2009

Biochemical and Genetic Studies of Beclin 1 Function in Autophagy

Yun Zhong

Biochemical and Genetic Studies of Beclin 1 Function in Autophagy

A Thesis Presented to The Faculty of

The Rockefeller University

in Partial Fulfillment of the Requirements for

The degree of Doctor of Philosophy

by

Yun Zhong

June 2009

Biochemical and Genetic Studies of Beclin 1 Function in Autophagy

Yun Zhong, Ph.D.

The Rockefeller University 2009

Beclin 1 is a mammalian autophagy protein and has important functions in development, tumor suppression and neurodegeneration. Beclin 1 exists in a protein complex with Vps34, which is a class III phosphatidylinositol (PtdIns) 3-kinase and mediates multiple vesicle trafficking pathways including autophagy and endocytosis. However the precise role of Beclin 1 in autophagy regulation is not well understood and information is lacking regarding the function of Beclin 1 in neuronal development and degeneration. In a study that combines mouse genetics and biochemistry, three novel Beclin 1 interaction proteins Atg14L (yeast Atg14-like), Rubicon (RUN domain and cysteine-rich domain containing, Beclin 1-interacting protein) and Nrbf2 were identified from mouse tissues. Gel filtration and co-immunoprecipitation show that these proteins co-exist in one large *in vivo* protein complex, from which multiple sub-complexes may be generated. Functional assays reveal that Atg14L positively regulates Vps34/PtdIns3K kinase activity and autophagy while Rubicon shows negative regulatory effects. Moreover, Beclin 1 and Atg14L synergistically promote autophagosome biogenesis while over-expression of Rubicon causes formation of aberrant late endosomes/early lysosomes and blocks autophagosome maturation. Therefore Atg14L and Rubicon regulate autophagy in opposite directions and at different steps, possibly through forming distinctive complexes with Beclin 1 and mediating Vps34/PtdIns3K kinase activity. Meanwhile, to study the function of Beclin 1 in neuronal development and degeneration,

targeted deletion of *beclin 1* was performed in pyramidal cells of the hippocampus and the cerebral cortex and in cerebellar Purkinje cells. Consequently, the deletion leads to rapid and severe degeneration in these cells. In degenerating pyramidal cells, there is intracellular protein accumulation that may have resulted from impaired autophagy, and activation of apoptotic pathway is also observed. In Purkinje cells, electron microscopy studies show a large number of aberrant electron dense structures and they are closely associated with intracellular membranes. Meanwhile, immuno-staining shows that deletion of *beclin 1* induces localization change of PtdIns(3)P, the product of Vps34/PtdIns3K. Therefore it is suggested that Beclin 1 is critical for normal neuronal development and that its deletion not only results in impaired autophagy but also may induce abnormal membrane and vesicle trafficking, possibly due to disrupted regulation of Vps34/PtdIns3K.

To my wife Xuan, daughter Michelle and my parents

Acknowledgements

I would like to thank my advisor, Dr. Nathaniel Heintz, for his guidance throughout my PhD years. His unique style of mentoring allows students to have the biggest freedom and independence, and thanks to that I was able to choose to work on the biological questions that I truly felt interested in. Hand-off as he is when everything is on track, whenever I had questions or problems, big or small, or felt lost and didn't know how the next step should be made, I was always able to receive advice from him that pointed me to the correct direction. The experience and training I was able to get in his lab gave me the confident to face the next challenge. I would also like to thank my thesis committee members, Dr. Hermann Steller, Dr. Shai Shaham, and Dr. David Sulzer for all their advice at my committee meetings and for their time and effort in evaluating my thesis work. I would like to thank Dr. Zhenyu Yue, a previous member in the lab who initiated the whole project and taught me the basics about mouse genetics, and with whom I had a very happy and fruitful collaboration. Without his help and expertise my accomplishments wouldn't have been possible. Many thanks as well to my collaborator Dr. Qingjun Wang and her adviser Dr. Brain Chait at Rockefeller. I learned a lot from her careful planning before experiments and critical thinking afterwards, and I feel honored to share with her the first authorship of our paper. I would like to thank Dr. Shiaoching Gong from the Gensat project, for developing highly efficient shuttle vectors and Bacterial Artificial Chromosome (BAC) modification protocols and generously sharing them with me. I would like to thank Wendy Yang of Heintz Lab, who helped me with cell culture all the time and never complained to any unreasonable request that I have made. I would like to thank my baymate Dr. Skirmantas Kriaucionis for his advice on protein purification and other daily discussion, and Ms. Judith Walsh of Heintz Lab for her help with ordering and all other administrative issues. Many thanks to all other Heintz Lab members for their technical help with my experiments. I would like to thank Drs. Chingwen Yang and Jing Gao of the Rockefeller Transgenic Facility for helping me generate the conditional knockout mice, and Ms. Eleana Sphicas and Ms. Helen Shio of Electron Microscopy Resource Center for their great help with my EM experiments. I would also like to thank members of the Dean's office for their superb support to graduate students, which I believe cannot be found anywhere else, and the Dean, Dr.

Sidney Strickland, for his advice when I was worried about not being able to make enough progress in my research. Finally I would like to thank my family for their support and patience, without which nothing would have been possible.

Table of Contents

List of Figures

Chapter I

Introduction

1.1 Autophagy

The balance between protein synthesis and degradation is important for normal function and survival of cells. While the ubiquitin-proteasome pathway is responsible for specific clearance of short-lived proteins, long-lived proteins are delivered to lysosomes by autophagy, which is the major inducible pathway for general turnover of bulk cytoplasmic components including entire organelles such as mitochondria (Klionsky and Emr, 2000; Levine and Klionsky, 2004; Levine and Kroemer, 2008). There are three types of autophagy: macroautophagy, microautophagy, and chaperone-mediated autophagy. In microautophagy, cytosolic components are directly engulfed by lysosomal limiting membrane at lysosome surface (Uttenweiler and Mayer, 2008), while in chaperone-mediated autophagy, specific cytosolic proteins with certain motif structures are degraded through chaperone complexes both in the cytocol and associated with lysosomal membranes (Massey et al., 2006). Macroautophagy is the most widely studied type of autophagy among these three types, and is usually referred to as autophagy. The initial step of autophagy is the synthesis of *de novo* single membrane sac named isolation membrane, which fuses at the edges and thereby enwraps cytosolic proteins and organelles into a double-membrane structure called autophagosome. The outer membrane of autophagosomes finally fuses with the membrane of lysosomes, releasing the inner membrane and the content for hydrolytic enzyme mediated degradation in lysosomes.

Although the morphology of autophagy has been widely studied in animal cells, the molecular mechanism was poorly understood, until a screening experiment was performed in the budding yeast *Saccharomyces cerevisiae*. In yeast, autophagy is induced by nitrogen deprivation. The vacuoles generated in response to starvation, which are equal to autophagosomes in mammalian cells, can be easily monitored by light microscopy. From screening for mutant yeast cells in which autophagic vacuoles do not accumulate under starvation conditions and as a result bulk protein degradation, sporulation and cell viability are affected, fifteen autophagy-related (Atg) genes were identified and later a few more were discovered (Tsukada and Ohsumi, 1993; Klionsky et al., 2003). Almost all of these Atg genes have orthologs in higher eukaryotic cells such as mammalian cells, suggesting that the machinery of autophagy is well conserved.

1.2 Two ubiquitin-like conjugation systems

Autophagy starts from autophagosome formation, and two ubiquitin-like conjugation systems are important for this initial step. One is Atg5-Atg12 system (Mizushima et al., 1998b). Atg12p forms a conjugate with Atg5p via a covalent bond between the carboxy-terminal glysine of Atg12p and a lysine of Atg5p at residue 149. This conjugation reaction is mediated by two other Atg proteins, Atg7p and Atg10p. Apg7 shows significant homology to the ubiquitin activating enzyme (E1) (Tanida et al., 1999), and Apg10p is considered to be a ubiquitin conjugating enzyme (E2)-like protein (Nemoto et al., 2003). Finally, another protein, Atg16p, binds to the conjugated Atg5p and oligomerizes to link a pair of Atg12p-Atg5p conjugates to form a complex (Mizushima et al., 1999; Kuma et al., 2002). Similar conjugation was also found in

human cells (Mizushima et al., 1998a) so it is highly conserved. In mammalian cells, Apg5p-Apg12p conjugates localize on the isolation membrane and dissociate upon autophagosome formation, therefore it is essential for the autophagosomal precursors to form.

Another ubiquitin-like modification that is important for initiation of autophagy is the processing of Atg8p, and in this process, Atg7p and Atg3p act as E1 and E2 like enzymes respectively (Ichimura et al., 2000). Unlike Atg12p, Atg8p is finally conjugated to phosphatidylethanolamine (PE), and it must first undergo a series of posttranslational modification before it finally associates to the autophagosome membrane. A critical step is a proteolytic cleavage of the C terminal of Apg8p, removing the arginine residue from the nascent Atg8p precursor to expose a conserved glysine residue, and this step is catalyzed by a constitutively expressed cysteine protease, Atg4p.

LC3 (microtubule-associated protein 1 (MAP1) light chain 3), the mammalian orthologue of Atg8, is the first mammalian autophagy gene identified to be associated specifically to the autophagosome membrane. Therefore, it can be used as a molecular marker for the autophagic membrane (Kabeya et al., 2000). *In vivo* studies using a GFP-LC3 tansgenic mouse reveal that under starvation conditions, increased numbers of punctate dots are observed in most tissues, indicating the induction of autophagy (Mizushima et al., 2004). Targeting of LC3 to the isolation membrane also requires Atg5-Atg12 conjugate, as is shown by a study using Atg5-deficient mouse embryonic stem cells (Mizushima et al., 2001).

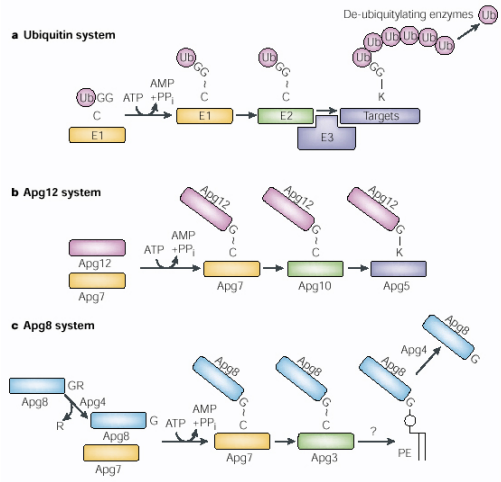

Two ubiquitin-like systems are required for autophagy. **(a)** The ubiquitin system. **(b)** The Atg12-Atg5 system. **(c)** The Atg8 system. (From Ohsumi Y, Nature Reviews Molecular Cell Biology, 2001)

1.3 Beclin 1

Another protein that is important for autophagy induction and yet has distinct function from the two ubiquitin-like conjugation systems is Beclin 1. *Beclin 1* is the mammalian ortholog of yeast gene *Atg6/Vps30*, and is one of the first identified mammalian orthologs of Atg genes.

In yeast, *Atg6* is identical to *Vps30*, one of vacuolar protein sorting (VPS) genes that are required for correct targeting of soluble hydrolases from late-Golgi to vacuoles (Horazdovsky et al., 1995). Atg6p/Vps30p exists in two distinctive protein complexes that both contain Vps34p, a phosphoinositide 3-kinase (PI3K), and its activator Vps15p. One Atg6p/Vps30p complex contains Atg14p and is essential for autophagy induction, and the other contains Vps38p and functions in vacuolar protein carboxypeptidase Y (CPY) sorting pathway that delivers CPY and other vacuolar proteins from the late Golgi to the vacuole (Kametaka et al., 1998; Kihara et al., 2001b). *Atg14* mutants exhibit defective autophagy but display normal CPY sorting, and the over production of Atg14p

partially reverses the autophagy defect induced by *Atg6/Vps30* mutation but has no effect on CPY sorting defect (Kametaka et al., 1998). Meanwhile, *Vps38* mutants exhibit disrupted CPY sorting but intact autophagy levels. Moreover, Atg14p and Vps38p do not co-immunoprecipitate. Therefore, the Atg14p containing and Vps38p containing Atg6p/Vps30p-Vps34p-Vps15p complexes are two distinctive complexes and function separately, and Atg6p/Vps30p is unique and different from other Atg proteins in that it is not required for autophagy alone. Given the fact that loss of Atg38 dramatically disruptes interaction between Atg6p/Vps30p and Vps34p-Vps15p while deletion of Atg14 has little effect, it is estimated that Vps38p containing complex is much more abundant in yeast cells (Kihara et al., 2001b).

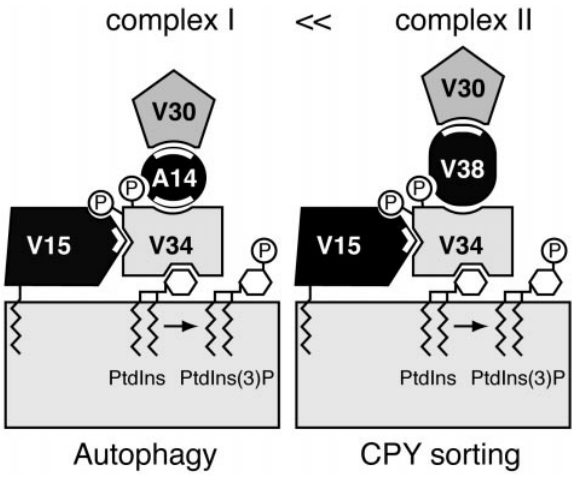

Model for two distinct Atg6p/Vps30p-Vps34p-Vps15p complexes (from Kihara et al., 2001)

In yeast, several autophagy proteins, including Atg5p, Atg16p and Atg8p that reside on autophagosome membrane, and Atg1p, a kinase functioning in autophagosome formation, are all localized on perivacuolar structures prior to autophagosome formation.

These structures were named pre-autophagosomal structures (PASs) and both Atg6/Vps30p and Atg14p are important for delivering other Atg proteins from cytosol to PASs (Kihara et al., 2001b; Suzuki et al., 2001).

In mammalian cells Beclin 1 was first identified as a novel coiled-coil protein that interacts with cell death inhibitor Bcl-2 through a yeast two-hybrid screen using an adult mouse brain library. From deletion mutation analysis it is estimated that the putative Bcl-2 binding domain is localized at the N-terminus of the protein, while the BH1 domain in Bcl-2 is responsible for its interaction with Beclin 1 (Liang et al., 1998). Recently Beclin 1 was further shown to be a Bcl-2-homology-3 (BH3)-only protein (Maiuri et al., 2007; Oberstein et al., 2007). Beclin 1 is mono-allelically deleted in a high percentage of human breast, ovarian and prostate carcinomas (Aita et al., 1999), and its gene transfer inhibits cell growth in human breast cancer cell line as well as tumorigenesis in nude mice (Liang et al., 1999). Therefore *Beclin 1* is considered a haploinsufficient tumor suppressor gene in mammals. Moreover, homozygous targeted disruption of *beclin1* in mice caused the mice to die between embryonic day 7.5 (E7.5) and E8.5, indicating that Beclin 1 is important for embryonic development, and heterozygous disruption results in increased spontaneous tumorigenesis (Qu et al., 2003; Yue et al., 2003).

Like yeast Atg6p/Vps30p, Beclin 1 also mediates autophagy in mammalian cells. Transformation of *beclin 1* into *Atg6/Vps30*-disrupted yeast restored the autophagy to normal levels, and transfer of *beclin 1* gene into MCF7 human breast carcinoma cells that do not express detectable levels of endogenous Beclin 1 increased the autophagy levels after serum and amino-acid deprivation (Liang et al., 1999). *Beclin* $1^{-/-}$ ES cells show defect in nutrient deprivation induced autophagy but no significant changes in apoptosis

(Yue et al., 2003), and *Beclin 1*$^{+/-}$ mice show reduced autophagy levels in tissues (Qu et al., 2003; Yue et al., 2003). Therefore the function of Atg6p/Beclin 1 in autophagy is well conserved.

1.4 Vps34/PtdIns3K and its function in regulation of autophagy

In mammalian cells, quantitative analyses show that Beclin 1 localizes both in cytosol and on membranes, and that all Beclin 1 is associated with Vps34/PtdIns3K, a type III phosphoinositide 3 (PI 3)-kinase that generates phosphotidylinositol 3-phosphate (PtdIns(3)P) from the substrate phosphatidylinositol (PI) (Schu et al., 1993; Kihara et al., 2001a). The Beclin 1-Vps34/PtdIns3K complex localizes to the trans-Golgi network (TGN) , and Vps34/PtdIns3K is recruited from the cytosol to the membrane and is activated by its activator Vps15p, which is a membrane associated serine/threonine protein kinase that helps activate the PI 3-kinase activity of Vps34/PtdIns3K (Stack et al., 1993; Stack et al., 1995).

Vps34/PtdIns3K functions in multiple vesicle trafficking pathways including endocytosis and is also essential for autophagy induction (Simonsen et al., 2001; Lindmo and Stenmark, 2006). Deletion of Vps34p in yeast disrupts starvation induced autophagy (Kihara et al., 2001b), and in HT-29 human colon cancer cells treatment with PI 3-kinase inhibitors wortmannin, LY294002 or 3-methyladenie (3-MA), as well as down-regulation of Vps34/PtdIns3K, inhibits autophagy. In contrast, adding Vps34/PtdIns3K product PtdIns(3)P to the cells promotes autophagy (Petiot et al., 2000). Among the PI 3-kinase inhibitors, 3-MA preferentially inhibits class III PI 3-kinases and is widely used as an inhibitor of autophagy.

Like in yeast, the function of Beclin 1-Vps34/PtdIns3K complex in the regulation of autophagy is likely to be at the initial step of autophagy induction. With Beclin 1, Vps34/PtdIns3K participates in the nucleation of autophagosome formation, and also mediates localization of other autophagy proteins to the preautophagosomal structure (PAS) (Kihara et al., 2001b; Suzuki et al., 2001). The dynamic membrane trafficking mediated by Vps34/PtdIns3K complex is important for autophagy induction.

The Vps34/PtdIns3K product PtdIns(3)P has several known protein effectors that have specific domains. The first identified PtdIns(3)P binding domain is FYVE (for conserved in Fab1, YOTB, Vac1 and EEA1) zinc finger domain (Stenmark et al., 2002), and another one is conserved Phox-homology (PX) domain (Ellson et al., 2002). From their specific binding to PtdIns(3)P, these domains can be used as probes to study the localization of PtdIns(3)P.

Although Beclin 1 is essential for regulatory function of Vps34/PtdIns3K on autophagy it is not necessary for the other function of Vps34/PtdIns3K on protein trafficking. Forced expression of *beclin 1* in yeast strains that are deficient in *Atg6/Vps30* does not rescue the disrupted CPY sorting pathway (Liang et al., 1999). Furthermore, knockdown of Beclin 1 in mammalian cells does not affect the lysosomal enzyme sorting and protein trafficking in the endocytic pathway (Zeng et al., 2006).

1.5 Pro-survival or pro-death?

It has long been debated what the function of autophagy is in cell death, and in yeast it is considered that autophagy generally functions in favor of cell survival under stressful conditions such as starvation. Yeast with Atg gene mutations fail to initiate

autophagy and die under starvation conditions (Tsukada and Ohsumi, 1993; Klionsky et al., 2003). Evidence supports that this is also true in other species because in autophagy, cytoplasm components are degraded to generate an internal reserve of nutrients, and amino acids from lysosomal degradation can be used as energy source and for novel protein synthesis.

In the nematode *Caenorhabditis elegans*, in order to survive unfavorable environment such as food limitation or increased temperature, *C elegans* enter dauer, a stage of developmental arrest. Animals that carry a loss of function mutation in insulin-like tyrosine kinase receptor *daf-2* show constitutive entry into dauer at 25°C and extended adult life-span at lower temperatures. When the expression of *bec-1*, the C. elegans ortholog of *Atg6/Vps30*, was inhibited with RNA interference (RNAi), animals showed abnormal dauer morphogenesis and died within a few days at 25°C. Treatment with *bec-1* RNAi also reduced the extension of life-span of *daf-2* mutant animals. RNAi treatment targeting other autophagy genes induced similar phenotypes, indicating that autophagy genes are important for dauer morphogenesis and life-span extension in C. elegans (Melendez et al., 2003). In the fruitfly *Drosophila melanogaster*, the fat body formed during the larval period functions as a sensor for nutritional levels. Starvation induces a significant increase in the level of autophagy in the fat body, and either larva ubiquitous or fat body targeted inhibition of autophagy with RNAi against *Drosophila* ortholog of *Atg5* resulted in reduced larva or cell size (Rusten et al., 2004; Scott et al., 2004). In mammalian cells, when primary cells or immortalized interleukin-3 (IL-3) dependent cells generated from the bone marrow of Bax/Bak double knockout mice (in which deletion of the two pro-apoptotic members of the Bcl-2 family makes the cells

resistance to apoptosis) are deprived of IL-3, cells are not able to utilize the nutrients in the extracellular media and activate autophagy to degrade intracellular contents for ATP production and survival maintenance. Treatment of IL-3 deprived cells with either small hairpin RNA (shRNA) against autophagy gene *Atg5* or *Atg7*, or with an autophagy inhibitor, induces cell death. This can be reversed by supplying the cells with alternative metabolic substrate for oxidative phosphorylation at mitochondria to make up for the loss of autophagy. This indicates that in the situation of growth factor withdraw autophagy functions to maintain cell survival (Lum et al., 2005). Furthermore, the autophagy level in mice is low during embryogenesis but is transiently activated after birth to maintain adequate amino acid levels so as to combat the nutrient limitation that neonates face. Mice deficient in either *Atg5* or *Atg7* are defective in autophagy and die within one day after delivery, showing reduced amino acid levels in tissues and signs of energy depletion. This suggests that autophagy in essential for mammalian survival during neonatal starvation (Kuma et al., 2004; Komatsu et al., 2005). In conclusion, from yeast to mammalian cells conserved autophagy is induced to maintain cell and animal survival in stressful conditions such as starvation.

In some other cases, autophagy constitutes a pathway that contributes to cell death, possibly through excessive self-digestion. This pathway is called autophagic cell death or type II programmed cell death, in contrast to apoptosis or type I programmed cell death. In a number of mammalian cell lines, treatment with the caspase inhibitor (O-methyl)-fluoro-methylketone (zVAD) induces non-apoptotic cell death that shows characteristics of autophagy, and the cell death can be blocked with either the autophagy inhibitor 3-MA or wortmannin, or by knockdown of autophagy gene *Atg7* or *beclin 1* (Yu et al., 2004).

Moreover in $Bax^{-/-}/Bak^{-/-}$ mouse embryonic fibroblast cells, apoptotic death stimulation induces non-apoptotic cell death that exhibits autophagy induction, and this cell death can be suppressed with autophagy inhibitor treatment. It is also dependent on autophagy proteins Atg5 and Beclin 1 (Shimizu et al., 2004). In addition, in human cervical carcinoma Hela cells, Atg5 interacts with Fas-associated protein with death domain (FADD) to contribute to autophagic cell death, which can be inhibited with Atg5 knockdown or 3-MA treatment (Pyo et al., 2005). Therefore autophagy may function in both directions, to maintain cell survival and to mediate cell death, depending on the context.

1.6 The complex role of Beclin 1 in autophagy and apoptosis

As the possible contributing force to type II programmed cell death, autophagy has complex crosstalk with type I programmed cell death (apoptosis), and one intriguing function of Beclin 1 is its coordination of autophagy and apoptosis. Beclin 1 was first identified as interaction protein of Bcl-2, and it contains a BH3 domain that is both necessary and sufficient for its interaction with Bcl-X_L, both of which are members of the Bcl-2 family that have pro-survival functions in the apoptotic pathway (Maiuri et al., 2007; Oberstein et al., 2007). The interaction between Beclin 1 and Bcl-2 may occur on outer membranes of mitochondria or endoplasmic reticulum (ER), and forced expression of ER-targeted Bcl-2 inhibits binding of Beclin 1 to Vps34/PtdIns3K as well as Beclin 1 dependent autophagy while Beclin 1 mutants that cannot bind to Bcl-2 induce excess level of autophagy (Pattingre et al., 2005). Meanwhile, treatment of cells with BH3-mimetic compound ABT737, which inhibits the Beclin 1-Bcl-2/ Bcl-X_L interaction in a

competitive manner, stimulates Beclin 1-dependent autophagy (Maiuri et al., 2007). Furthermore, Bcl-2 down-regulation in human leukemic HL60 cells with expression of antisense message induces massive cell death accompanied with activated autophagy (Saeki et al., 2000). Therefore, Bcl-2 and other apoptotic proteins have regulatory effect on autophagy and this occurs through interaction with Beclin 1.

Change in autophagy levels can also affect apoptosis. In fact inhibition of autophagy often leads to activation of apoptosis. In *C elegans*, the Beclin 1 ortholog BEC-1 forms a complex with Bcl-2 ortholog CED-9, and disruption of *bec-1* induced apoptosis (Takacs-Vellai et al., 2005). In nutrient depleted mammalian cells, inhibition of autophagy either with siRNA targeting critical Atg genes including *beclin 1* or with chemical autophagy inhibitors often leads to cell death that is dependent on mitochondrial outer membrane permeabilization and caspase activation and is therefore apoptotic (Boya et al., 2005). Similarly, inactivation of LAMP2 by RNAi inhibits fusion of autophagosomes with lysosomes, and induces accumulation of autophagosomes under starvation that is followed by cell death with features of apoptosis (Gonzalez-Polo et al., 2005).

Reagents that inhibit apoptosis can also induce autophagy. Treatment of HL-60 human myeloid leukemian cells with vitamin D3 inhibits apoptosis but induces autophagy, possibly through up-regulation of Beclin 1 and Vps34/PtdIns3K protein levels (Wang et al., 2008).

In summary, in response to various stimuli, autophagy and apoptosis are selectively induced in cells, and altering one pathway often leads to changes in the other.

Beclin 1 may be the key protein in coordinating the two pathways through forming different protein complexes with different interaction partners.

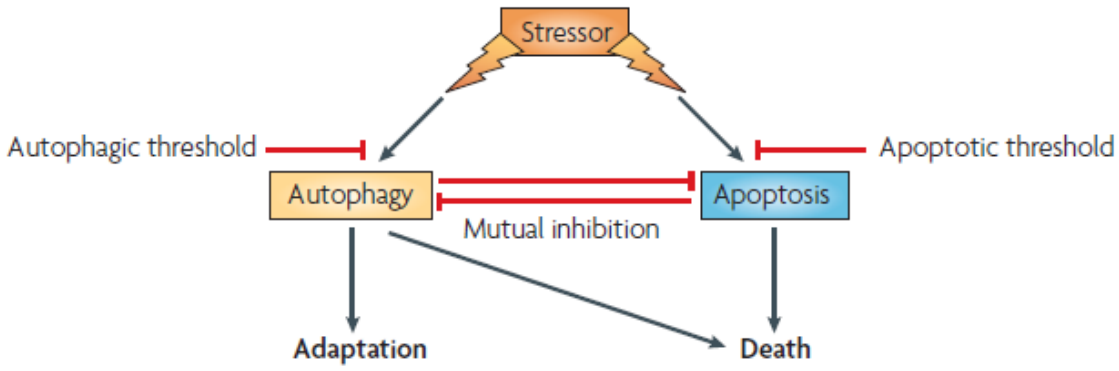

The relationship between apoptosis and autophagy (From Maiuri M et al., Nature Reviews Molecular Cell Biology, 2007)

1.7 Beclin 1 interacting proteins

In addition to Bcl-2 and Vps34/PtdIns3K, recently several novel Beclin 1 interaction proteins have been identified. UV irradiation resistance-associated gene (UVRAG) was identified as a protein that immunoprecipitated with Bcl-2-Beclin 1-Vps34/PtdIns3K multiprotein complex. It binds directly to Beclin 1 through the coiled-coil domains in itself and in Beclin 1, and they interdependently promote autophagy and induce autophasosome formation, possibly thorough positive regulation of Vps34/PtdIns3K lipid kinase activity by UVRAG. Like *beclin 1*, *UVRAG* is also monoallelically deleted in various human cancers, and ectopic expression of UVRAG in one type of these cells (human colon cancer HCT116 cells) suppresses cell proliferation and inhibits tumorigenicity of the cells (Liang et al., 2006). Bif 1, originally discovered as a Bax-binding protein that localizes on intracellular membranes, was shown to form a

complex with Beclin 1. This interaction is thought to be bridged by UVRAG, through binding between the C-terminal SH3 domain of Bif1 and UVRAG, and like UVRAG, Bif-1 also positively regulates Vps34/PtdIns3K lipid kinase activity and autophagy (Takahashi et al., 2007). *Ambra1* (activating molecule in Beclin 1-regulated autophagy) is a gene involved in nervous system development that was isolated from a large-scale mutagenesis approach. Homozygous disruption of *Ambra1* induces neural tube defects, unbalance cell proliferation and excessive apoptosis. Yeast two-hybrid screening with a portion of Ambra1 identified Beclin 1, suggesting that Ambra1 is also a Beclin 1 interaction protein, and Ambra1 o positively regulates autophagy. Consistent with this function, *Ambra1* deficient embryos show severe defect in autophagy and accumulation of ubiquitinated proteins (Fimia et al., 2007).

However, despite the recent discoveries, the exact role of Beclin 1 in autophagy regulation and its autophagy unrelated functions still remain to be characterized. Although yeast Atg6/Vps30p forms two distinctive complexes that have different functions, it is not known how many Beclin 1-containing protein complexes mammalian cells possess and the composition of the complex(es). Furthermore the molecular mechanism underlying the function of Beclin 1 in autophagy regulation still remains unknown. Unlike *atg5*$^{-/-}$ and *atg7*$^{-/-}$ mice that are born almost normally and then die within one day, *beclin 1*$^{-/-}$ mice die as early as on embryonic day 7.5 and show excessive developmental defect. Moreover, neither tumorigenesis nor abnormal cell proliferation was observed in atg5 or atg7 (homozygous or heterozygous) deficient mice. These results suggest that Beclin 1 may have a more important function in embyogenesis and tumor suppression and this function may or may not be related to autophagy.

1.8 Beclin 1 and autophagy in neuronal development and diseases

Although the pathways of autophagy are well characterized in yeast and its function widely studied in many tissues of mammalian animals, its exact function in the nervous system is not well understood. Its morphological features such as excessive double membrane autophagosome formation and high electron density lysosomes have been reported in many human neurodegenerative diseases such as transmissible spongiform encephalopathies, Polyglutamine diseases, Alzheimer's disease (AD) and Parkinson's disease (PD) (Williams et al., 2006; Rubinsztein et al., 2007). However it is still in debate whether autophagy is one of the cell death executing forces in neurodegenerative diseases, whether it is a failed attempt at protection, or just a secondary effect. Many *in vivo* studies in disease model mice and *in vitro* studies using cultured primary neurons have suggested that autophagy is a self protective response to the stress that is induced by accumulation of toxic proteins in many neurodegenerative diseases (Larsen and Sulzer, 2002).

Consistent with this possible protective function, *beclin 1* expression level has been shown to decrease in human brains in an age-dependent manner, and Beclin 1 mediated autophagy reduces intracellular Huntingtin accumulation (Shibata et al., 2006). Meanwhile, Beclin 1 levels are reduced in cortical gray matter from AD patients, and heterozygous deletion of *beclin 1* in a mouse model for AD increased the amyloid β (Aβ) accumulation in neurons as well as extracellular Aβ deposit (Pickford et al., 2008). In addition, after closed head injury, Beclin 1 levels increases quickly and dramatically in both neurons and surrounding astrocytes at the injury site, suggesting that Beclin 1 is involved in brain response to head trauma (Diskin et al., 2005). Up-regulation

of Beclin 1 level and activation of autophagy are also observed in Niemann-Pick type C disease, one type of inherited sphingolipid storage diseases that cause neurodegeration and cognitive impairment (Pacheco et al., 2007).

Induction of autophagy is also observed in non-apoptotic Purkinje cell death in Lurcher (Lc) mice, an extensively used model of Purkinje cell degeneration. Purkinje cells are specifically lost in various neurodegenerative conditions such as spinalcerebellar ataxia, ataxia telangectasia, autism and certain prion encephalopathies, but the molecular mechanism underlying Purkinje cell death is poorly understood. Lurcher is a spontaneous, semidominant mouse neurological mutation. A point mutation in Purkinje cell specific glutamate receptor δ2 changes the receptor to a constitutive active form, and excessive influx of calcium induces cell-autonomous death of cerebellar Purkinje cells (Zuo et al., 1997). Degenerating Purkinje cells exhibit elevated levels of autophagy, and yeast two-hybrid study using C terminal cytosolic tail of glutamate receptor δ2 as a bait identified Beclin 1, suggesting that Beclin1 mediated autophagy may be related to Lurcher Purkinje cell degeneration (Yue et al., 2002).

Autophagy may be a quick response by the brain to protect itself in response to injury or accumulation of toxic protein aggregates. Furthermore, the basal level of autophagy is important in maintaining the normal function of the brain, since inhibition of basal autophagy in the brain has been shown to induce neurodegeneration.. When *Atg5* or *Atg7* expression is specifically deleted in the central nervous system, cytosolic proteins in neurons accumulate, and ultimately become inclusion bodies that are ubiquitin positive, and activated apoptosis and neurodegeneration were observed. This suggests that basal level of autophagy is essential for maintaining normal functions of neurons by

clearing cytosolic proteins and preventing them from forming aggregates (Hara et al., 2006; Komatsu et al., 2006).

In addition to its critical function in mediating cell survival and cell death, autophagy is also important in cellular and tissue development and remodeling, through turnover and recycling of organelles and proteins. *Unc51*, which is a C. elegans ortholog of *Atg1*, is important for axonal elongation (Ogura et al., 1994), while Drosophila ortholog of Apg4 was identified as modifier of Notch signaling pathway, and its loss of function affected wing development (Thumm and Kadowaki, 2001). From its involvement in recycling of proteins and membranes, it can be hypothesized that autophagy may also be related to dynamic morphological changes of neuronal and synaptic structures, and that it may be involved in plasticity in the central nervous system.

1.9 Summary

As an essential protein for autophagy induction, Beclin 1 is part of the Vps34/PtdIns3K complex and functions at the initial step of autophagosome formation. Moreover, through its organelle specific binding with Bcl-2, Beclin 1 is also important in mediating cross talk between autophagy and apoptosis. Although it has been shown in yeast that Atg6p forms two distinctive complexes with different functions, and recently several novel Beclin 1 interaction proteins have been identified in mammalian cells, the exact nature of Beclin 1 complex(es) is unclear. Information regarding the function of Beclin 1 on neuronal development is still lacking. Therefore in this study, we combined genetic and biochemical approaches to study the formation of Beclin 1 complex(es) in mammalian cells and the function of Beclin 1 in the central nervous system.

Chapter II

Identification and Characterization of Beclin 1 Interaction Proteins

2.1 Generation of *beclin 1-EGFP* transgenic mice

Beclin 1-EGFP transgenic mice were generated using bacterial artificial chromosome (BAC) techniques. As a result of homologous recombination through BAC modification, EGFP-coding cDNA was inserted immediately in front of the stop codon of *beclin 1* gene inside the BAC, and CsCl purified BAC DNA was pro-nuclear injected to generate transgenic mice (Fig. 1a). Positive mice that have *EGFP* integrated into the genome were identified with PCR and further confirmed with southern blot (data not shown). Two founder mice were obtained from injection, and both gave germ line transmission. Expression of Beclin 1-EGFP protein was confirmed with western blot using brain tissue homogenate. Using Beclin 1 antibody, it was observed that one line had higher expression level of Beclin 1-EGFP fusion protein than the other and the level was comparable to that of endogenous Beclin 1 protein (data not shown). This line was used for further study. Immuno-fluorescence studies on tissue sections using anti-GFP antibody confirmed that Beclin 1-GFP fusion protein was localized diffusely in the cytoplasm, which is consistent with the reported localization of the endogenous Beclin 1 protein (Arsov et al., 2008).

2.2 Generation of *beclin 1*$^{-/-}$*; beclin 1-EGFP* rescued mice

Since *beclin 1* homozygous deletion is embryonic lethal, it was tested whether Beclin 1-EGFP fusion protein could restore the Beclin 1 protein function and rescue the embryonic

Figure 1-1. *Beclin 1-EGFP* transgene rescued the embryonic lethality of *beclin 1* homozygous deletion (*beclin 1* $^{-/-}$)

(a) Schematic representation of EGFP insertion in BAC-mediated Beclin 1-EGFP transgenics.

(b) Breeding strategy for generating mice in which *beclin 1-EGFP* transgene replaces the endogenous *beclin 1* alleles. *Beclin 1-EGFP* mice were crossed with *beclin 1* $^{+/-}$ mice to generate "rescued mice" (*beclin 1* $^{-/-}$; *beclin 1-EGFP*).

(c) Western blot analysis confirmed the replacement of endogenous Beclin 1 with Beclin 1-EGFP in *beclin 1* $^{-/-}$; *beclin 1-EGFP* mice, as detected by anti-Beclin 1 antibody.

(d) Theoretical distribution (Mendeline ratio) of each mouse genotype in the breeding experiments. In the breeding to generate rescued mice, the theoretical ratio of the rescued mice to the whole litter is 1/7. In this study, 11 out of a total of 69 mice (from 8 litters) were the *beclin 1* $^{-/-}$; *beclin 1*-EGFP genotype (*chi* square test with the value 0.22, $p>0.6$, df=1). In the second round breeding with the rescued mice, the theoretical ratio of the rescued mice born to the whole litter is 1/3, and 12 out of 36 mice (from 6 litters) were of that genotype. Therefore Beclin 1-EGFP completely rescued the early embryonic lethality in *beclin 1* $^{-/-}$ mice, and thus can functionally substitute for the endogenous Beclin 1 protein.

Figure 1-1

a

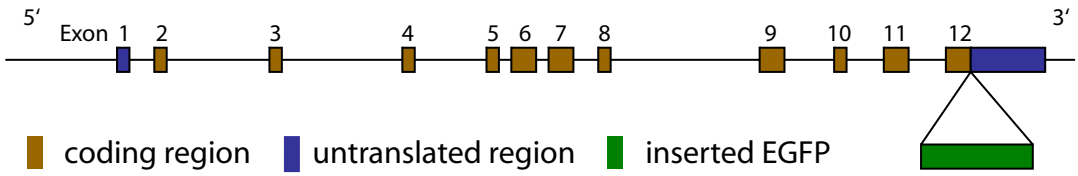

b

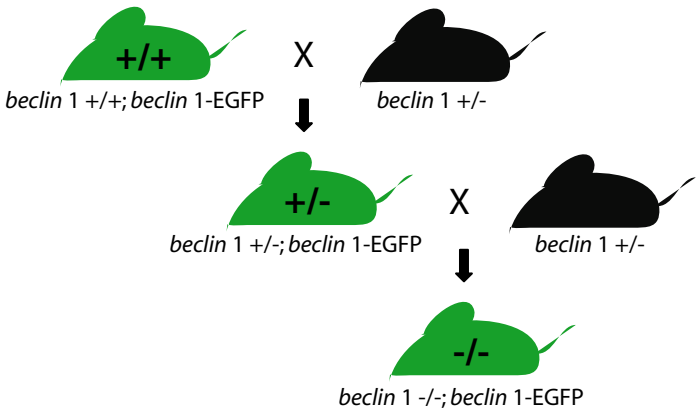

c

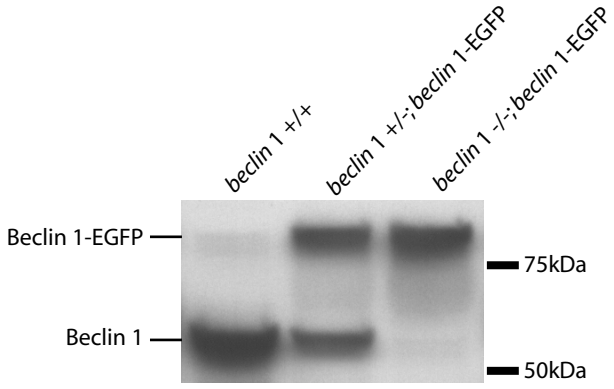

d

beclin 1 +/-; *beclin* 1-EGFP X *beclin* 1 +/-

ratio	genotype
1/7	*beclin* 1 +/+
2/7	*beclin* 1 +/-
1/7	*beclin* 1 +/+; *beclin* 1-EGFP
2/7	*beclin* 1 +/-; *beclin* 1-EGFP
1/7	*beclin* 1 -/-; *beclin* 1-EGFP

beclin 1 -/-; *beclin* 1-EGFP X *beclin* 1 +/-

ratio	genotype
1/3	*beclin* 1 +/-
1/3	*beclin* 1 +/-; *beclin* 1-EGFP
1/3	*beclin* 1 -/-; *beclin* 1-EGFP

lethal phenotype. *Beclin 1-EGFP* transgenic mice were first crossed with *beclin 1* $^{+/-}$ mice to generate *beclin* $1^{+/-}$; *beclin 1-EGFP* mice, and these mice were further crossed with *beclin* $1^{+/-}$ mice (Fig. 1b). Tail clips were cut and protein was extracted for western blot with anti-Beclin 1 antibody. *Beclin* $1^{-/-}$*; beclin 1-EGFP* mice were identified as having only Beclin 1-EGFP fusion protein but no endogenous Beclin 1 protein (Fig. 1c). Rescued mice showed a similar life span to control mice, and did not show significant phenotypic abnormality (data not shown). Mating was repeated and in total 69 mice were born from 8 mating pairs, and among them 11 mice were confirmed to be rescued mice. The ratio of rescued mice to total litter size was close to 1:7, which is the predicted number if Mandel's law is followed (chi-square test with the value 0.22, $p>0.6$, df=1, Fig. 1d). Rescued mice were further crossed with *beclin* $1^{+/-}$ mice to test if they can reproduce normally. Within totally 36 mice born from 6 breeding pairs, 12 mice were rescued mice, and the ratio again followed the 1:3 predicted by Mandel's law (Fig. 1d). Therefore it can be concluded that over-expression of Beclin 1-EGFP fusion protein completely rescued embryonic lethal phenotype of *beclin 1* homozygous deletion, and that the Beclin 1-EGFP fusion protein possesses the physiological function of the endogenous Beclin 1 protein.

2.3 Identification of Beclin 1 interaction proteins

Rescued mice were used for identification of Beclin 1 interaction proteins so that no endogenous Beclin 1 protein would compete for binding. Whole brains, livers and thymuses were dissected out from rescued mice and littermate control mice, and homogenate was prepared. After immunoprecipitation was performed using anti-GFP

Figure 1-2. Identification of novel Beclin 1-interaction proteins from *beclin 1* $^{-/-}$; *beclin 1-EGFP* mice

(a) Coomassie-stained SDS-PAGE gel revealed the Beclin 1-interacting proteins immuno-isolated from the brain and liver tissues of the "rescued" mice by using anti-GFP antibody (Lane 2 and 4). Protein bands in the gel were isolated and identified by mass spectrometric analysis as Vps15/p150 (band 1), Vps34/ PtdIns3K (band 3), UVRAG (band 4), Beclin 1-EGFP (band 5), Nrbf2 (band 7, asterisk) and two novel proteins Atg14L (band 6, asterisk, gi|27369860) and Rubicon (band 2, asterisk, gi|45708948). The control mice were the beclin 1 $^{+/-}$ littermates (P16) (Lane 1 and 3).

(b) Schematic diagrams of the domain structures of Atg14L, Rubicon and Nrbf2. Atg14L contains two coiled-coil domains (CCD1 and CCD2), which are also homologous to SMC domain (Structural Maintenance of Chromosomes). Rubicon contains an N-terminal RUN (for RPIP8, UNC-14 and NESCA) domain, a C-terminal cysteine-rich domain, and a CCD domain in the central of the protein sequence. Nrbf2 contains a coiled-coil domain in the central part of the protein.

(c and d) HEK 293T cells were transiently transfected with either N-terminal FLAG-tagged (d) or C-terminal EGFP-tagged (e) Atg14L, Nrbf2 and Rubicon. Immunoprecipitation was performed with anti-FLAG (d) or anti-GFP antibody (e). The endogenous Beclin 1 co-immunoprecipitated was detected by western blot analysis using anti-Beclin 1 antibody. WCL: whole cell lysate; IP: immunoprecipitated.

Figure 1-2

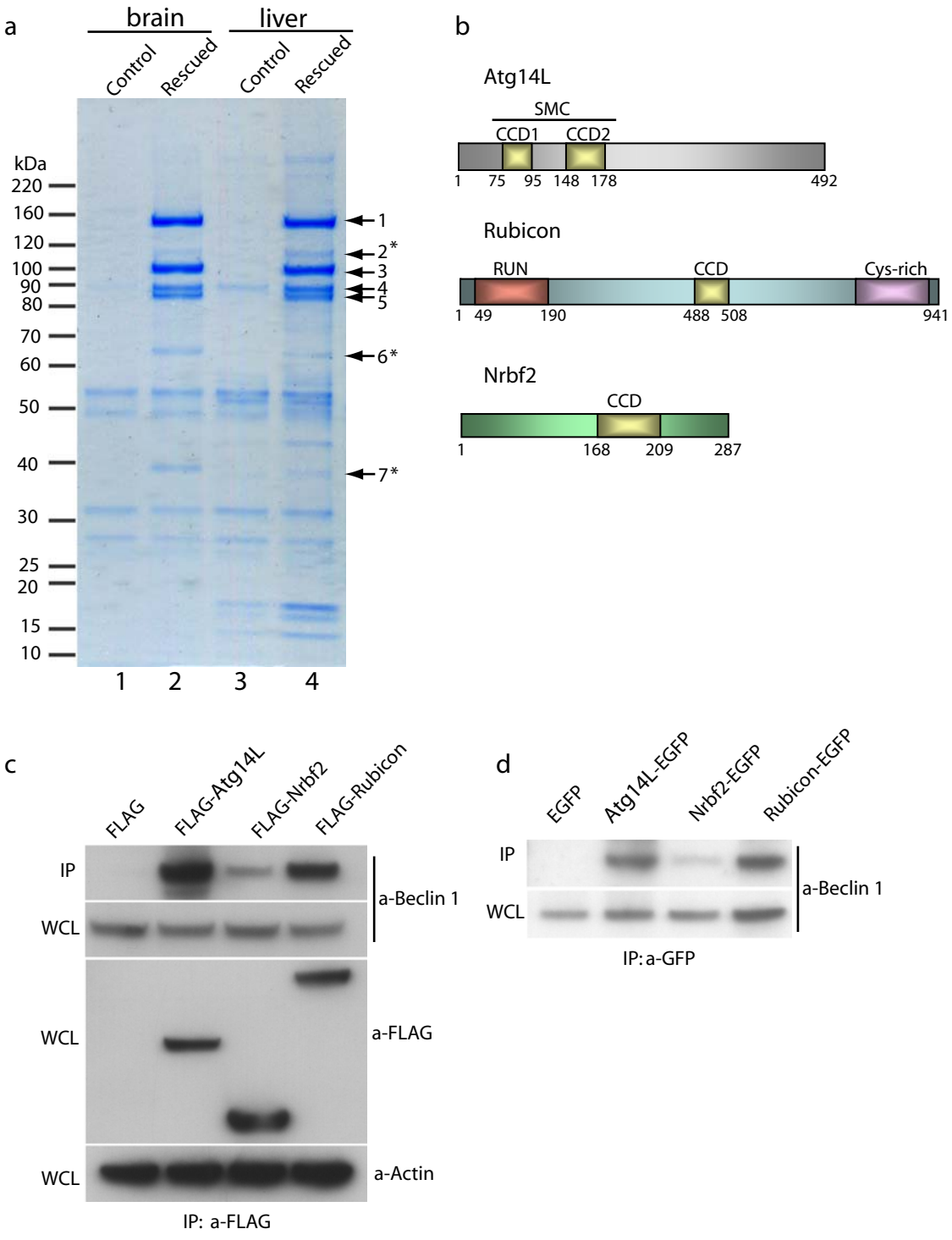
a
brain
liver
Control
Rescued
Control
Rescued
kDa
220
160
120
100
90
80
70
60
50
40
30
25
20
15
10
1
2*
3
4
5
6*
7*
1
2
3
4
b
Atg14L
SMC
CCD1
CCD2
1
75
95
148
178
492
Rubicon
RUN
CCD
Cys-rich
1
49
190
488
508
941
Nrbf2
CCD
1
168
209
287
c
FLAG
FLAG-Atg14L
FLAG-Nrbf2
FLAG-Rubicon
IP
WCL
a-Beclin 1
WCL
a-FLAG
WCL
a-Actin
IP: a-FLAG
d
EGFP
Atg14L-EGFP
Nrbf2-EGFP
Rubicon-EGFP
IP
WCL
a-Beclin 1
IP: a-GFP

antibody, proteins were separated in SDS-PAGE gel, followed by visualization with coomassie blue staining. Distinct bands that were only observed from rescued mice but not from control mice were cut out and proteins were identified with mass spectrometry. From rescued mouse tissues, at least seven bands were identified that were not seen from control tissues. In addition to Beclin 1-EGFP fusion protein itself, three were known Beclin 1 interaction proteins: Vps34/PtdIns3K, its activator Vps15 and UV Resistance Associated Gene (UVRAG). The remaining three proteins were identified as two novel proteins and Nuclear Receptor Binding Factor 2 (Nrbf2) (Fig. 2a). The first novel protein (gi|27369860) has 492 amino acids (~60 kD), has two coiled-coil domains (aa 75-95 and aa 148-178) and also contains homology to the conserved SMC (Structural Maintenance of Chromosomes) motif. The second novel protein (gi|45708948) contains 941 amino acids (~124 kD) and has a conserved RUN (for RPIP8, UNC-14 and NESCA) domain (aa 49-190) near the N-terminus, a cysteine-rich domain (aa 837-890) near the C-terminus, and a coiled-coil domain (aa 488-508) in the central region. Since yeast Atg6p binds to either Atg14p or Vps38p, alignment study was performed between the two novel proteins and Atg14p or Vps38p. The first novel protein showed a modest 15% homology to yeast Atg14p, therefore was named Atg14-Like (Atg14L) (Fig. 3). The second novel protein showed no significant homology to either Atg14p or Vps38p, therefore was named after its domain structure as Rubicon for RUN domain and cysteine-rich domain containing, Beclin 1-interacting protein (Fig. 2b).

Figure 1-3. Moderate homology between Atg14L and yeast Atg14

Protein sequences of Atg14L and yeast Atg14 were aligned to analyze possible homology between them. Alignment was done suing T-Coffee package (**T**ree based **C**onsistency **O**bjective **F**unction **F**or **A**lignm**E**nt **E**valuation) available at server: www.tcoffee.org., and analysis was performed with GeneDoc application. The exact match between Atg14L and yeast Atg14 is 15%, and juxtaposition greater than zero is 27%. The numbers indicate similar groups: 1, DN; 2, EQ; 3, ST; 4, KR; 5, FYW; 6, LIVM.

Figure 1-3

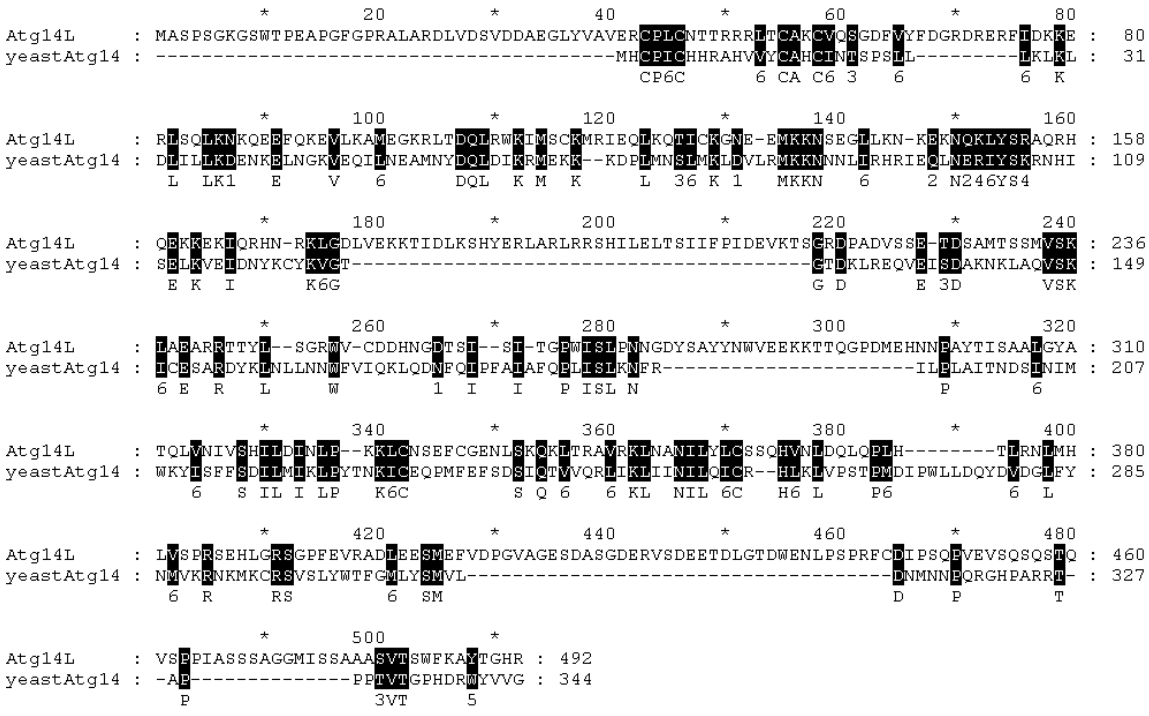
Atg14L : MASPSGKGSWTPEAPGFGPRALARDLVDSVDDAEGLYVAVERCPLCNTTRRRLTCAKCVQSGDFVYFDGRDRERFIDKKE : 80
yeastAtg14 : ----------MHCPICHHRAHVVYCAHCINTSPSLL---------LKLKL : 31
Atg14L : RLSQLKNKQEEFQKEVLKAMEGKRLTDQLRWKIMSCKMRIEQLKQTICKGNE-EMKKNSEGLLKN-KEKNQKLYSRAQRH : 158
yeastAtg14 : DLILLKDENKELNGKVEQILNEAMNYDQLDIKRMEKK--KDPLMNSLMKLDVLRMKKNNNLIRHRIBQLNERIYSKRNHI : 109
Atg14L : QEKKEKIQRHN-RKLGDLVEKKTIDLKSHYERLARLRRSHILELTSIIFPIDEVKTSGRDPADVSSE-TDSAMTSSMVSK : 236
yeastAtg14 : SELKVEIDNYKCYKVGT----------GTDKLREQVEISDAKNKLAQVSK : 149
Atg14L : LAEARRTTYL--SGRWV-CDDHNGDTSI--SI-TGPWISLPNNGDYSAYYNWVEEKKTTQGPDMEHNNPAYTISAALGYA : 310
yeastAtg14 : ICESARDYKLNLLNNWFVIQKLQDNFQLPFALAFQPLISLKNFR----------ILPLAITNDSINIM : 207
Atg14L : TQLVNIVSHIIDINLP--KKLCNSEFCGENLSKQKLTRAVRKLNANILYLCSSQHVNLDQLQPLH--------TLRNIMH : 380
yeastAtg14 : WKYISFFSDIIMIKLEYTNKICEQPMFEFSDSIQTVVQRLIKLIINILQICR--HLKLVPSTPMDIPWLLDQYDVDGIFY : 285
Atg14L : LVSPRSEHLGRSGPFEVRADLEESMEFVDPGVAGESDASGDERVSDEETDLGTDWENLPSPRFCDIPSQPVEVSQSQSTQ : 460
yeastAtg14 : NMVKRNKMKCRSVSLYWTFGMLYSMVL----------DNMNNPQRGHPARRT- : 327
Atg14L : VSPPIASSSAGGMISSAAASVTSWFKAYTGHR : 492
yeastAtg14 : -AP----------PPTVTGPHDRWYVVG : 344

2.4 Confirmation of interaction with immunoprecipitation

To confirm specific interaction between identified proteins and Beclin 1, *in vitro* reverse immunoprecipitation was performed in cultured cells. Atg14L, Rubicon and Nrbf2 were cloned into pEGFP-N3 vector and pCMV-FLAG2 vector, and constructs were transfected into human embryonic kidney (HEK) 293T cells to express C-terminal EGFP-tagged or N-terminal FLAG-tagged proteins. Cell lysates were collected and immunoprecipitations were performed using either anti-GFP or anti-FLAG antibody. Both antibodies pulled down endogenous Beclin 1 as well as tagged proteins (Fig. 2c and 2d). Therefore the interaction between Beclin 1 and the three identified proteins is indeed real and specific, and is not dependent on protein tags. Among these three identified proteins, Atg14L and Rubicon pulled down much more Beclin 1 than Nrbf2, suggesting that Atg14L and Rubicon interact with Beclin 1 much more strongly than Nrbf2. Therefore, we decided to focus our study on Atg14L and Rubicon first.

2.5 Mapping binding domains

Beclin 1 has three domains: Bcl-2-binding domain (BD), coiled-coil domain (CCD) and evolutionary conserved domain (ECD). Bcl-2 binding domain, as the name indicates, is essential for interaction between Beclin 1 and Bcl-2 (Pattingre et al., 2005). The evolutionary conserved domain is important for interaction between Beclin 1 and Vps34/PtdIns3K, while the coiled-coil domain was shown to be mediating direct binding between Beclin 1 and UVRAG (Furuya et al., 2005; Liang et al., 2006). In order to determine which domains within Beclin 1 are mediating its interaction with Atg14L and Rubicon, either single domains of Beclin 1 or two neighboring domains in different

Figure 1-4. Mapping of the binding domains within Beclin 1 that mediate its interaction with Atg14L and Rubicon

(a) Schematic representations of Beclin 1 domain structures and the construction of multiple deletion mutants. All Beclin 1 mutants were tagged with FLAG at N-termini.

(b and c) Domains within Beclin 1 that mediate its binding with Atg14L or Rubicon. HEK293T cells were co-transfected with FLAG-tagged Beclin 1 mutant constructs and GFP-tagged full-length Atg14L (c) or Rubicon (d). The immunoprecipitation was performed with anti-GFP antibody, followed by Western blot with anti-FLAG antibody. The results of these experiments are summarized in a table under panel c and d. "+" or "-" indicated positive or negative interactions between the tested protein domains. These experiments showed that coiled-coil domain of Beclin 1 alone (FlAG-CCD) is sufficient for binding with Atg14L but with evolutionarily conserved domain added (FLAG-CE) the binding became much stronger; only FLAG-CE of Beclin 1, not other Beclin 1 mutants, bound to Rubicon. Abbreviations: B – Bcl2 binding domain, C – Coiled-coil domain, and E – evolutionarily conserved domain.

Figure 1-4

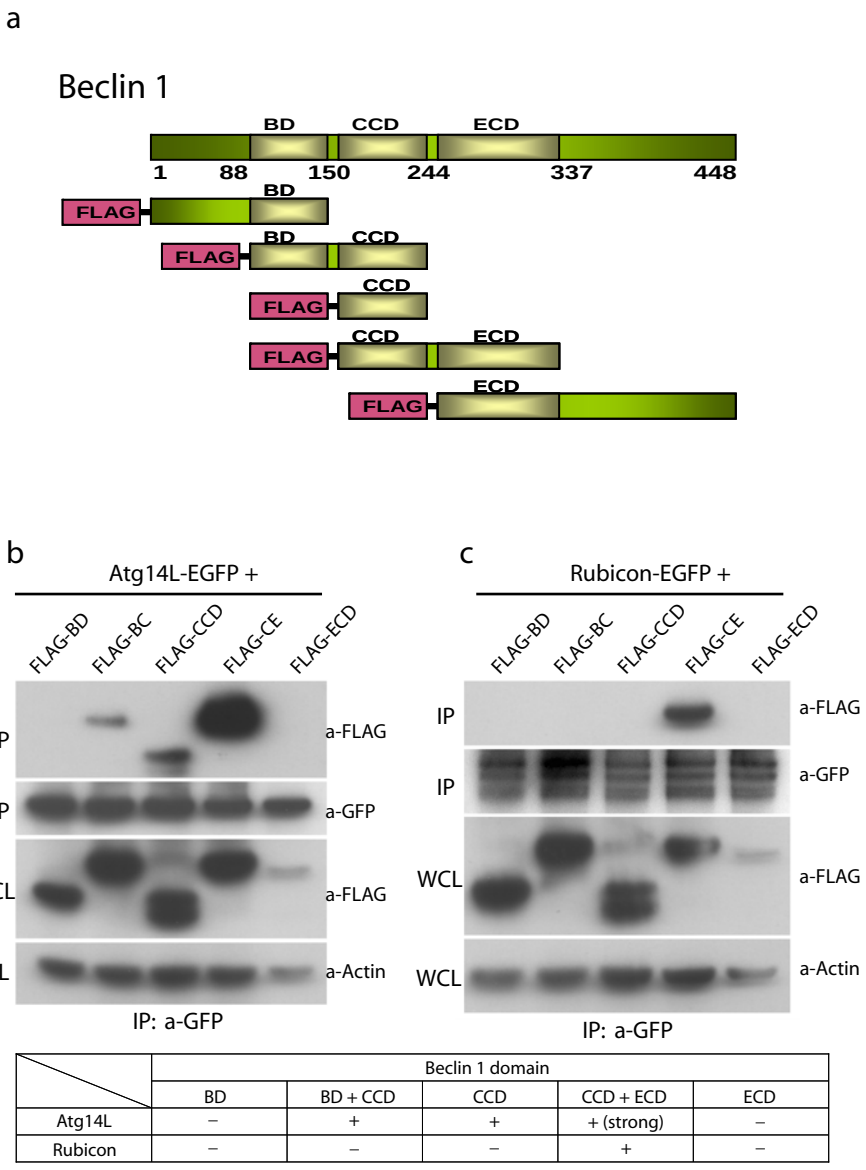

	Beclin 1 domain				
	BD	BD + CCD	CCD	CCD + ECD	ECD
Atg14L	–	+	+	+ (strong)	–
Rubicon	–	–	–	+	–

combinations were cloned into pCMV-FLAG2 vector to generate a series of deletion mutants (Fig. 4a). These mutation constructs were co-transfected into HEK 293T cells with either Atg14L-EGFP or Rubicon-EGFP, and immunoprecipitation was performed using anti-GFP antibody, followed by western blot using anti-FLAG antibody. As a result, Atg14L-EGFP pulled down FLAG-CCD, FLAG-BC (BD and CCD) and FLAG-CE (CCD and ECD), suggesting that CCD of Beclin 1 alone is sufficient for its interaction with Atg14L. Interestingly, the amount of immunoprecipitated FLAG-CE was significantly higher than that of FLAG-CCD, while the amount of immunoprecipitated FLAG-BC was comparable to that of FLAG-CCD, suggesting that ECD of Beclin 1 is not essential for but greatly enhances its interaction with Atg14L (Fig. 4b). Meanwhile, Rubicon-EGFP pulled down only FLAG-CE, but not any other deletion mutant of Beclin 1, suggesting that CCD and ECD of Beclin 1 are both required for its interaction with Rubicon (Fig. 4c).

A similar strategy was used to determine the domains within Atg14L and Rubicon that mediate their binding to Beclin 1. A series of deletion mutants of Atg14L and Rubicon were generated and transfected into HEK293T cells to test their ability to pull down endogenous Beclin 1 and Vps34/PtdIns3K proteins (Fig. 5a). Atg14L-EGFP with the first coiled-coil domain deleted pulled down smaller amount of endogenous Beclin 1 than full length Atg14L-EGFP, and when both coiled-coil domains were deleted, no endogenous Beclin 1 was detectable from immunoprecipitation. This result suggested that both coiled-coil domains within Atg14L are important for it to maintain sufficient interaction with Beclin 1. Likewise, Atg14L without coiled-coil domains was not able to pull down Vps34/PtdIns3K either (Fig. 5b).

Figure 1-5. Mapping domains within Atg14L and Rubicon that are required for their interaction with Beclin 1

(a) Schematic representations of Atg14L and Rubicon domain structures and the construction of multiple deletion mutants. All Atg14L and Rubicon mutants were tagged with EGFP at C-termini.

(b and c) Domains within Atg14L or Rubicon that are required for their binding with Beclin 1. HEK293T cells were transfected with EGFP-tagged Atg14L (b) or Rubicon (c) mutant constructs. The immunoprecipitation was performed with anti-GFP antibody, followed by Western blot analyses of endogenous Beclin 1 and Vps34/PtdIns3K with anti-Beclin 1 and Vps34/PtdIns3K antibodies. The results of these experiments are summarized in a table at bottom of panel b and c. "+" or "-" indicated positive or negative interactions between the tested protein domains. These experiments showed that both CCD1 and CCD2 of Atg14L are important for its binding to Beclin 1. Meanwhile, neither RUN nor Cys-rich domain of Rubicon is required for its binding to Beclin 1. Thus, central region containing CCD is important for the binding. In addition, Rubicon mutants lacking RUN, Cys-rich domain or both domains have increased binding to Beclin1. Abbreviations: RUN – RUN domain, Cys– cysteine-rich domain.

Figure 1-5

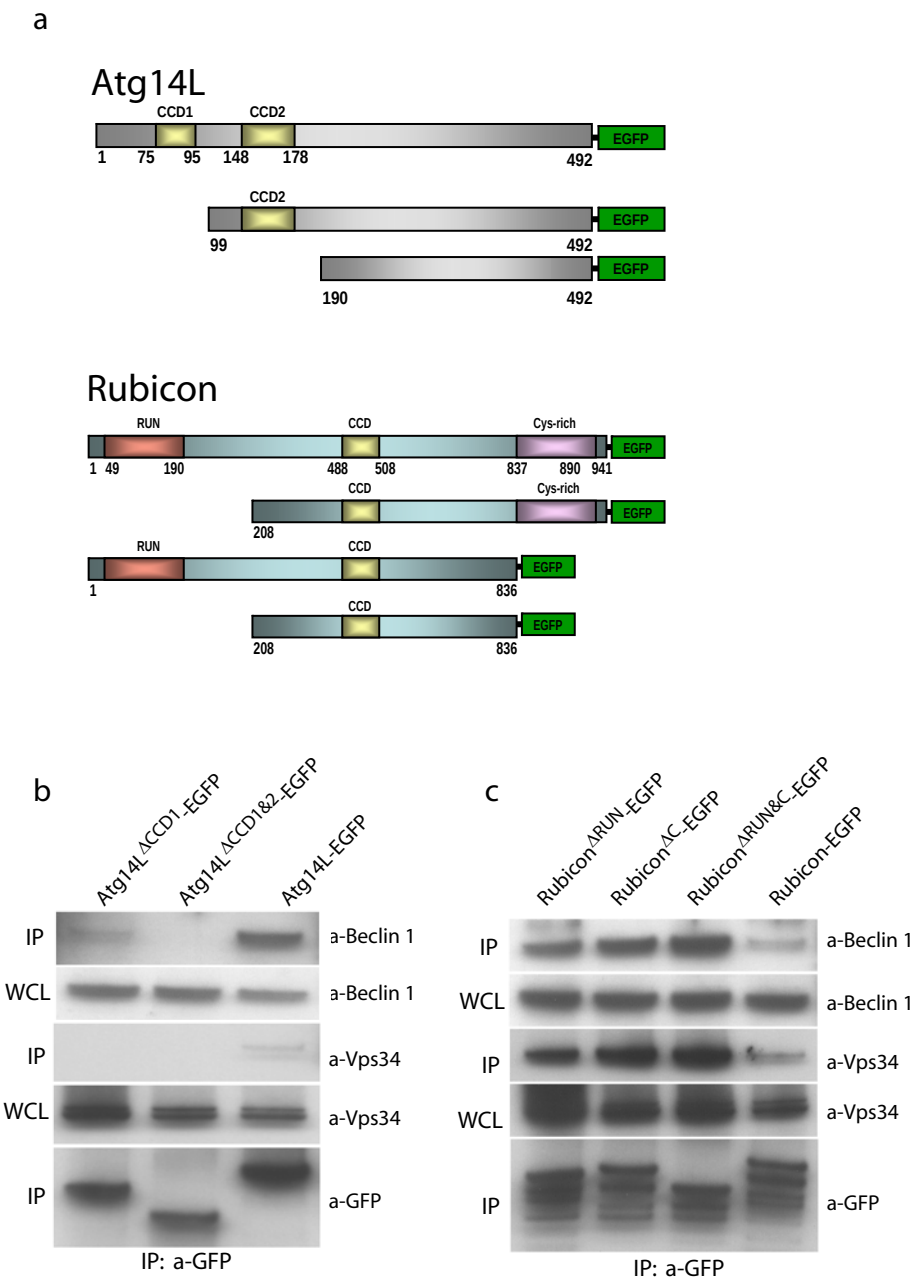

	Atg14L			Rubicon			
	DCCD1	DCCD2	full length	DRUN	DFYVE	DRUN&C	full length
Beclin 1	+	–	++	++	++	++	+

Interestingly, when either RUN domain or cysteine-rich domain was deleted from Rubicon-EGFP, larger amount of endogenous Beclin 1 was immunoprecipitated, and Rubicon-EGFP with both domains simultaneously deleted pulled down the largest amount of Beclin 1. It is therefore suggested that RUN domain and cysteine-rich domain are not only unnecessary but also somehow inhibitory for the interaction between Rubicon and Beclin 1, and that the interaction with Beclin 1 is probably mediated by the coiled-coil domain in the central region of Rubicon. The same pattern was observed for interaction between Rubicon and Vps34//PtdIns3K (Fig. 5c).

2.6 Identification of Beclin 1-containing protein complexes

In yeast, Atg6p/Vps30p forms two distinctive protein complexes. One contains Atg14p and is essential for autophagy induction, and the other contains Vps38p and functions in vacuolar protein carboxypeptidase Y (CPY) sorting pathway (Kihara et al., 2001b). However in mammalian cells it is still unknown whether there are multiple Beclin 1 complexes and what are the components of the complex(es). The *in vivo* immunoprecipitation in this study identified at least six Beclin 1 interaction proteins, and it is an interesting question how many protein complexes these proteins can form. To answer this question, immunoprecipitation was first performed in NIH/3T3 mouse fibroblast cells using anti-Atg14L and anti-Rubicon antibodies. As a result, anti-Atg14L antibody pulled down Beclin 1 and Vps34/PtdIns3K, but not Rubicon or UVRAG, while anti-Rubicon antibody pulled down Beclin 1 and Vps34/PtdIns3K as well as UVRAG, but not Atg14L (Fig. 6a). This suggested that like yeast there may also be distinctive multiple Beclin 1 complexes in mammalian cells as well, that Atg14L and Rubicon may

Figure 1-6. Analysis of protein interactions among endogenous proteins in NIH/3T3 cells and HEK293 cells stably expressing Atg14L-EGFP or Rubicon-EGFP

(a) Immunoprecipitation of endogenous proteins that interact with Atg14L and Rubicon using anti-Atg14L and anti-Rubicon antibodies from NIH/3T3 cell lysate. The control experiments were preformed using the corresponding pre-immune serum for each antibody. The whole cell lysate (WCL) and immunoprecipitated samples (IP) were examined by western blot using antibodies against UVRAG, Vps34/PtdIns3K, Atg14L and Rubicon.

(b) Immunoprecipitation of endogenous proteins that interact with Atg14L and Rubicon using anti-GFP antibodies from HEK293 cells stably expressing Atg14L-EGFP or Rubicon-EGFP. The whole cell lysate (WCL) and immunoprecipitated samples (IP) were examined by western blot with antibodies against UVRAG, GFP, Vps34//PtdIns3K and Beclin 1. Atg14L-EGFP co-immunoprecipitated with Vps34 and Beclin 1; Rubicon-EGFP co-immunoprecipitated with Vps34, Beclin 1 and UVRAG.

Figure 1-6

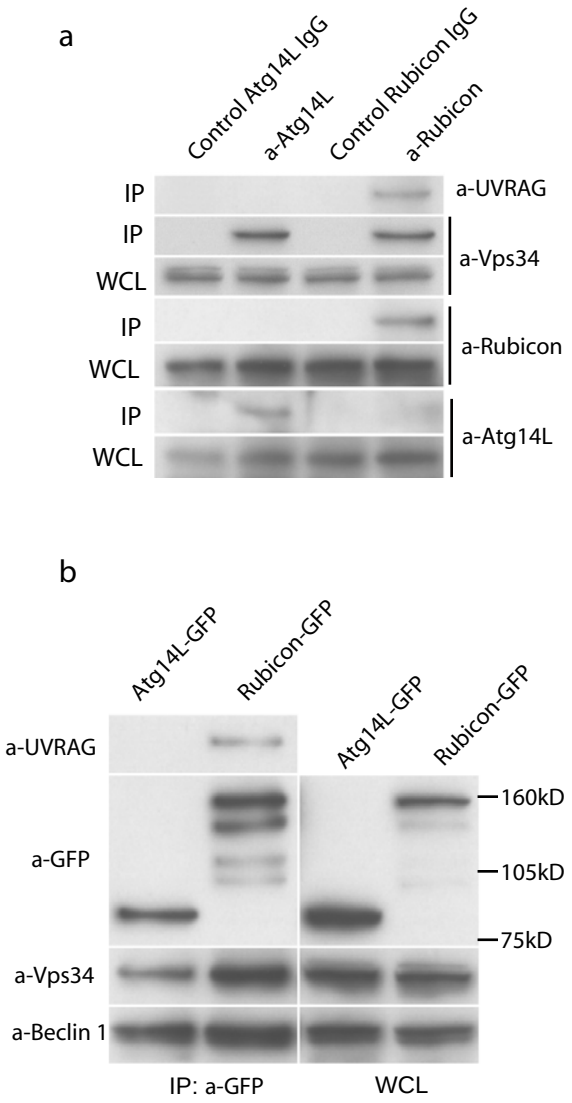
a
Control Atg14L IgG
a-Atg14L
Control Rubicon IgG
a-Rubicon
IP
a-UVRAG
IP
WCL
a-Vps34
IP
WCL
a-Rubicon
IP
WCL
a-Atg14L
b
Atg14L-GFP
Rubicon-GFP
Atg14L-GFP
Rubicon-GFP
a-UVRAG
a-GFP
160kD
105kD
75kD
a-Vps34
a-Beclin 1
IP: a-GFP
WCL

exist in separate Beclin 1-containing protein complexes, and that UVRAG may be in the same complex with Rubicon but not with Atg14L. Consistent with this idea, immunoprecipitation with anti-GFP antibody performed in HEK293 cells stably expressing either Atg14L-EGFP or Rubicon-EGFP showed that only Rubicon-EGFP pulled down UVRAG although they both pulled down endogenous Beclin 1 and Vps34/PtdIns3K (Fig. 6b).

To further characterize the composition of possible Beclin 1 protein complexes *in vivo*, size exclusion chromatography (gel filtration) was performed. In this technique protein complexes are separated according to their sizes (uisng mild condition). Wild-type or "rescued" mouse livers were homogenized and soluble cytosolic protein extract was prepared with centrifugation, after which the extract was run through a column. Eighty fractions were collected and analyzed by western blot using anti-Atg14L, anti-Rubicon, anti-Vps34/PtdIns3K, anti-Beclin 1 and anti-UVRAG antibodies. From both wild-type and "rescued" mice, Vps34/PtdIns3K and Beclin 1 proteins were detected in similar fractions and their levels peaked in the same fractions of 39-40 (Beclin 1-GFP in "rescued" mice). Interestingly, Atg14L and Rubicon levels also showed similar distribution among all fractions and the strongest signals in the similar fractions (Figs. 7a & 7b), suggesting that these fractions contain a major Beclin 1-Vps34/PtdIns3K complex that may include both Atg14L and Rubicon proteins. From protein size markers, it was estimated that the size of this protein complex was over 700 kD.

Figure 1-7. Analysis of protein composition in the Beclin 1 complex(es)

(a) Western blot analyses of Beclin 1, Vps34, Atg14L and Rubicon in the gel filtration fractions from wild type mouse liver extract. The peak levels of each protein were found co-eluded in the same fractions (39-40). Atg14L was also found eluted at the second peak levels in later fractions (53-54). The cell lysate of FLAG-Atg14L-transfected HEK 293T was loaded as a positive control (labeled with "1") for the migration position of the Atg14L protein. The adjacent lane (labeled with "2) was loaded with cell lysates without transfection.

(b) Western blot analyses of Beclin 1, Vps34, Atg14L and Rubicon in the gel filtration fractions from the "rescued" mice liver samples. The liver lysate was prepared from "rescued" mice *beclin 1* $^{-/-}$*; beclin 1-GFP and* applied in gel filtration experiment. Western blot analyses of Beclin 1, Vps34, Atg14L and Rubicon in the gel filtration fractions is shown. The peak levels of each protein were found co-eluded in the same fractions (~41-43). Atg14L was also found eluted at the second peak levels in later fractions (53-55). These results are consistent with the observation using wild-type mice (a).

Figure 1-7

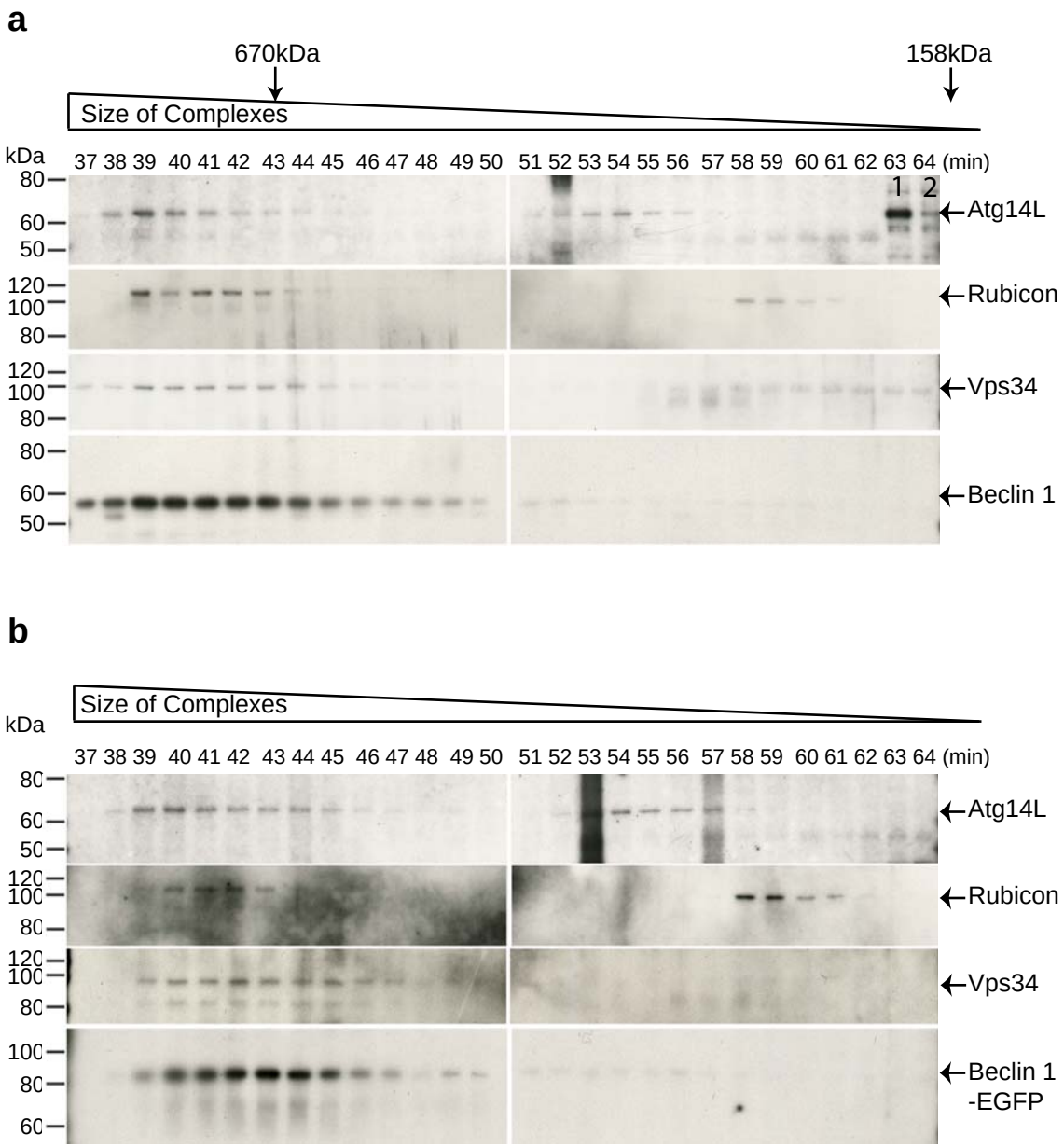
a
670kDa
158kDa
Size of Complexes
kDa
37 38 39 40 41 42 43 44 45 46 47 48 49 50 51 52 53 54 55 56 57 58 59 60 61 62 63 64 (min)
1 2
Atg14L
Rubicon
Vps34
Beclin 1
b
Size of Complexes
kDa
37 38 39 40 41 42 43 44 45 46 47 48 49 50 51 52 53 54 55 56 57 58 59 60 61 62 63 64 (min)
Atg14L
Rubicon
Vps34
Beclin 1
-EGFP

To validate the protein detection by anti-Atg14L or anti-Rubicon antibodies in the above study, the same experiment was repeated using cell lysate from HEK293 cells stably expressing either Atg14L-EGFP or Rubicon-EGFP, followed by western blot analyses with anti-GFP and anti-Beclin 1 antibodies (Fig. 8). The results from the Atg14L-EGFP stable cell lysate again showed that the fractions containing peak levels of Beclin 1 overlapped with that of Atg14L-EGFP (both peak fractions eluted at 39-40; Fig. 8), confirming the results using anti-Atg14L antibody for detecting endogenous proteins in the liver (Fig. 7). Interestingly, the samples prepared from starved Atg14L-EGFP stable cells showed no difference in the distribution pattern for Atg14L or Beclin 1 as compared to that from non-starved cells (Fig. 8), suggesting that starvation does not increase or decrease the binding between Atg14L and Beclin 1. Similar studies using lysate from Rubicon-EGFP stable cells also confirmed the results using anti-Rubicon antibodies for detecting endogenous Rubicon protein in mouse liver, and starvation did not change the interaction between Rubicon and Beclin 1 (Fig. 8).

Western blot was also performed on liver and cell lysate fractions with UVRAG antibody. However, no clear signal was detected. The possible reason may be the quality of the anti-UVRAG antibody used, or that the binding of UVRAG in the whole protein complex is not stable or strong enough to endure the experimental procedures of gel filtration, and therefore UVRAG may have eluted as single molecules in late fractions that were not collected.

In conclusion, gel filtration experiments showed that there is one major *in vivo* Beclin 1-containing protein complex that contains both Atg14L and Rubicon, and that Atg14L may exist in another smaller complex as well.

Figure 1-8. Gel filtration analyses of protein distribution using stably transfected cells

(a) Western blot analyses of Atg14L-EGFP and Beclin 1 in the gel filtration fractions of non-starved (left panel) and starved (for 2h, right panel) using Atg14L-EGFP HEK293 stable cell lysate. Atg14L-EGFP (recognized by anti-GFP antibody as a ca. 85 kDa band) and Beclin 1 co-eluted in fractions around 39-40, supporting the specificity of the anti-Atg14L antibody (Fig. 7a&b). No change in the elution pattern was detected after the cells were starved for 2h.

(b) Western blot analyses of Rubicon-EGFP and Beclin 1 in the gel filtration fractions of non-starved (left panel) and starved (for 2h, right panel) using Rubicon-EGFP HEK293 stable cell lysate. Rubicon-EGFP and Beclin 1 co-eluted in many fractions, supporting the specificity of the anti-Rubicon antibody (Fig. 7a&b). No change in the elution pattern was detected after the cells were starved for 2h.

Figure 1-8

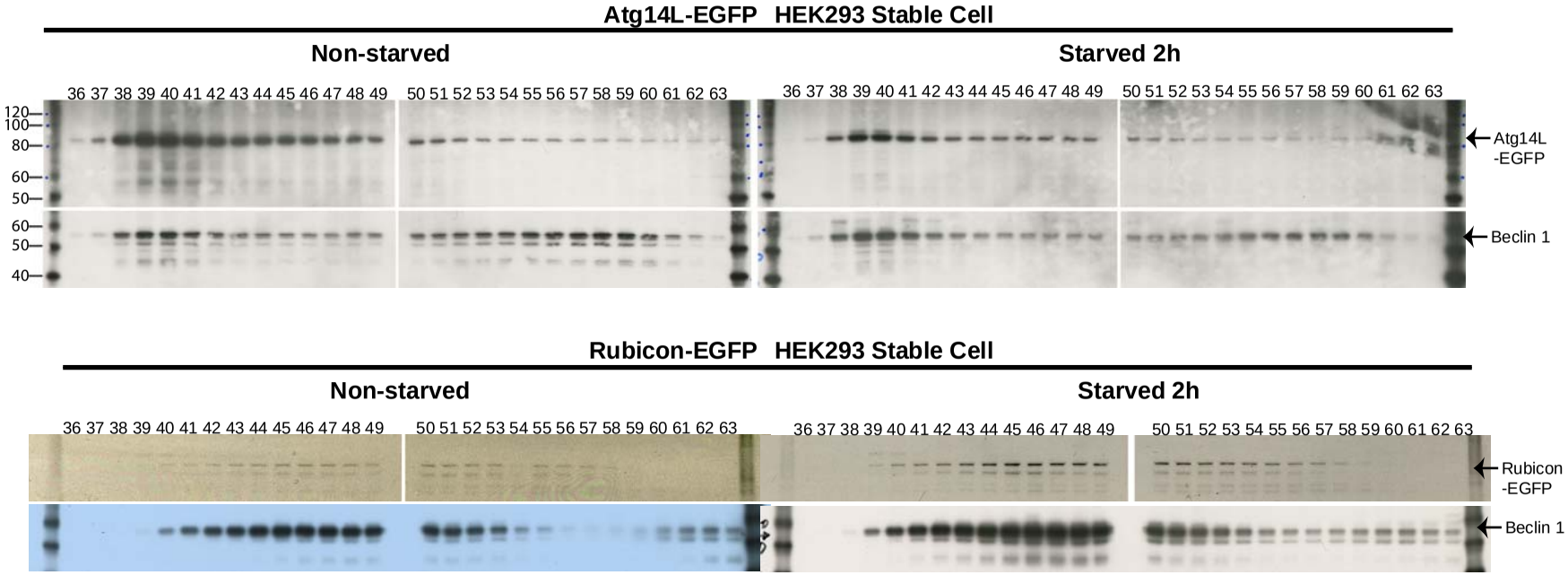
Atg14L-EGFP HEK293 Stable Cell
Non-starved
Starved 2h
36 37 38 39 40 41 42 43 44 45 46 47 48 49
50 51 52 53 54 55 56 57 58 59 60 61 62 63
120
100
80
60
50
60
50
40
Atg14L -EGFP
Beclin 1
Rubicon-EGFP HEK293 Stable Cell
Non-starved
Starved 2h
Rubicon -EGFP
Beclin 1

2.7 Co-immunoprecipitation

In order to confirm the results from gel filtration that Atg14L and Rubicon are able to co-exist in the same protein complex, tagged proteins were expressed in cultured HEK293T cells and co-immunoprecipitation with anti-GFP antibody was performed. As a result, Atg14L-EGFP was able to pull down FLAG-Rubicon (Fig. 9a), and Rubicon-EGFP pulled down FLAG-Atg14L as well (Fig. 9b). In both cases, Atg14L-EGFP and Rubicon-EGFP were able to pull down endogenous Beclin 1, indicating that Beclin 1 was also in the protein complex. Since gel filtration results did not indicate binding of UVRAG in the protein complex, co-immunoprecipitation was performed in HEK293T cells to study the binding between UVRAG-EGFP and FLAG-Atg14L or FLAG-Rubicon. With anti-GFP antibody, UVRAG-EGFP pulled down both FLAG-Atg14L and FLAG-Rubicon, as well as endogenous Beclin 1 and Vps34/PtdIns3K, indicating that UVRAG can also be in the same protein complex (Fig. 9c).

2.8 Binding inter-relations

When multiple proteins form a protein complex, they may affect the binding affinity of each other in either positive way, in which case a certain protein may increase the binding between other proteins, or in negative way, in which case a certain protein may inhibit the binding between other proteins. In order to study whether such interactions exist among the proteins of Beclin 1-Vps34/PtdIns3K complex, co-transfection of tagged proteins and co-immunoprecipitation was performed.

Figure 1-9. Protein interactions among Beclin 1, ATG14L, Rubicon and UVRAG assayed in transiently transfected cells

(a-b) Co-immunoprecipitation experiments showing protein-protein interaction between Atg14L and Rubicon. HEK293T cells were co-transfected with EGFP-tagged Atg14L and FLAG-tagged Rubicon (a), or EGFP-tagged Rubicon and FLAG-tagged Atg14L (b). Cell lysate was used for immunoprecipitation with anti-GFP antibody, followed by western blot with anti-FLAG antibody. EGFP-tagged Atg14L was able to pull down FLAG-tagged Rubicon (a), and vice versa (b). WCL: whole cell lysate; IP: immunoprecipirated.

(c) Protein interaction between co-expressed UVRAG and Atg14L/Rubicon. HEK293T cells were co-transfected with UVRAG-EGFP and FLAG-Atg14L or FLAG-Rubicon. Immunoprecipitation was performed with anti-GFP antibody, followed by detection with anti-FLAG antibody. The result shows that both FLAG-Atg14L and FLAG-Rubicon was co-immunoprecipitated with UVRAG-EGFP.

Figure 1-9

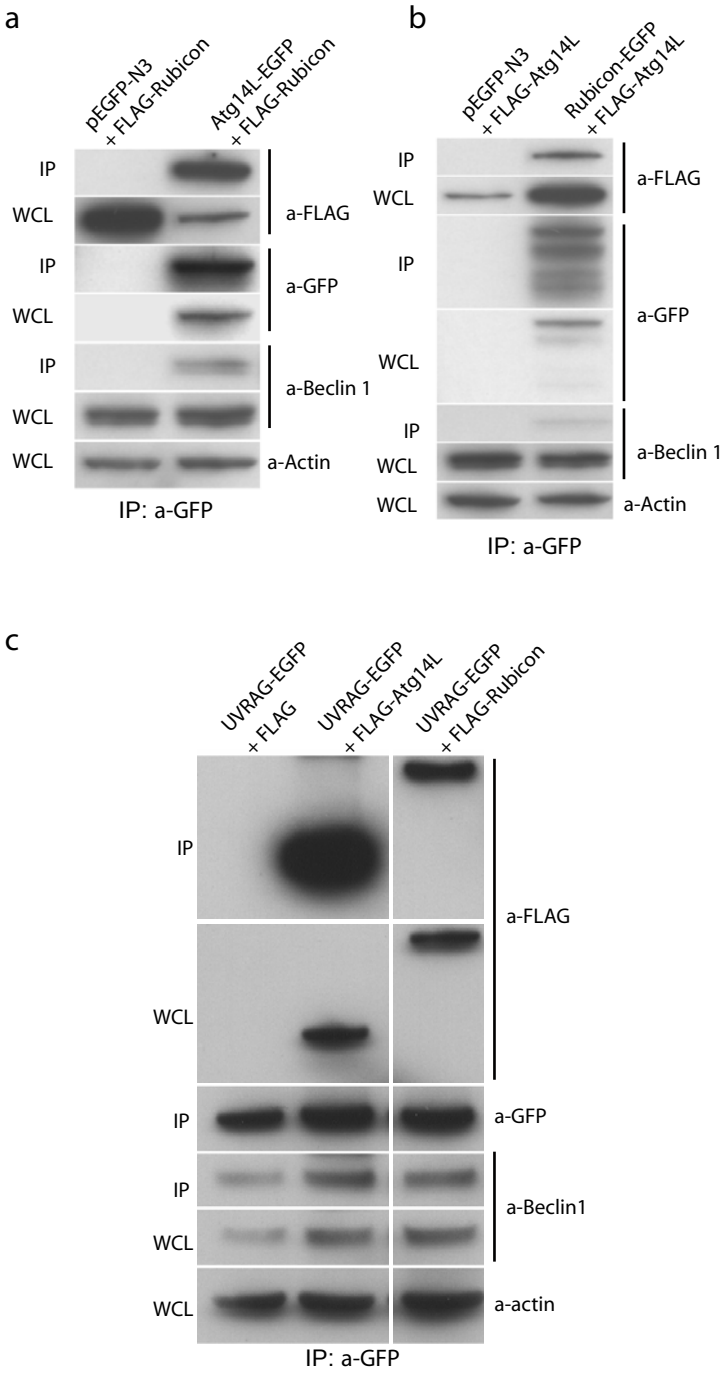
a
pEGFP-N3 + FLAG-Rubicon
Atg14L-EGFP + FLAG-Rubicon
IP
WCL
a-FLAG
a-GFP
a-Beclin 1
a-Actin
IP: a-GFP
b
pEGFP-N3 + FLAG-Atg14L
Rubicon-EGFP + FLAG-Atg14L
IP: a-GFP
c
UVRAG-EGFP + FLAG
UVRAG-EGFP + FLAG-Atg14L
UVRAG-EGFP + FLAG-Rubicon
a-Beclin1
a-actin

2.8.1 Atg14L increases, and Rubicon reduces, interaction between Beclin 1 and Vps34/PtdIns3K

Previous study showed that in mammalian cells, almost all Beclin 1 protein forms complexes with Vps34/PtdIns3K while not all Vps34/PtdIns3K is interacting with Beclin 1 (Kihara et al., 2001a). In order to study if the presence of Atg14L or Rubicon affects the interaction between Beclin 1 and Vps34/PtdIns3K, two sets of co-transfection experiments were performed. In the first set, Beclin 1-EGFP was co-transfected into HEK293T cells with empty pCMV-FLAG vector, FLAG-tagged Atg14L or FLAG-tagged Rubicon, followed by immunoprecipitation using anti-GFP antibody. The level of endogenous Vps34/PtdIns3K protein that was immunoprecipitated with the anti-GFP antibody was detected with western blot and compared. In the second set, Myc-tagged Vps34/PtdIns3K was co-transfected into HEK293T cells with empty pCMV-FLAG vector, FLAG-tagged Atg14L or FLAG-tagged Rubicon, followed by immunoprecipitation using anti-Myc antibody. And the level of endogenous Beclin 1 protein that was immunoprecipitated was detected and compared. In the first set, compared to empty vector control, FLAG-Rubicon significantly reduced the level of Vps34/PtdIns3K that was pulled down with Beclin 1-EGFP while FLAG-Atg14L did not show significant effect (Fig. 10a). Meanwhile in the second set, when empty vector was co-transfected Myc-Vps34/PtdIns3K was only able to pull down extremely small amount of endogenous Beclin 1, probably due to the low efficiency of immunoprecipitation with anti-Myc antibody. However when FLAG-Atg14L was co-transfected, an increased amount of endogenous Beclin 1 was pulled down. And with co-transfection of FLAG-Rubicon, the amount of Beclin 1 pulled down was too small to assess the effect of

Figure 1-10. Binding inter-relationship among Beclin 1 interaction proteins

(a) Co-immunoprecipitation of endogenous Vps34/PtdIns3K with Beclin 1-EGFP in the presence of over-expressed FLAG-Atg14L or FLAG-Rubicon. Beclin 1-EGFP was co-expressed with FLAG-Atg14L, FLAG-Rubicon or control FLAG vector in HEK 293T cells. Immunoprecipitation was performed with anti-GFP antibody, followed by western blot with anti-Vps34 antibody to detect endogenous Vps34/PtdIns3K. Notably, over-expression of FLAG-Rubicon, but not FLAG-Atg14L, repressed the amount of endogenous Vps34/PtdIns3K that interacted with Beclin 1-EGFP.

(b) Co-immunoprecipitation of endogenous Beclin 1 with Myc-Vps34/PtdIns3K in the presence of over-expressed FLAG-Atg14L or FLAG-Rubicon. Immunoprecipitation was performed with anti-Myc antibody, followed by Western blot with anti-Beclin 1 antibody to detect Endogenous Beclin 1. Over-expression of FLAG-Atg14L increased the amount of endogenous Beclin 1 that interacted with Myc-Vps34/PtdIns3K.

(c) Co-immunoprecipitation of Beclin 1 and Vps34/PtdIns3K with Atg14L-EGFP or Rubicon-EGFP. Atg14L-EGFP or Rubicon-EGFP was co-expressed with Myc-Vps34/PtdIns3K, either with or without Beclin 1-AsRed in HEK293T cells. Immunoprecipitation was performed using anti-GFP antibody followed by blotting with anti-Vps34/PtdIns3K and anti-Beclin 1 antibodies. Over-expression of Beclin 1-AsRed increased the binding between Atg14L-EGFP and Myc-Vps34/PtdIns3K

(d-e) Effect of Beclin 1 over-expression on protein interaction between co-expressed UVRAG and Atg14L/Rubicon. UVRAG-EGFP was co-expressed with either FLAG-Atg14L or FLAG-Rubicon in HEK 293T cells, in the absence or in the presence of Beclin 1-Myc. Immunoprecipitation was performed with anti-GFP antibody, followed by detection with anti-FLAG and anti-Myc antibodies. The results show that Beclin 1 over-expression markedly increased the amount of FLAG-Rubicon that was co-immunoprecipitated with UVRAG-EGFP (e) while having little effect on interaction between FLAG-Atg14L and UVRAG-EGFP (d).

For (a-e), WCL: whole cell lysate; IP: immunoprecipirated.

Figure 1-10

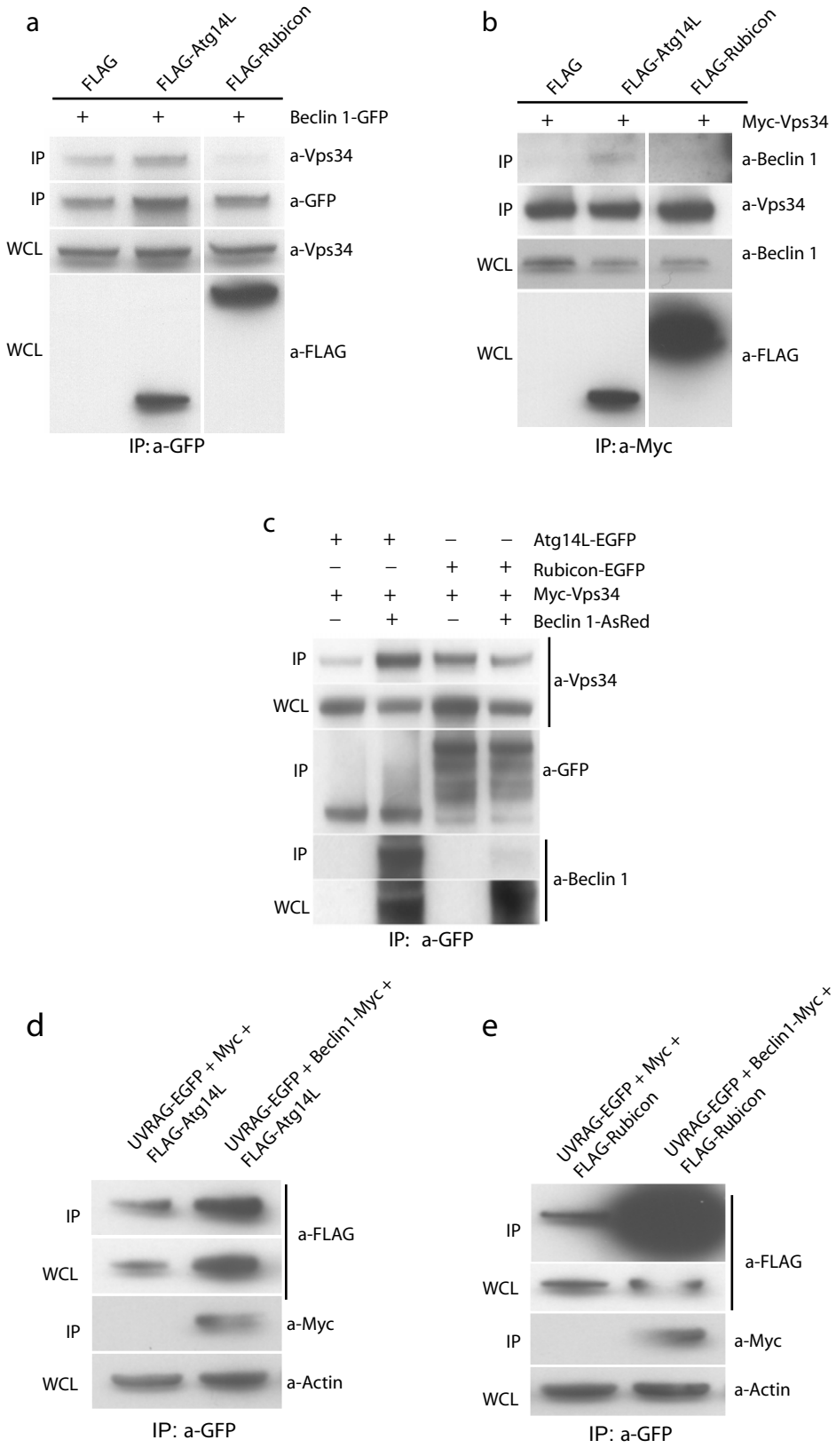
a
FLAG
FLAG-Atg14L
FLAG-Rubicon
+ + + Beclin 1-GFP
IP a-Vps34
IP a-GFP
WCL a-Vps34
WCL a-FLAG
IP: a-GFP
b
FLAG
FLAG-Atg14L
FLAG-Rubicon
+ + + Myc-Vps34
IP a-Beclin 1
IP a-Vps34
WCL a-Beclin 1
WCL a-FLAG
IP: a-Myc
c
+ + – – Atg14L-EGFP
– – + + Rubicon-EGFP
+ + + + Myc-Vps34
– + – + Beclin 1-AsRed
IP a-Vps34
WCL
IP a-GFP
IP a-Beclin 1
WCL
IP: a-GFP
d
UVRAG-EGFP + Myc + FLAG-Atg14L
UVRAG-EGFP + Beclin1-Myc + FLAG-Atg14L
IP a-FLAG
WCL
IP a-Myc
WCL a-Actin
IP: a-GFP
e
UVRAG-EGFP + Myc + FLAG-Rubicon
UVRAG-EGFP + Beclin1-Myc + FLAG-Rubicon
IP a-FLAG
WCL
IP a-Myc
WCL a-Actin
IP: a-GFP

Rubicon (Fig. 10b). The results from these two sets of co-immunoprecipitation experiments suggested that Atg14L increased while Rubicon reduced the interaction between Beclin 1 and Vps34/PtdIns3K.

2.8.2 Effect of Beclin 1 on interaction between Atg14L/Rubicon and Vps34/PtdIns3K

As a component of the Vps34/PtdIns3K complex, Beclin 1 may as well affect binding of other protein components to the Vps34/PtdIns3K. Therefore co-transfection and immunoprecipitation experiments were performed to test the effect of Beclin 1 on interaction between Atg14L or Rubicon and Vps34/PtdIns3K. For this purpose, triple transfection was performed using Atg14L-EGFP/Rubicon-EGFP, Myc-Vps34/PtdIns3K and either empty pAsRed2-N1 vector or Beclin 1-AsRed. Immuno-precipitation was performed with anti-GFP antibody, and the level of Myc-Vps34/PtdIns3K that was pulled down was detected with Vps34 antibody and compared between the conditions of empty vector co-trasfection and Beclin 1-AsRed co-transfection. As a result, the presence of Beclin 1-AsRed greatly increased the amount of Myc-Vps34/PtdIns3K that was pulled down with Atg14L-EGFP yet had no significant effect on that pulled down with Rubicon-EGFP. This suggested that Beclin 1 increased the interaction between Atg14L and Vps34/PtdIns3K but did not affect the interaction between Rubicon and Vps34/PtdIns3K.

Taken together, the co-immunoprecipitation experiments showed that Beclin 1 and Atg14L increase each other's interaction with Vps34/PtdIns3K, and that Rubicon inhibits the interaction between Beclin 1 and Vps34/PtdIns3K.

2.8.3 Effect of Beclin 1 on interaction between Atg14L/Rubicon and UVRAG

Immunoprecipitation with Atg14L or Rubicon antibodies from NIH/3T3 cells or with GFP antibody from HEK293 cells stably expressing Atg14L-EGFP or Rubicon-EGFP showed that Rubicon has strong interaction with UVRAG but Atg14L does not (Fig. 6a and 6b). Meanwhile, immunoprecipitation from transiently transfected cells showed that UVRAG could be in the same complex with both Atg14L and Rubicon. In order to study how their interaction is related to Beclin 1, triple transfection was performed in which UVRAG-EGFP, FLAG-Atg14L or FLAG-Rubicon, and either control empty vector or Beclin 1-Myc were co-transfected into HEK293T cells. Immunoprecipitation was performed with anti-GFP antibody, followed by western blot with anti-FLAG and anti-Myc antibodies. The results showed that the amount of FLAG-Rubicon that immunoprecipitated with UVRAG-EGFP increased dramatically when Beclin 1 was co-transfected, indicating that Beclin1 significantly increased binding between UVRAG and Rubicon (Fig. 10e). However Beclin 1 co-transfection had no effect on the interaction between UVRAG-EGFP and FLAG-Atg14L (Fig. 10d).

2.9 Functional assays of Atg14L

2.9.1 Atg14L positively regulates autophagy

Beclin 1 forms a protein complex with Vps34/PtdIns3K and regulates the level of autophagy in mammalian cells. In order to study the function of the novel protein Atg14L, its effect on autophagy levels was first studied. RNA interference (RNAi) was used to suppress the expression of endogenous *Atg14L* gene and knock down the protein level of Atg14L in NIH/3T3 cells. First, LC3 protein levels from the cell lysate were examined

after siRNA transfection. LC3 is the mammalian ortholog of Atg8, and undergoes modification from LC3 I form that is localized in the cytosol to LC3 II form that is bound to the autophagosome membrane. Anti-LC3 antibody detects both forms, and the ratio between the cytosolic I form and the membrane bound II form is correlated with the number of autophagosome and therefore the autophagy level in the cells. Compared to control siRNA, Atg14L siRNA transfection greatly increased the LC3 II form level, indicating that autophagy level was changed (Fig. 11a). However, the increase in LC3 II form level can be either from an increase of autophagosome formation, which means an increase of autophagy level, or from a decrease of lysosomal degradation of autophagosomes, which means a decrease of autophagy level. Interestingly, transfection of Beclin 1 siRNA also induced a significant increase of LC3 II level that is comparable to that induced by Atg14L siRNA transfection. Beclin 1 functions in autophagy induction and deletion of Beclin 1 inhibits autophagy. The similar changes in LC3 II form levels that Atg14L siRNA and Beclin 1 siRNA induced suggested that Atg14L is related to autophagy regulation and that it may function in the same direction as Beclin 1. To confirm the function of Atg14L on autophagy regulation, the level of another autophagy related protein, p62/SQSTM1 was examined. P62/SQSTM1 was identified as a LC3 interaction protein and is degraded by autophagy (Komatsu et al., 2007b; Pankiv et al., 2007). Therefore the p62/SQSTM1 protein level can be used as a more reliable marker for autophagy level. Western blot with anti-p62/SQSTM1 antibody showed that transfection of both Atg14L and Beclin 1 siRNA significantly increased the p62/SQSTM1 protein level compared to control siRNA. This result confirmed that like Beclin 1, knockdown of Atg14L protein resulted in accumulation of p62/SQSTM1,

Figure 1-11. **Atg14L functions in positive regulation of autophagy**

(a) Beclin 1 or Atg14L RNAi knock-down in the NIH/3T3 cells led to increased levels of p62/SQSTM1 and LC3 II form as detected with anti-p62/SQSTM1 and LC3 antibodies under both normal (left panel) and nutrient-starvation conditions (right panel). Notably, Beclin 1 RNAi knock-down markedly reduced levels of Atg14L expression. β-actin was blotted as the loading control.

(b) Confocal images of MLE12 cells stably expressing GFP-LC3 showed that Atg14L RNAi knock-down resulted in markedly increased number of large size GFP-LC3 puncta, as compared to the control RNAi treatment. Scale bar, 10 μm.

(c-d) Confocal images of MLE12 cells stably expressing GFP-LC3 showed that Atg14L-RNAi-induced large-size GFP-LC3 puncta (in green) colocalized with p62/SQSTM1 (c, in red) and ubiquitin (d, in red). Scale bar, 10 μm.

(e) Atg14L siRNA, as compared to control siRNA, decreased long-lived protein degradation in NIH/3T3 cells under both normal (p=0.007) and starvation (p=5E-6) conditions (asterisks, one-tailed Student's t-test with equal variances, n = 4). This difference was diminished when the starved cells were treated with 3-methyladenine (3MA), a PI-3K inhibitor.

Figure 1-11

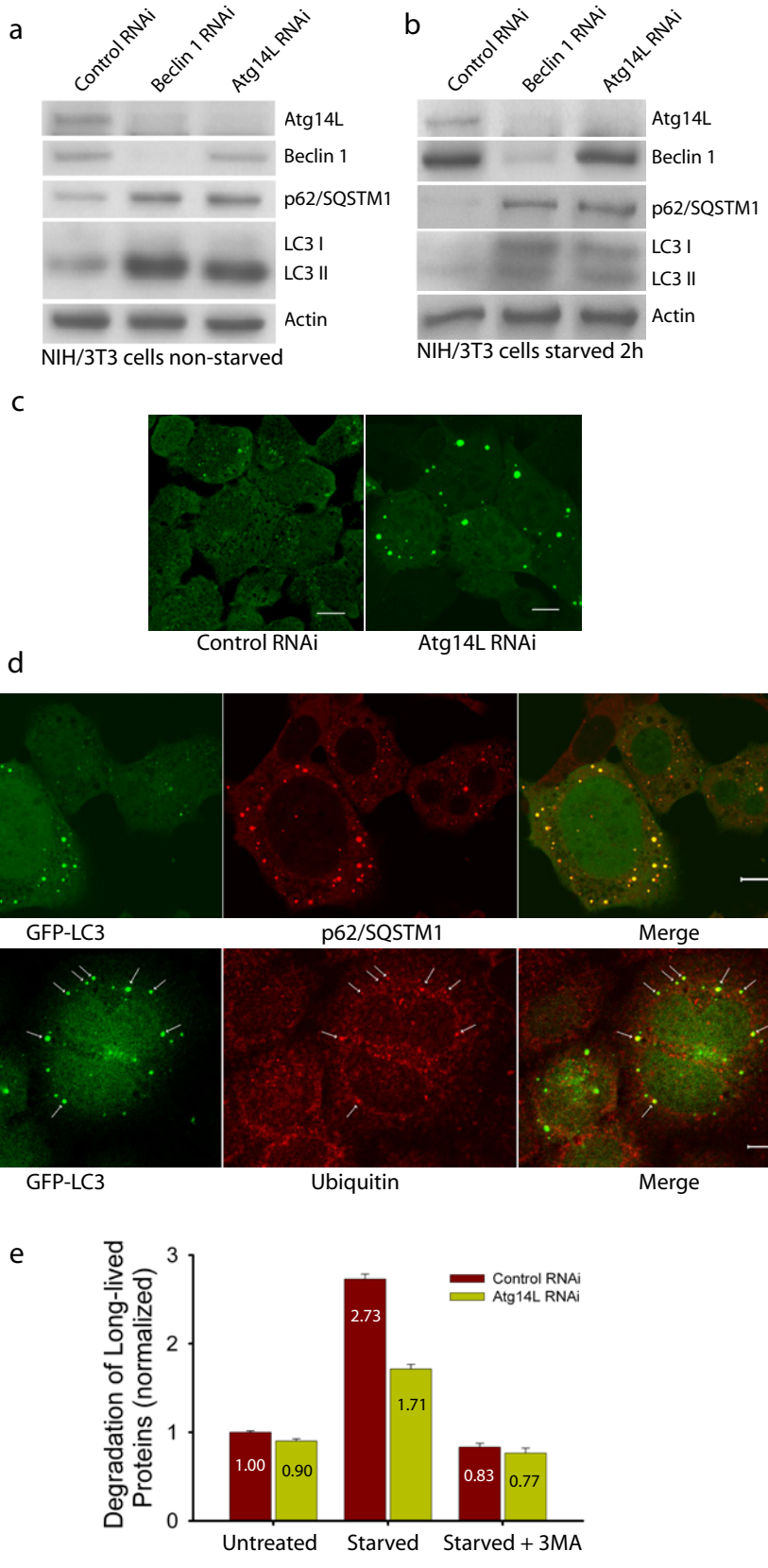
a
Control RNAi
Beclin 1 RNAi
Atg14L RNAi
Atg14L
Beclin 1
p62/SQSTM1
LC3 I
LC3 II
Actin
NIH/3T3 cells non-starved
b
Control RNAi
Beclin 1 RNAi
Atg14L RNAi
Atg14L
Beclin 1
p62/SQSTM1
LC3 I
LC3 II
Actin
NIH/3T3 cells starved 2h
c
Control RNAi
Atg14L RNAi
d
GFP-LC3
p62/SQSTM1
Merge
GFP-LC3
Ubiquitin
Merge
e
Degradation of Long-lived Proteins (normalized)
Control RNAi
Atg14L RNAi
1.00
0.90
2.73
1.71
0.83
0.77
Untreated
Starved
Starved + 3MA

thereby indicating that like Beclin 1, knockdown of Atg14L impaired autophagy level in the cells. When cells were deprived of serum and amino acids to induce autophagy, transfection of Beclin 1 or Atg14L siRNA resulted in the same accumulation of p62/SQSTM1 and both LC3 I and II forms, indicating that autophagy was inhibited as well under starvation conditions (Fig. 11b). Interestingly, Beclin 1 siRNA transfection also resulted in a significant decrease of Atg14L protein level, suggesting that Beclin 1 may be essential for stabilization of Atg14L.

In a parallel experiment, Atg14L protein levels were knocked down in MLE12 cells that stably expressed the autophagy reporter, GFP-LC3 fusion protein. Compared to control siRNA, Atg14L siRNA transfection resulted in accumulation of many large-sized punctate structures that were positive for GFP-LC3 (Fig. 11c). These structures were stained positively with anti-p62/SQSTM1 and anti-ubiquitin antibodies, indicating that they are accumulation of ubiquitinated proteins they failed to be degraded by lysosomes because of down-regulation of autophagy (Fig. 11d).

To further confirm the positive regulation of autophagy by Atg14L, long-lived protein degradation rate was measured and compared in control or Atg14L siRNA trasnfected NIH/3T3 cells. Unlike short-lived proteins that are degraded by ubiquitin-proteasome system, long-lived proteins are degraded by autophagy and therefore the rate of degradation can be used as an indicator of the level of autophagy. When the long-lived protein degradation rate in control siRNA transfected cells under normal culture conditions was set as 1.00 fold as normalization standard, Atg14L siRNA transfection reduced the degradation to 0.90 fold, which is a small yet significant difference ($p<0.001$). Upon starvation, autophagy in cells was induced and the long-lived protein degradation

rate in control RNAi transfected cells increased to 2.73 folds, and again Atg14L siRNA transfection reduced it to 1.71 folds (~37%, *p*=5E-6). Finally when cells were put under starvation conditions and treated with a specific autophagy inhibitor 3-methyladenie (3-MA), long-lived protein degradation rates in control siRNA and Atg14L siRNA transfected cell were reduced to 0.83 fold and 0.77 fold respectively, and no significant difference was observed between the two conditions (Fig. 11e). These results indicated that knockdown of Atg14L protein level indeed inhibited autophagy, therefore Atg14L positively regulates autophagy.

2.9.2 Atg14L positively regulates Vps34/PtdIns3K lipid kinase activity

Vps34/PtdIns3K is essential for autophagy induction, and it is a type III phosphoinositide 3 (PI 3)-kinase that generates phosphotidylinositol 3-phosphate (PtdIns(3)P) from the substrate phosphatidylinositol (PI). Recently identified Beclin 1 interaction proteins UVRAG and Bif-1 both positively regulate Vps34/PtdIns3K kinase activity and autophagy. To study whether Atg14L may also function on Vps34/PtdIns3K, a kinase activity assay was performed. A plasmid that contains both Myc-tagged Vps34/PtdIns3K and its co-activator Vps15 was used, since the co-expression of Vps15 was reported to enhance Vps34/PtdIns3K kinase activity and therefore increase the sensitivity of the assay (Yan et al., 2008). Myc-Vps34/PtdIns3K-Vps15 was co-transfected with either empty pCMV-FLAG vector or FLAG-Atg14L, and IP was performed using Myc antibody. Immunoprecipitated Myc-Vps34/PtdIns3K was subsequently used for *in vitro* kinase activity assay, and generated PtdIns(3)P was separated with thin layer chromatography (TLC) (Fig. 12a).

Figure 1-12. Atg14L positively regulates Vps34/ PtdIns3K kinase activity

(a) HEK 293T cells were co-transfected with myc-Vps34/PtdIns3K-Vps15 and FLAG-Atg14L or FLAG vector, either in the absence or in the presence of Beclin 1-EGFP. Myc-Vps34-Vps15 was immunoprecipitated with anti-Myc antibody for the *in vitro* kinase activity assay. The resulting radioactive PtdIns(3)P was separated by thin layer chromatography (TLC) (lower panel), quantified and normalized against the amount of immunoprecipitated myc-tagged Vps34/PtdIns3K as measured by Western blot (upper panel).

(b) The quantified results showed that over-expressing Atg14L significantly up-regulated the Vps34 kinase activity by 2.5 folds with simultaneous over-expression of Beclin 1 (asterisk, p=0.04, one-tailed Student's t-test with unequal variances, n=5). Without over-expressed Beclin 1, no significant difference was observed.

Figure 1-12

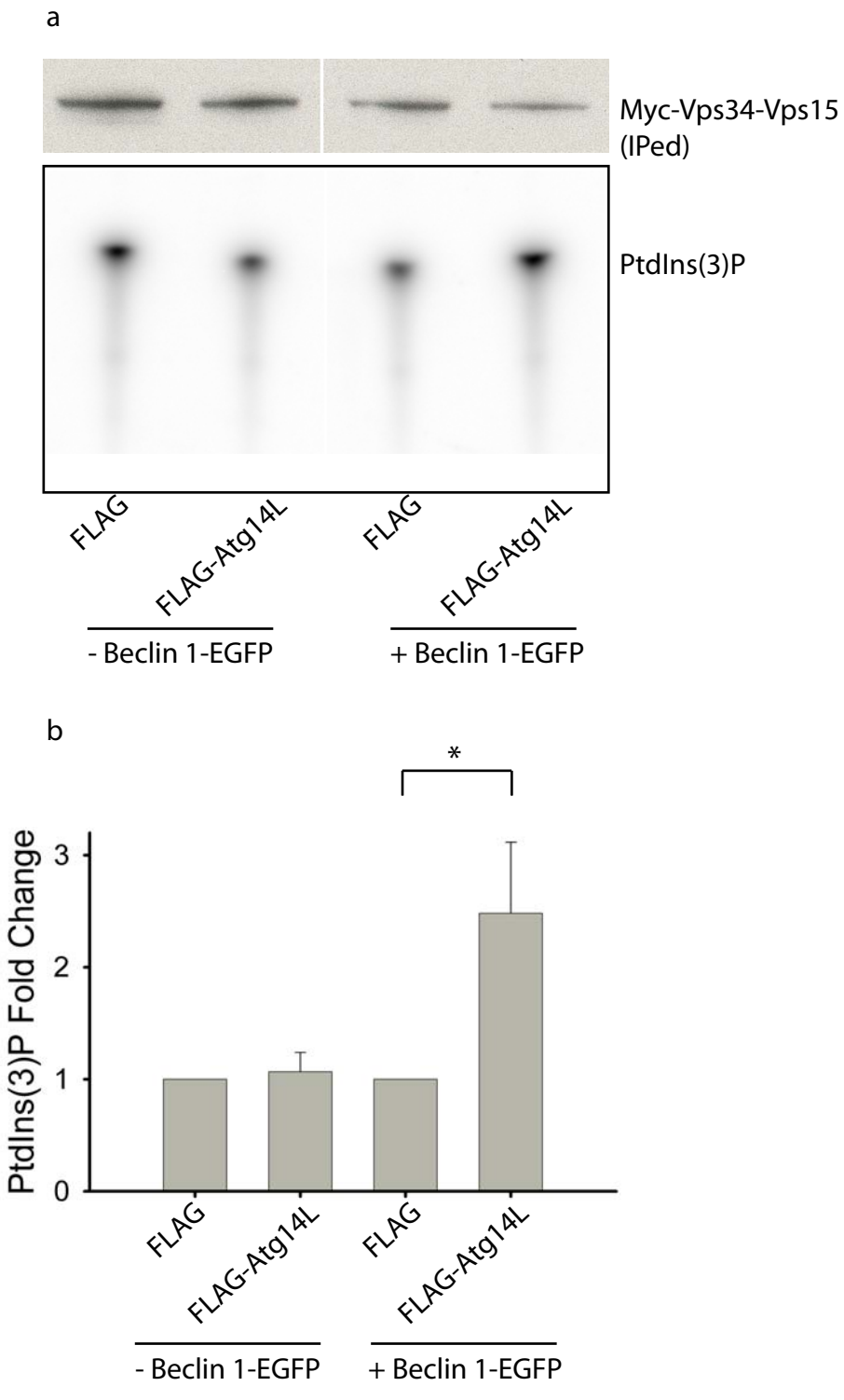
a
Myc-Vps34-Vps15
(IPed)
PtdIns(3)P
FLAG
FLAG-Atg14L
FLAG
FLAG-Atg14L
- Beclin 1-EGFP
+ Beclin 1-EGFP
b
*
PtdIns(3)P Fold Change
0
1
2
3
FLAG
FLAG-Atg14L
FLAG
FLAG-Atg14L
- Beclin 1-EGFP
+ Beclin 1-EGFP

When only two plasmids were co-transfected, FLAG-Atg14L did not change the Vps34/PtdIns3K kinase activity compared to empty control vector. However, when Beclin 1-EGFP was co-transfected with FLAG-Atg14L, there was a significant 2.5 folds change in Vps34/PtdIns3K kinase activity compared to control vector (Fig. 12b). Therefore, Atg14L positively regulates Vps34/PtdIns3K kinase activity, and Beclin 1 is essential for this regulatory function.

2.9.3 Beclin 1 and Atg14L synergistically promote autophagosome biogenesis

Although it has been shown that Beclin 1 is localized on trans-Golgi network (TGN) and near mitochondria, the majority of it is diffusely localized throughout the cytosol, and half of the protein is within soluble portion of the cells (Kihara et al., 2001a; Pattingre et al., 2005). Staining of tissue sections from Beclin 1-EGFP mice also showed diffuse intracellular localization of Beclin 1-EGFP in cells (Arsov et al., 2008). The intracellular localization of Beclin 1-EGFP after transient transfection or in Beclin 1-EGFP HEK293 stable cells was consistent with these previous reports (Fig. 13a). Meanwhile, Atg14L-EGFP mainly showed diffuse intacellular localization in HEK293 cells stably expressing Atg14L-EGFP (Fig. 13a). In order to study the inter-relation between localization of Beclin 1 and Atg14L, Beclin 1-AsRed and Atg14L-EGFP were co-transfected into Hela cells. Upon co-transfection, both proteins showed dramatic changes in intracellular localization and both became localized on numerous punctate structures. On these punctate structures, Beclin 1-AsRed and Atg14L-EGFP showed complete co-localization (Fig. 13b). In order to reveal the identity of the punctate structures, electron microscopy (EM) studies were performed on HEK293T cells

Figure 1-13. Synergistic effects of Beclin 1 and Atg14L in promoting double membrane formation

(a) Beclin 1-EGFP and Atg14L-EGFP are diffuse in cytoplasm of HEK-293 cells stably transfected with Beclin 1-EGFP or Atg14L-EGFP plasmids. Scale bar: 10 μm.

(b) Co-expression and co-localization of Atg14L-EGFP (green) & Beclin 1-AsRed (red) on punctate structures in co-transfected HeLa cells, with Pearson's coefficient (PC) 0.91. Scale bar: 10 μm.

(c) Electron microscopic images showed that co-transfection with Atg14L-EGFP and Beclin 1-AsRed caused the formation of large size organelles (red asterisks) that were often enwrapped with double membranes in HEK 293T cells: (c1) concentric membrane "rings"; (c2) two large structures (3-5 μm in diameter) containing materials with high electron density. The inset shows high magnification of enwrapping double membranes; (c3) formation of many autophagosomes (yellow arrows) in cytoplasm; (c4) Immuno-electron microscopic image showing a structure enwrapped with concentric membrane "rings" labeled with anti-GFP antibody. Abbreviations: M – mitochondria, N – nucleus. Scale bar: 500 nm.

(d) Co-localization of Beclin 1-myc (blue), Atg14L-AsRed (red) and GFP-LC3 (green). HeLa cells stably expressing GFP-LC3 were transiently transfected with Beclin 1-myc and Atg14L-AsRed and stained with anti-Myc antibody. Scale bar: 10 μm.

(e-f) Atg12-EGFP and Atg5-EGFP (green) were colocalized with the puncta associated with the Atg14L-AsRed (red) and Beclin 1-Myc (blue) (arrows) in transfected HeLa cells. Some of these puncta (yellow arrows) appeared to be "ring" shape (see the inset). Scale bar: 10 μm.

Figure 1-13

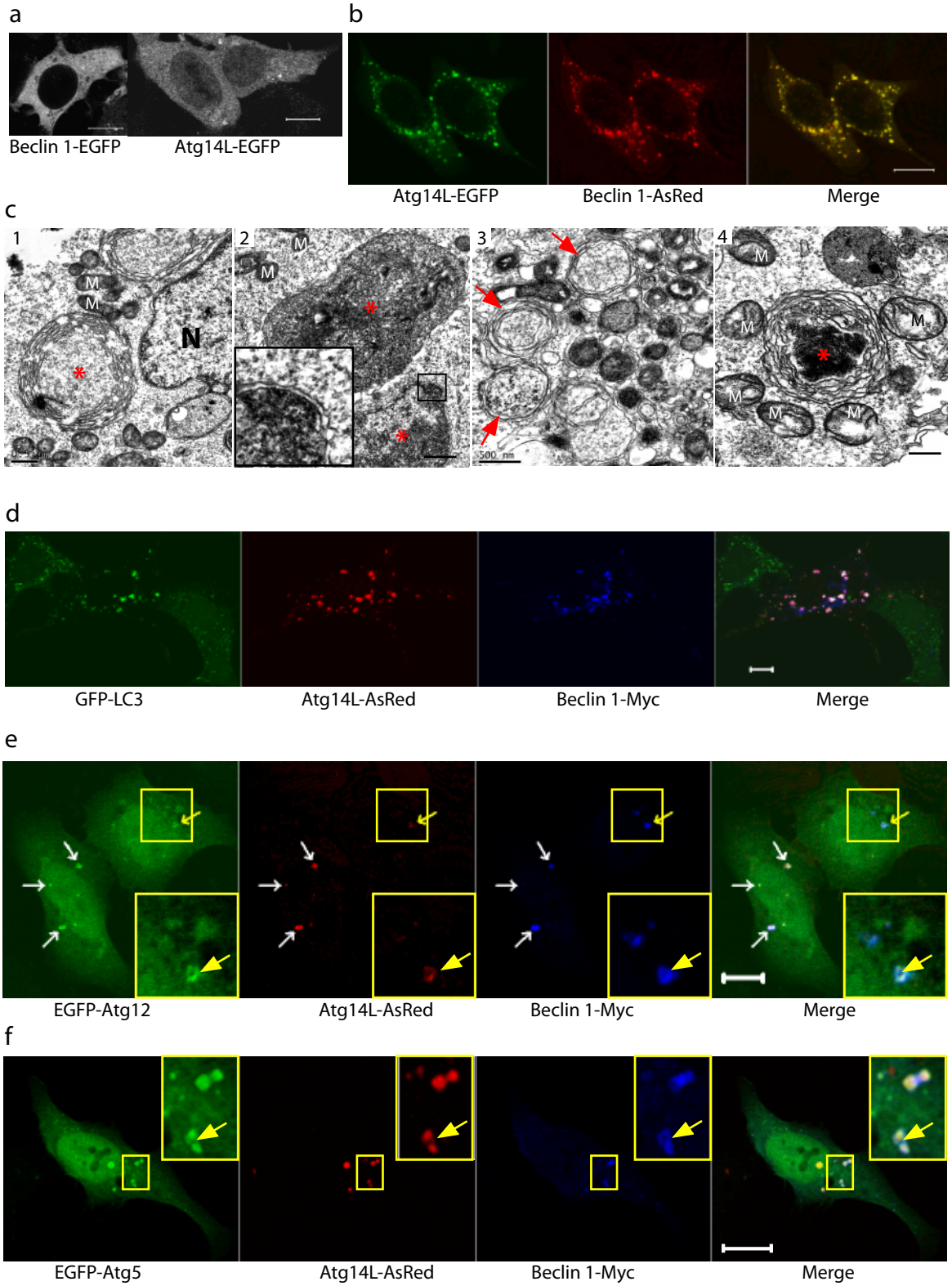
a
Beclin 1-EGFP
Atg14L-EGFP
b
Atg14L-EGFP
Beclin 1-AsRed
Merge
c
1
2
3
4
M
N
d
GFP-LC3
Atg14L-AsRed
Beclin 1-Myc
Merge
e
EGFP-Atg12
Atg14L-AsRed
Beclin 1-Myc
Merge
f
EGFP-Atg5
Atg14L-AsRed
Beclin 1-Myc
Merge

co-transfected with Beclin 1-AsRed and Atg14L-EGFP. Under EM, numbers of electron dense structures that have large-size (~3-5 micron in diameter) were observed, and such structures were virtually absent in single plasmid or control empty vector transfected cells (data not shown). Some of these structures displayed concentric "rings" with double membranes (Fig. 13c1), and many were large vacuoles filled with materials of high electron density (Fig. 13c2). Interestingly, these large organelles were enwrapped with double-membranes (e.g., Fig. 13c2 inset), which are distinguished from typical aggresomes or protein aggregates that are usually not associated with limiting membranes. Meanwhile, increased numbers of double membrane autophagosomes were also observed in the cells overexpressing Atg14L-EGFP and Beclin 1-AsRed (Fig. 13c3). In addition, as shown by immuno-EM using anti-GFP antibody, these large organelles were mostly positive for Atg14L-EGFP (Fig. 13c4), indicating that they are the punctate structures on which Beclin 1-AsRed and Atg14L-EGFP co-localized under fluorescence microscopy (Fig. 13b).

Like Atg6 in yeast, Beclin 1 functions with Vps34/PtdIns3K at the nucleation step of autophagosome formation. They are localized on pre-autophagosomal structure (PAS), and are also essential for localization of other autophagy protein to PAS (Kihara et al., 2001b; Suzuki et al., 2001). To further study the relationship of Beclin 1-Atg14L-labeled structures to other autophagy proteins, Beclin 1-Myc and Atg14L-AsRed were co-transfected into HeLa cells stably expressing GFP-LC3. Again, co-expression of Beclin 1-Myc (blue) and Atg14L-AsRed (red) causes formation of Beclin 1-BISC punctate structures, and GFP-LC3 was also localized on these structures (green) (Fig. 13d), suggesting that the Beclin 1-Atg14L structures likely recruit LC3. Moreover, when

transfection of Atg14L-AsRed, Beclin 1-Myc and EGFP-Atg12 (or EGFP-Atg5) was performed in HeLa cells, EGFP-Atg12 or EGFP-Atg5 (green) was also co-localized on the Atg14L-Beclin 1 punctate structures (red and blue, respectivley) (Fig. 13e&f), suggesting that these Beclin 1-Atg14L structures may also recruit Atg12 and Atg5, whose conjugation is required for autophagosome expansion and association of LC3 to autophagosome membranes (Mizushima et al., 2001).

Taken together, the results suggest that Beclin 1 and Atg14L synergistically induce formation of specific structures on which autophagy protein Atg5, Atg12 and LC3 are localized, and that they also synergistically promote the formation of double membranes during the process of autophagosome biogenesis.

2.10 The functions of Rubicon

2.10.1 Rubicon negatively regulates autophagy

To study the possible functions of Rubicon on autophagy regulation, the Rubicon protein level was knocked down in NIH/3T3 cells with siRNA transfection, after which LC3 and p62/SQSTM1 protein levels were examined with western blot. Compared to control siRNA, Rubicon siRNA transfection reduced both LC3 I/II forms and p62/SQSTM1 levels, indicating that knockdown of Rubicon induced activation of autophagy, which resulted in elevated p62/SQSTM1 protein degradation and faster LC3 I/II protein turnover by autophagy (Fig. 14a). When transfected cells were deprived of serum and amino acids, the same results were observed, indicating that when autophagy was induced by starvation, knockdown of Rubicon further activated autophagy (Fig. 14a). These results suggest that Rubicon inhibits autophagy. In order to confirm this, the effect

Figure 1-14. **Rubicon is a negative regulator of autophagy**

(a) Rubicon RNAi knock-down in the NIH/3T3 cells led to decreased levels of p62/SQSTM1 and LC3 II as detected with anti-p62/SQSTM1 and LC3 antibodies under both normal and starvation conditions.

(b) Over-expression of Rubicon resulted in increased levels of p62/SQSTM1 under both normal and starvation conditions in both HEK293 cells stably expressing Rubicon-EGFP (upper panel) and HEK293T cells transiently transfected with Rubicon-EGFP (lower panel). The control cells were transfected with EGFP-N3 vector.

(c) Vps34/PtdIns3K kinase activity assay. HEK293T cells were co-transfected with Myc-Vps34/PtdIns3K-Vps15 and FLAG-tagged Rubicon or empty vector, either in the absence or in the presence of Beclin 1-EGFP. Myc-tagged Vps34/PtdIns3K that was immunoprecipitated using anti-Myc antibody was used for *in votro* kinase activity assay. The resulting radioactive PtdIns(3)P was separated by thin layer chromatography (TLC) and visualized by radiograph. The amount of radioactive PtdIns(3)P was normalized against the amount of immunoprecipitated Myc-tagged Vps34/PtdIns3K.

(d) The results were quantified and showed that in the absence of Beclin 1, overexpessed Rubicon significantly reduced Vps34/PtdIns3K kinase activity (ratio=0.58, p=0.04 for the one-tailed Student's t-test with unequal variances, n=4, labeled by asterisk). No significant difference was observed when Beclin 1 was co-transfected.

(e) Starvation increased interaction between Rubicon and Beclin 1. HEK293T cells were transiently transfected with Atg14L-EGFP or Rubicon-EGFP. Cells were either maintained in complete media or under starvation conditions for 4 hours. After that immunoprecipitation was performed using anti-GFP antibody. Anti-Beclin 1 and anti-Vps34/PtdIns3K antibody were used to detect the endogenous proteins that were immunoprecipitated.

Figure 1-14

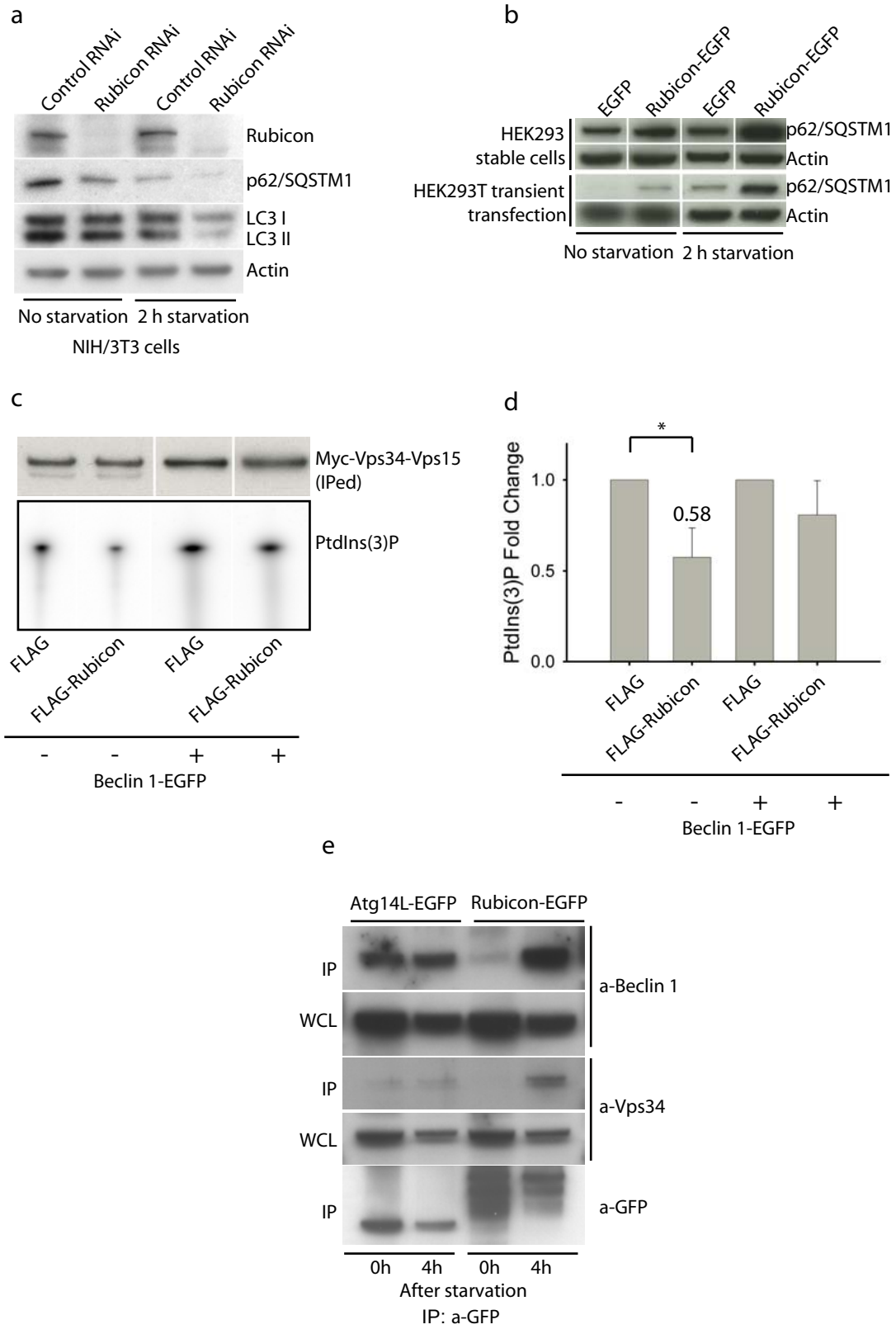
a
Control RNAi
Rubicon RNAi
Control RNAi
Rubicon RNAi
Rubicon
p62/SQSTM1
LC3 I
LC3 II
Actin
No starvation
2 h starvation
NIH/3T3 cells
b
EGFP
Rubicon-EGFP
EGFP
Rubicon-EGFP
HEK293 stable cells
p62/SQSTM1
Actin
HEK293T transient transfection
p62/SQSTM1
Actin
No starvation
2 h starvation
c
Myc-Vps34-Vps15 (IPed)
PtdIns(3)P
FLAG
FLAG-Rubicon
FLAG
FLAG-Rubicon
- - + +
Beclin 1-EGFP
d
*
PtdIns(3)P Fold Change
1.0
0.5
0.0
0.58
FLAG
FLAG-Rubicon
FLAG
FLAG-Rubicon
- - + +
Beclin 1-EGFP
e
Atg14L-EGFP
Rubicon-EGFP
IP
WCL
IP
WCL
IP
a-Beclin 1
a-Vps34
a-GFP
0h 4h 0h 4h
After starvation
IP: a-GFP

of Rubicon over-expression on autophagy levels was studied in transiently transfected HEK293T cells or in HEK293 cells stably expressing Rubicon-EGFP. Compared to control conditions, under both normal culture conditions and starvation conditions, over-expression of Rubicon-EGFP resulted in increased p62/SQSTM1 protein levels in both transiently transfected cells and stable cells, indicating that Rubicon indeed inhibits autophagy (Fig. 14b).

2.10.2 Rubicon negatively regulates Vps34/PtdIns3K kinase activity

Since Rubicon is associated with Beclin 1-Vps34/PtdIns3K complex, its inhibitory effect on autophagy may be through regulation of Vps34/PtdIns3K kinase activity. To test this possibility, Myc-Vps34/PtdIns3K-Vps15 was co-transfected with either empty pCMV-FLAG vector or FLAG-Rubicon, and immunoprecipitated Myc-Vps34/PtdIns3K was used for *in vitro* kinase activity assay (Fig. 14c). Compared to control condition, co-transfection of FLAG-Rubicon significantly reduced the kinase activity of Myc-Vps34/PtdIns3K. Interestingly, when Beclin 1-EGFP was also over-expressed in the cells, this reduction of kinase activity largely diminished, indicating that Beclin 1 is not required for and furthermore interferes with the negative regulation of Vps34/PtdIns3K by Rubicon (Fig. 14c&d).

2.10.3 Interaction between Beclin 1 and Rubicon increases under starvation conditions

Rubicon reduces the interaction between Beclin 1 and Vps34/PtdIns3K (Fig. 10a), while Beclin 1 inhibits Rubicon's regulation on Vps34/PtdIns3K (Fig. 14c&d). To characterize the possible function of Beclin 1-Rubicon interaction in autophagy, how

activation of autophagy affects this interaction was examined. To do this, HEK293T cells transfected with Rubicon-EGFP were either maintained in normal culture media or subjected to nutrient and amino acid starvation for 4 hours. Immunoprecipitation using anti-GFP antibody was then performed and immunoprecipitated endogenous Beclin 1 and Vps34/PtdIns3K were detected with western blot. Under starvation conditions, Rubicon-EGFP pulled down significantly larger amount of Beclin 1 and Vps34/PtdIns3K, indicating that they have much stronger binding when autophagy is activated (Fig. 14e). In contrast, the interaction between Atg14L and Beclin 1 or Vps34/PtdIns3K showed no changes under starvation conditions (Fig. 14e).

2.10.4 Rubicon blocks autophagosome acidification and maturation

Vps34/PtdIns3K functions at various steps of intracellular membrane trafficking. In order to identify which step of autophagy may be affected by Rubicon, a previously developed double-tagged LC3 reporter, mCherry-GFP-LC3, was used to examine the maturation of autophagosomes, such as autophagosome acidification following fusion with late endosomes/lysosomes (Pankiv et al., 2007). Immature autophagosoms labeled with mCherry-GFP-LC3 emit both GFP and mCherry fluorescence and will appear yellow when two channels are merged under fluorescence microscope. However, since GFP is pH sensitive and cannot emit green fluorescence in acidic environments, mCherry-GFP-LC3 labeled mature autophagosomes that have fused with late endosomes/lysosomes will only show red color (Fig. 15a). In Hela cells co-transfected with FLAG-Rubicon and mCherry-GFP-LC3, the majority fluorescent punctate structures

Figure 1-15. Rubicon blocks autophagosome maturation

(a) Schematic representation of mCherry-GFP-LC3 construct. pH Neutral autophagosome will appear yellow under fluorescence microscope while mature autophagsomes that have fused with lysosomes will appear red.

(b) Effect of over-expressing FLAG-Rubicon on autophagosome acidification, as monitored by mCherry-GFP-LC3 fluorescence. HeLa cells were transiently co-transfected with mCherry-GFP-LC3 and FLAG-Rubicon (or control FLAG vector). Cells co-expressing mCherry-GFP-LC3 and control FLAG vector contained many red-only puncta along with yellow (indicating presence of both red and green) puncta, suggesting both autolysosomes and nascent autophagosomes (upper panel). In contrast, cells co-expressing mCherry-GFP-LC3 and FLAG-Rubicon contained primarily yellow puncta, suggesting only nascent autophagosomes (lower panel, white arrows). Notably, some cells that did not express detectable levels of FLAG-Rubicon contained many red-only puncta (low panel, yellow arrows).

(c) Quantitation of the results in (b) showed that over-expressing FLAG-Rubicon drastically reduced the percentage of red-only puncta (mCherry-LC3) from 39% in the control FLAG vector-transfected cells to 2% in the FLAG-Rubicon-transfected cells (asterisk, p=2E-26, one-tailed Student's t-test with unequal variances, n=30), indicating that over-expression of Rubicon blocks autophagosome acidification or maturation.

Figure 1-15

a

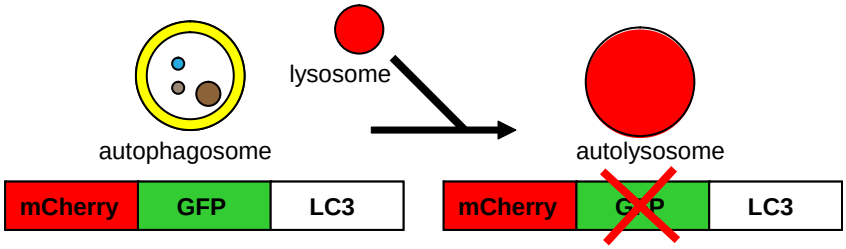

b

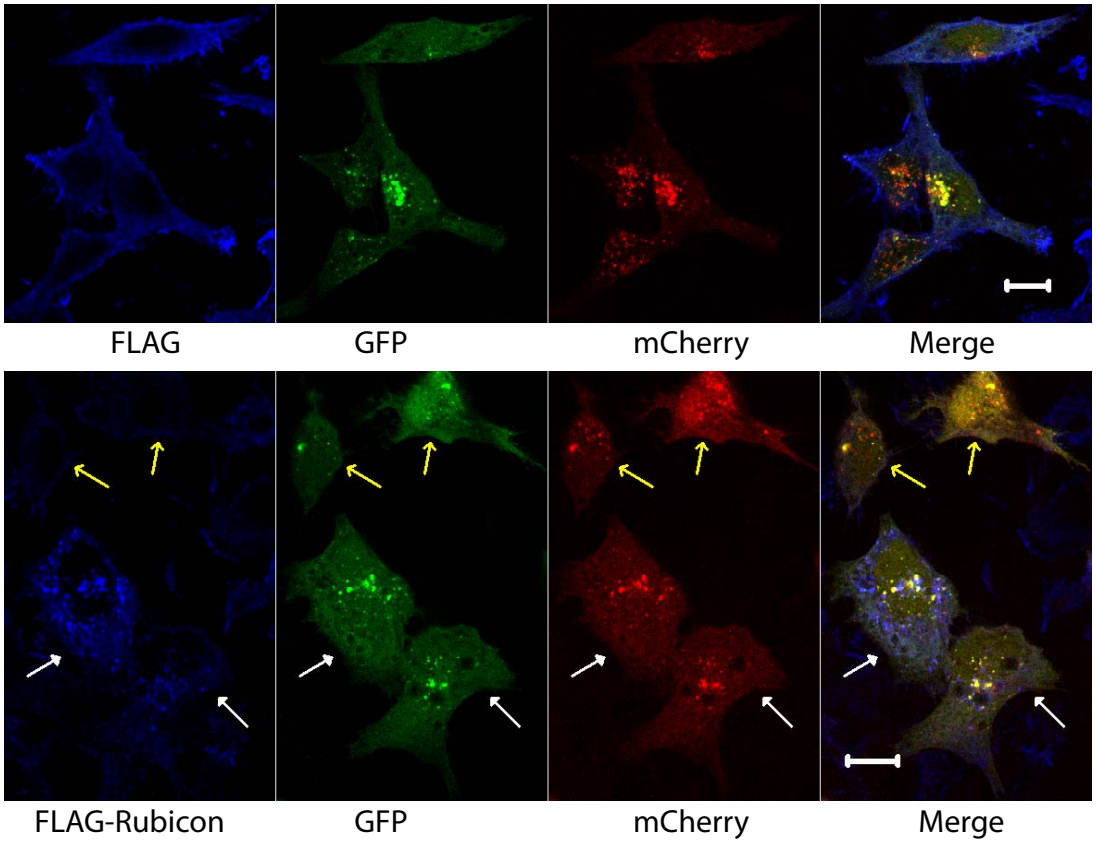

c

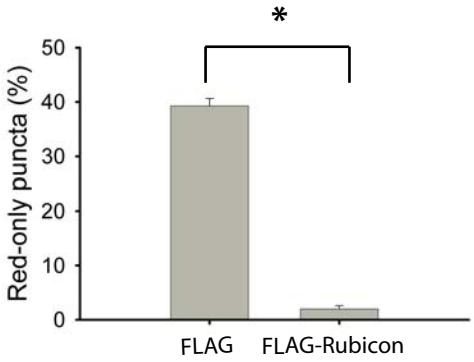

observed were yellow, indicating that most mCherry-GFP-LC3 labeled autophagosomes in the cells are immature, and only about 2% of the autophagosomes were mature (Fig. 15b and 15c). In contrast, in cells that were co-transfected with empty pCMV-FLAG vector or those that did not express detectable levels of FLAG-Rubicon, a significantly higher number of red punctate structures, which represented mature autophagosomes, were observed (Fig. 15b and 15c). These results suggest that over-expression of Rubicon blocked autophagosome acidification or maturation.

Taken the above results together, it can be concluded that Rubicon negatively regulates autophagy and that it may be functioning through negatively regulating Vps34/PtdIns3K kinase activity and inhibiting autophagosome maturation.

2.10.5 Over-expression of Rubicon causes aberrant expansion of late endosomes/lysosomes

In cells transiently transfected with Rubicon-EGFP or cells that stably express Rubicon-EGFP, localization of Rubion-EGFP on large numbers of punctate and vesicular structures was observed (Fig. 16a). Transient transfection of FLAG-Rubicon and staining with FLAG antibody confirmed that the localization pattern was unique to Rubicon and not due to EGFP tagging (data not shown). Some of these Rubicon-EGFP puncta were large in size and exhibited “ring” shapes (Fig. 16a, yellow arrows). To study the identity of these structures, Hela cells transiently transfected with Rubicon-EGFP were stained with a series of cellular organelle markers. The results showed that the Rubicon-EGFP structures were primarily positive for Lamp1, a late endosome/lysosome larker, although a small portion of them were positive for EEA1, an early endosome marker (Fig. 16a and

Figure 1-16. Over-expressing Rubicon causes aberrant expansion of late endosomes/lysosomes

(a) Co-localization of Rubicon-EGFP-associated structures (green) with the late endosome/lysosome marker Lamp1 (red, upper panel) (arrows) and partial co-localization of Rubicon-EGFP-associated structures (green) with the MVB marker LBPA (red, lower panel) (arrows) in the HeLa cells that were transfected with Rubicon-EGFP. Note that some of the Rubicon-EGFP-associated structures displayed "ring"-shape (yellow arrows). Scale bar: 10 μm.

(b) Representative ultrastructural images show aberrant expansion of late endosomes/lysosomes structures in the HEK 293T cells over-expressing Rubicon-EGFP. These abnormal organelles are large in size and contained high (orange arrows) or low (black arrows) electron density. Some enclose small vesicles (purple arrows) and some resemble MVB (blue arrows). Scale bars: 500 nm.

(c) Representative ultrastructural images showing late endosome/lysosome-like structures that are labeled by anti-GFP gold particles (panels 3-4) in the HEK 293T cells transiently transfected with Rubicon-EGFP. These structures are enwrapped by double membranes (panel 4 inset) and co-labeled by anti-GFP (developed by DAB) and anti-Lamp1 (gold enhanced) (panels 5-7). Note that mitochondria are mostly negative for Rubicon-EGFP (panel 4). The negative controls are without antibody (panels 1-2). M – mitochondria. Scale bars: 200 nm.

Figure 1-16

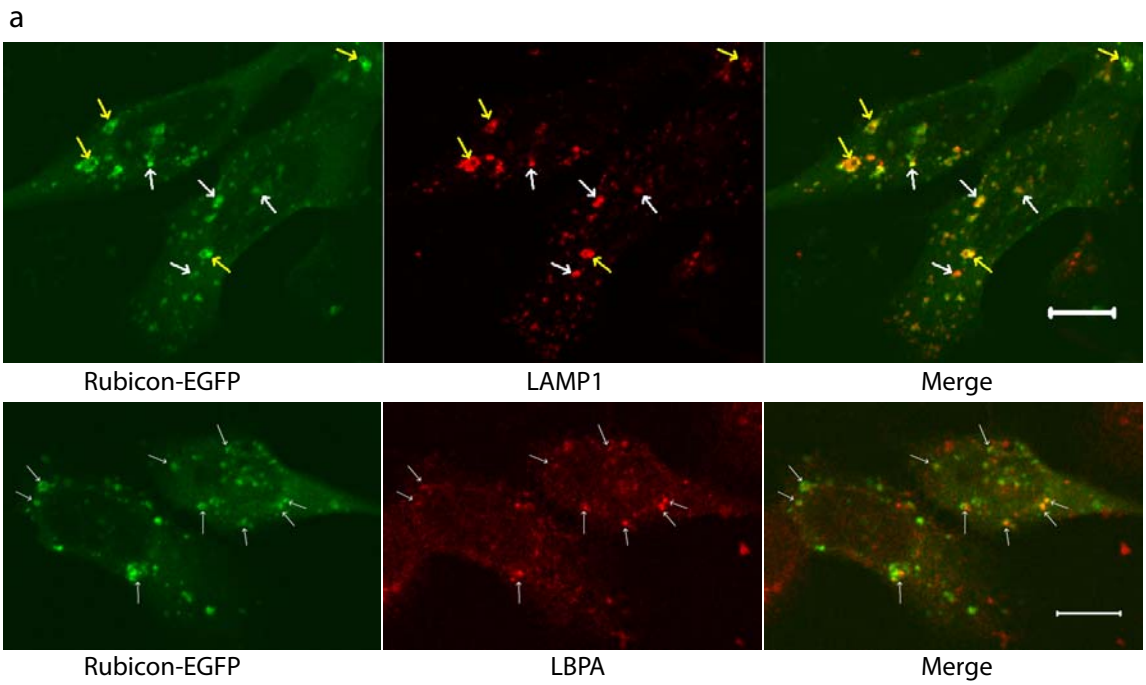
a
Rubicon-EGFP
LAMP1
Merge
Rubicon-EGFP
LBPA
Merge
b
1
2
3
4
c
No primary antibody
Anti-GFP
1
2
3
4
M
M
Anti-GFP DAB + Anti-Lamp1 Au-enhanced
5
6
7

data not shown). In addition, some of the structures were positively stained with an antibody against lysobisphosphatidic acid (LBPA) (Fig. 16b), an unusual eukaryotic lipid found only in multi-vesicular body (MVB). These results suggest that the function of Rubicon may also be related to endocytic pathway. In order to examine the Rubicon-EGFP-labeled structures at ultra-structural levels, electron microscopy (EM) analyses were performed. Under EM, many abnormally large-sized vacuoles (1-5μm in diameter) were observed in Rubicon-EGFP-transfected cells (Fig. 16b). In contrast, these large structures were not observed in cells over-expressing EGFP, Atg14L-EGFP or Beclin 1-EGFP (data not shown). Some of these large vacuoles contained high electron density (Fig. 16b1&2, orange arrows), characteristic of late endosomes/lysosomes; some had relatively less content with overall low electron density (more transparent), which may represent an early stage of endosomes (but with enlarged size) (Fig. 16b3, black arrows); interestingly, some contained numerous small vesicles of multiple-layers (Fig. 16b2&4, purple arrows), while others resembled multivesicular endosomal vesicles or MVB (Fig. 16c1&2, blue arrows). To ensure that these large organelles under EM are the same structures as those observed under fluorescence microscopy (Fig. 16a), immuno-EM was performed using anti-GFP antibody and extensive staining by the gold particles on the large vacuoles was observed (Fig. 16c3&4). These gold particles were found primarily associated to the outside of the limiting membranes, although some were also inside the membranes (Fig. 16c3&4). In addition, the immuno-EM results also confirmed the co-localization of Rubicon-EGFP and Lamp1 at ultrastructural level, as shown by extensive co-localization between anti-GFP antibody associated DAB and anti-Lamp1 antibody associated gold particles (Fig. 16d5-7).

2.10.6 C-terminal cysteine-rich domain is essential for Rubicon localization

Rubicon-EGFP exhibited distinctive punctate and vesicular localization in both transiently transfected cells and stably expressing cells (Fig. 16a and 17a). In order to identify which part of the Rubicon protein is critical for its intracellular localization, the localization pattern of previously generated deletion mutants of Rubicon (Fig. 5a) was studied in transiently transfected cells. When the N-terminal RUN domain was deleted, Rubicon(ΔRUN)-EGFP was still localized on numerous punctate and vesicular structures, and this pattern was very similar to that of full length Rubicon-EGFP. However, when the C-terminal cysteine-rich domain was deleted, Rubicon(ΔC)-EGFP was localized diffusely throughout the whole cytosol, and no punctate or vesicular structures were observed. Furthermore, when both RUN and cysteine-rich domains were deleted, Rubicon(ΔRUN&C)-EGFP showed the same diffuse pattern as Rubicon(ΔC)-EGFP (Fig. 17a). Therefore, the C-terminal cysteine-rich domain within Rubicon is essential for maintaining its intracellular localization and possibly its function as well.

Bioinformatic analysis of Rubicon sequence revealed that the several cysteine residues within the C-terminal cysteine-rich domain are conserved in FYVE domain, a well-characterized motif specific for PtdIns(3)P binding (Fig. 17b) (Stenmark et al., 2002). However, the sequence in Rubicon does not contain the key consensus sequences of typical FYVE domain, i.e., WxxD, R[R/K]HHCR and RVC (Fig. 17b, red bars). Moreover, Rubicon-EGFP from tansfected cell lysate failed to bind to PtdIns(3)P-conjugated sepharose beads, indicating that unlike other FYVE domain containing proteins, Rubicon does not bind to PtdIns(3)P directly (data not shown). Nevertheless, when Rubicon-AsRed was co-transfected into Hela cells with another PtdIns(3)P

Figure 1-17. Over-expressed Rubicon is localized on PtdIns(3)P enriched-structures and this loczalization if cysteine-rich domain dependent

(a) Subcellular localization of transiently transfected Rubicon-EGFP, Rubicon(ΔRUN)-EGFP, Rubicon(ΔC)-EGFP or Rubicon(ΔRUNΔC)-EGFP in HeLa cells. In contrast to punctate Rubicon-EGFP and Rubicon(ΔRUN)-EGFP, Rubicon(ΔC)-EGFP and Rubicon(ΔRUNΔC)-EGFP were localized diffusely in the cytoplasm. Abbreviations: ΔRUN – RUN domain deletion, ΔC – cysteine-rich domain deletion. Scale bars: 10 μm.

(b) Local sequence alignment between the C-terminal cystein-rich domain of Rubicon and FYVE domains of several known FYVE-containing proteins. Rubicon does not possess the key consensus sequences of a typical FYVE domain, i.e., N-terminal WxxD, central R[R/K]HHCR and C-terminal RVC (indicated by red bars).

(c) Co-localization of the PtdIns(3)P-enriched lipid domain marker p40 (phox)-PX-EGFP (green) and Rubicon-AsRed (red) on large punctate structures (arrows) in the co-transfected HeLa cells (upper panels). Upon short treatment with 75 nM wortmannin (another PI-3K inhibitor) for 1 hour, while the PtdIns(3)P-enriched lipid domains disappeared, the Rubicon-AsRed-positive structures was maintained (lower panels). Scale bars: 10 μm.

Figure 1-17

a

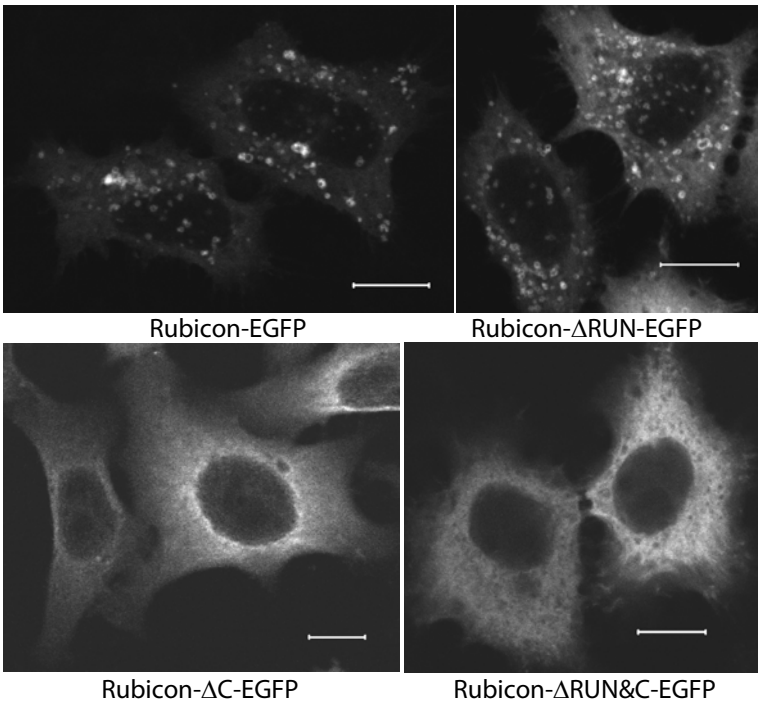

b

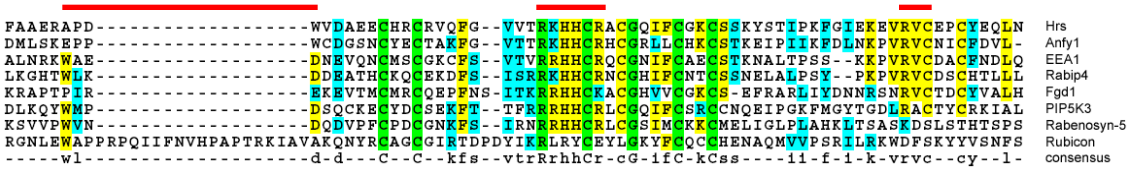

c

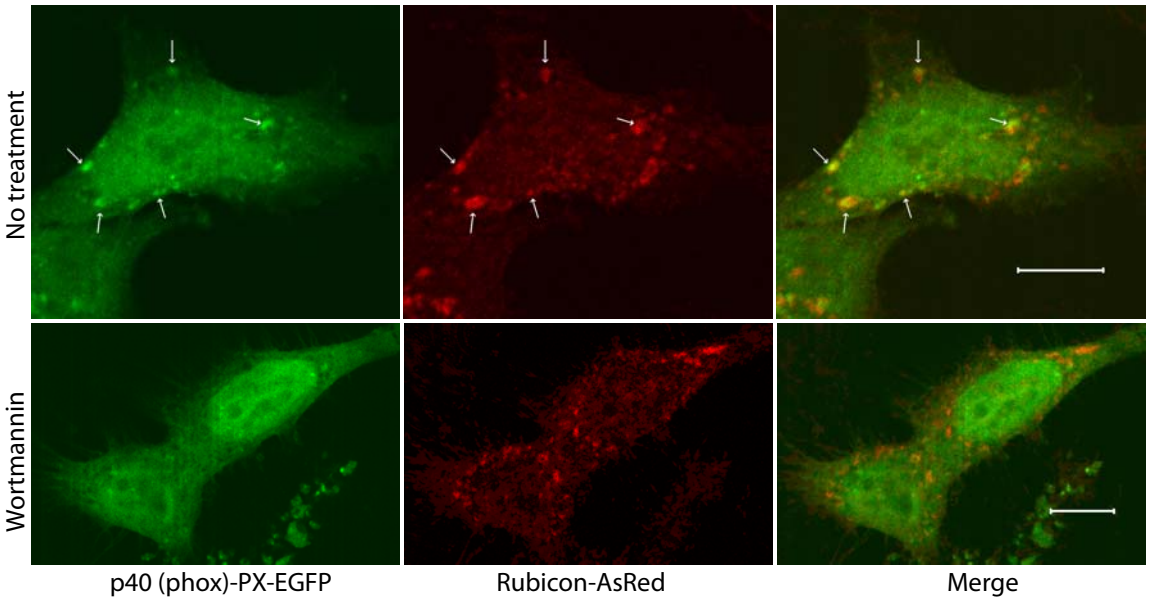

reporter, p40 (phox)-PX-EGFP, they showed extensive co-localization, suggesting that Rubicon associated structures are enriched in Vps34/PtdIns3K product PtdIns(3)P (Fig. 17c upper panel) (Kanai et al., 2001) Therefore, although the cysteine-rich domain is different from the typical FYVE domain and it does not directly bind to PtdIns(3)P, it is still closely related to the function of Vps34/PtdIns3K. In order to determine if the cysteine-rich domain dependent punctate/vesicular localization of Rubicon also depends on Vps34/PtdIns3K function, the cells co-transfected with Rubicon-AsRed and p40(phox)-PX-EGFP were treated with a chemical PI-3 kinase inhibitor wortmannin. Wortmannin treatment effectively dispersed punctate localization of p40(phox)-PX-EGFP, due to inhibition of Vps34/PtdIns3K activity. However the localization pattern of Rubicon-AsRed was not affected by wortmannin treatment, suggesting that formation of Rubicon-associated structures is not dependent on Vps34/PtdIns3K activity (Fig. 17c, lower panel).

2.10.7 Beclin 1 is not essential for formation of Rubicon-associated structures

Although formation of the Rubicon-associated structures is not dependent on Vps34/PtdIns3K activity, it is still closely related to it, as was indicated by co-localization of PtdIns(3)P reporter p40(phox)-PX-EGFP on these structures. It was shown that Rubicon negatively regulated Vps34/PtdIns3K kinase activity, and that presence of over-expressed Beclin 1 interfered with this regulatory effect. Since Rubicon was identified as a component of the Beclin 1-Vps34/PtdIns3K protein complex, the relation between Beclin 1 and the Rubicon associated structures was studied. First, Beclin 1-AsRed was transfected into cells that stably express Rubicon-EGFP. As a result, Beclin

Figure 1-18. Rubicon-associated structures do not have Beclin 1 on them and are Beclin 1-independent

(a-b) Absence of full-length Beclin 1 (a) or Beclin 1-CE mutant (b) (red) on the Rubicon-EGFP-positive structures (green) in the HEK293 cells stably expressing Rubicon-EGFP. These cells were transiently transfected with either Beclin 1-AsRed (a) or FLAG-Beclin 1-CE (b, i.e., the FLAG-tagged Beclin 1 mutant containing both CCD and ECD that mediate the Beclin 1-Rubicon interaction as shown in Fig. 4c). Scale bars, 10μm.

(c) The formation of the Rubicon-EGFP-positive structures was Beclin 1 independent. HEK293 cells stably expressing Rubicon-EGFP were transfected with Beclin 1 siRNA. Although the endogenous Beclin 1 level was significantly knocked down, as was confirmed with western blot using Beclin 1 antibody, the formation of Rubicon-EGFP associated structures was not affected. Scale bar, 10μm.

Figure 1-18

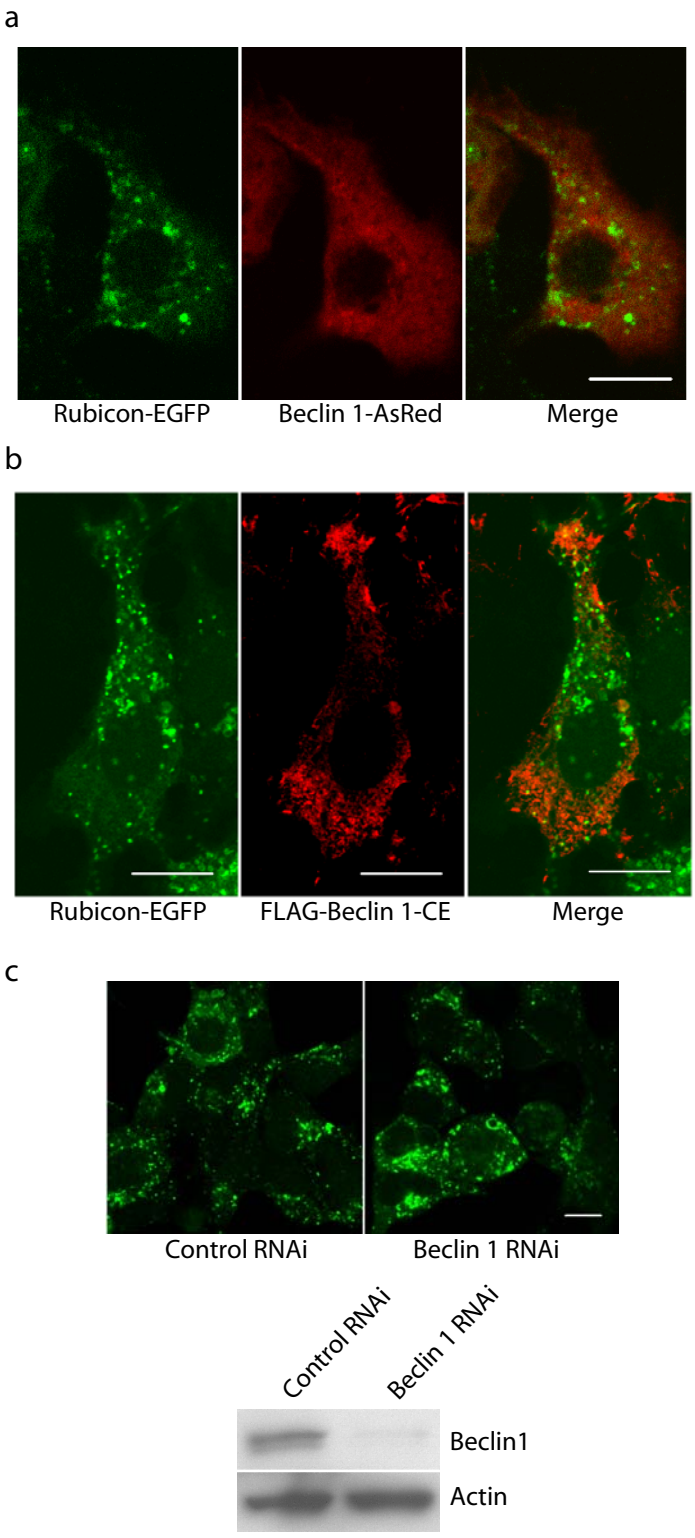
a
Rubicon-EGFP
Beclin 1-AsRed
Merge
b
Rubicon-EGFP
FLAG-Beclin 1-CE
Merge
c
Control RNAi
Beclin 1 RNAi
Control RNAi
Beclin 1 RNAi
Beclin1
Actin

1-AsRed localized diffusely throughout the cytosol and no obvious co-localization of Beclin 1-AsRed on the Rubicon-EGFP associated structures was observed (Fig. 18a). This suggested that Beclin 1 may not be associated with the structures. To further confirm this, coiled-coil and evolutionary conserved domains (CE) of Beclin 1 were tagged with FLAG and transfected into Rubicon-EGFP stable cells. Previous co-immunoprecipitation experiments showed that these two domains together mediate interaction between Beclin 1 and Rubicon (Fig. 4a&b). However, over-expressed FLAG-CE showed no co-localizaiton on Rubicon-EGFP associated structures either. Finally, endogenous Beclin 1 protein level was knocked down with RNAi in Rubicon-EGFP stable cells to study whether Beclin 1 is required for formation of Rubicon associated structures. After siRNA transfection, endogenous Beclin 1 level was significantly reduced, as was confirmed with western blot. However the formation Rubicon-EGFP associated structures was not affected and comparable numbers of Rubicon-EGFP positive punctate and vesicular structures were observed in Beclin 1 siRNA transfected cells and control siRNA transfected cells (Fig. 18c). In conclusion, Beclin 1 is neither localized on Rubicon-EGFP associated structure nor required for their formation.

Figure 1-19. A hypothetic model for the Beclin 1-Vps34/PtdIns3K protein complexes and their functions

In this model, a core Beclin 1 complex is composed of Vps34/PI-3K, p150/Vps15, Beclin 1, UVRAG and likely substoichiometric Atg14L (indicated by the tight binding and functional connection between Atg14L and Beclin 1). Under physiological conditions, a large Beclin 1-Vps34 complex is formed, including the core complex and Rubicon. From this large complex smaller functioning complexes may form such as an Atg14L-Beclin 1-containing complex and a Rubicon-containing complex. These smaller complexes are likely the functional units participating in autophagy regulation through modulating the Vps34 lipid kinase activity.

Figure 1-19

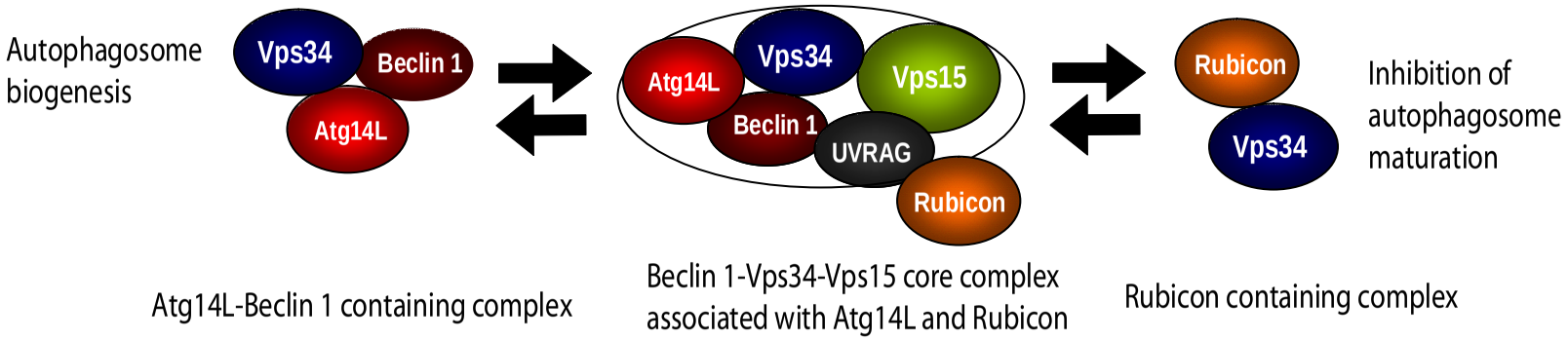
Autophagosome biogenesis
Vps34
Beclin 1
Atg14L
Atg14L
Vps34
Vps15
Beclin 1
UVRAG
Rubicon
Rubicon
Vps34
Inhibition of autophagosome maturation
Atg14L-Beclin 1 containing complex
Beclin 1-Vps34-Vps15 core complex associated with Atg14L and Rubicon
Rubicon containing complex

Chapter III

Generation and Characterization of *beclin 1* Conditional Knockout Mice

3.1 Generation of *beclin 1* conditional knockout mice

The *beclin 1*$^{flox/flox}$ mice were generated using bacterial artificial chromosome (BAC) recombination techniques in C57BL/6J strain background. The targeting BAC vector was generated so that two loxP sequences were inserted into the genome to flank the second exon of *beclin 1* gene, where the start codon is located, and the neomycin resistant gene pGKneo cassette with two flanking FRT sequences were inserted into the intron region between the second and the third exons (Fig. 1a). Purified BAC DNA was electroporated into embryonic stem (ES) cells derived from C57BL/6J-*Tyr*$^{c-2J}$/J mice, which are in C57BL/6J background but have white coat color due to a genetic mutation. After that cells were treated with G418 to select the ones that express the neomycin resistant gene. Two rounds of ES cell targeting were performed and overall 10 positive clones were obtained from screening 100 clones with southern blot. Further southern analysis confirmed that 8 within 10 clones were indeed positive clones in which homologous recombination happened in the correct way, resulting in an 8% targeting efficiency. Several positive clones were injected into C57BL/6J blastcyst, and chimera mice ranging from 5% to 40% were obtained. Successful germ line transmission from a 30% chimera mouse was confirmed with southern blot. After that the mice were crossed to transgenic mice that express FLP recombinase under the control of a broad promoter

Figure 2-1. Generation of *beclin 1*$^{flox/flox}$ mice

(a) Schematic illustration of *beclin 1* gene targeting construct. A modified bacterial artificial chromosome (BAC) clone was used as the targeting vector. Through homologous recombination, two loxP sites (black triangles) were inserted into the genome to flank the second axon of *beclin 1*, in which the start codon is located. The neomycin resistance gene pGKneo cassette was flanked by two FRT sites (black rectangles), and was later deleted by crossing to flipper mice. Southern blot to confirm correct recombination was performed using a probe that is located downstream of the homologous region B (arm B).

(b) PCR reaction and southern blot of mouse genotyping. PCR reaction was performed on genomic DNA extracted from mouse tail clips. The primers used were located outside the inserted loxP sites, so that a bigger-sized band was generated when the loxP sites were successfully inserted into the genome. The southern blot was performed on BglII and SwaI digested genomice DNA from mouse tail clips. With an extra SwaI site introduced into the genome from homologous recombination, a shorter band was detected from the floxed allele.

Figure 2-1

a

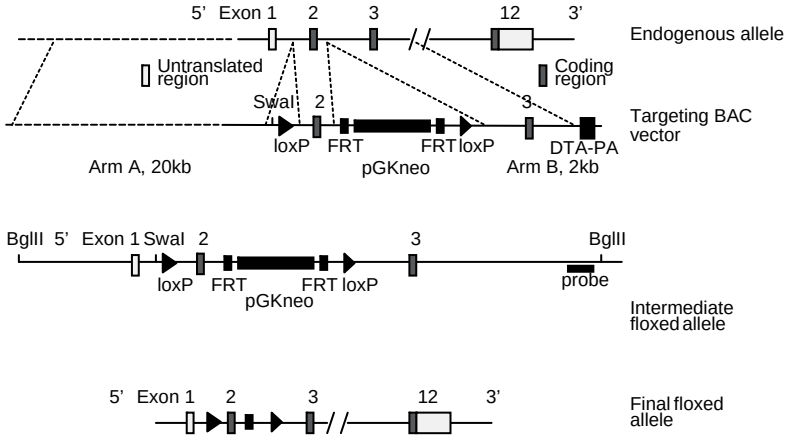
5' Exon 1 2 3 12 3'
Endogenous allele
Untranslated region
Coding region
SwaI 2 3
Targeting BAC vector
loxP FRT FRT loxP
DTA-PA
Arm A, 20kb
pGKneo
Arm B, 2kb
BglII 5' Exon 1 SwaI 2 3 BglII
loxP FRT FRT loxP
pGKneo
probe
Intermediate floxed allele
5' Exon 1 2 3 12 3'
Final floxed allele

b

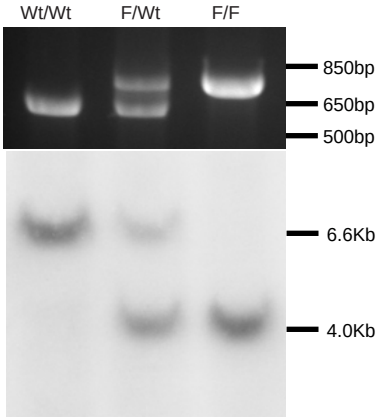
Wt/Wt
F/Wt
F/F
850bp
650bp
500bp
6.6Kb
4.0Kb

ROSA26 (flipper mice) to remove the pGKneo cassette flanked by FRT sequences (Fiering et al., 1993). The resulted *beclin 1*$^{flox/+}$ mice were crossed to each other to generate *beclin 1*$^{flox/flox}$ mice, and genotyping was performed using both polymerase chain reaction (PCR) and southern blot (Fig. 1b). Meanwhile, *beclin 1*$^{flox/+}$ mice were also crossed to transgenic mice that express the Cre recombinase under the control of various cell type specific promoters to generate *beclin 1*$^{flox/+}$; Cre mice (Nagy, 2000). Finally *beclin 1* conditional knockout mice were generated by crossing *beclin 1*$^{flox/flox}$ mice with *beclin 1*$^{flox/+}$; Cre mice to delete *beclin 1* expression in different cell populations.

3.2 Characterization of Beclin 1 function in Purkinje cells

3.2.1 Deletion of Beclin 1 protein in *beclin 1*$^{flox/flox}$; Pcp2-Cre Purkinje cells

Beclin 1$^{flox/flox}$ mice were crossed to transgenic mice that express Cre recombinase under the control of Purkinje cell protein 2 (Pcp2, also known as L7) promoter (Pcp2-Cre) to delete *beclin 1* expression in Purkinje cells. The Pcp2/L7 expression is restrict to Purkinje cells in the cerebellum and bipolar neurons in the retina (Oberdick et al., 1990). The gene expression starts from around postnatal day 2 (P2) and increases gradually to reach its peak at P15, and the Cre recombination driven by this promoter occurs between P15 and P19 (Nordquist et al., 1988; Komatsu et al., 2007a). To confirm that Beclin 1 protein is successfully deleted in Purkinje cells, brain sections from *beclin 1*$^{flox/flox}$ and *beclin 1*$^{flox/flox}$; Pcp2-Cre mice at the age of P21 were stained with anti-Beclin 1 antibody. In *beclin 1*$^{flox/flox}$ mice, the Purkinje cells showed clear staining, while in *beclin 1*$^{flox/flox}$; Pcp2-Cre mice the staining completely disappeared, indicating that Beclin 1 protein has been successfully deleted (Fig. 2, upper panel).

Figure 2-2. Immunohistochemistry of Beclin 1 protein expression in Purkinje cells of *beclin 1*$^{flox/flox}$ and *beclin 1*$^{flox/flox}$; Pcp2-Cre mice at P21

(a) Beclin 1 protein was detected in *beclin 1*$^{flox/flox}$ Purkinje cells but not in *beclin 1*$^{flox/flox}$; Pcp2-Cre Purkinje cells. Paraffin sections of the cerebella were stained with anti-Beclin 1 antibody and visualization was performed with DAB. Scale bar: 100 μm.

(b) Floating sections from the same cerebella were stained with anti-calbindin antibody and fluorescein conjugated secondary antibody, showing that loss of Beclin 1 protein expression in *beclin 1*$^{F/F}$; Pcp2-Cre Purkinje cells was not due to loss of Purkinje cells. Scale bar: 200 μm.

Figure 2-2

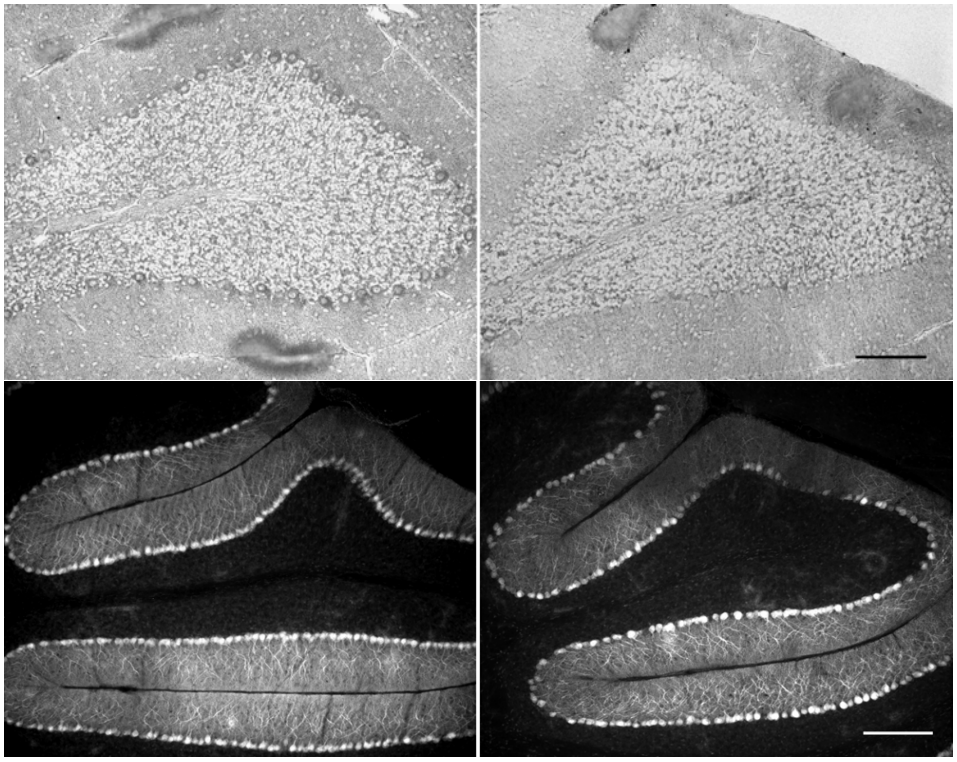

3.2.2 Degeneration of *beclin 1*$^{flox/flox}$; Pcp2-Cre Purkinje cells

To study if deletion of Beclin 1 induces any changes in Purkinje cells, sagittal brain sections from mice at different ages were first stained with an antibody against a Purkinje cell specific protein Calbindin. At P21, when the expression of *beclin 1* has been deleted and no protein can be detected in Purkinje cells, Calbindin staining showed no significant difference in Purkinje cell number between *beclin 1*$^{flox/flox}$; Pcp2-Cre mice and *beclin 1*$^{flox/flox}$ mice (Fig. 2, lower panel). However, by the age of 1 month, the Purkinje cell number in *beclin 1*$^{flox/flox}$; Pcp2-Cre mice has dramatically decreased, and the remaining Purkinje cells also showed features of severe degeneration (Fig. 3a). In order to study whether there is area specificity in Purkinje cell degeneration, coronal cerebellar sections were stained with anti-Calbindin antibody. At 1 month, the degeneration was mainly in medial part of the cerebellum, where the biggest decrease in cell number was observed. Meanwhile the number of Purkinje cells in the lateral part of the cerebellum remained largely unchanged (Fig. 3b). By the age of 2 months, almost all of the Purkinje cells in the medial part had disappeared (Fig. 3c).

3.2.3 Aberrant ultra-structures in early degenerating *beclin 1*$^{flox/flox}$; Pcp2-Cre Purkinje cells

In order to study the mechanism underlying the Purkinje cell degeneration in *beclin 1*$^{flox/flox}$; Pcp2-Cre mice, sections of the cerebellum were first stained with autophagy and apoptosis markers. P62/SQSTM1 is an LC3 interaction protein that is degraded by autophagy, and its accumulation in the cells is often viewed as a hallmark of impaired autophagy. However when cerebellum sections from *beclin 1*$^{flox/flox}$; Pcp2-Cre

Figure 2-3. Degeneration of *beclin 1*$^{flox/flox}$; Pcp2-Cre Purkinje cells

(a) Sagittal sections of cerebella from 1 month old *beclin 1*$^{flox/flox}$ and *beclin 1*$^{flox/flox}$; Pcp2-Cre mice were stained with anti-Calbindin antibody. Severe Purkinje cell loss was observed in *beclin 1*$^{flox/flox}$; Pcp2-Cre mice. Scale bar: 500 μm.

(b) A coronal section of the cerebellum from a 1 month old *beclin 1*$^{flox/flox}$; Pcp2-Cre mouse was stained with anti-Calbindin antibody. Severity of Purkinje cell degeneration showed area specificity. The medial region of the cerebellum showed more Purkinje cell loss than the lateral region. Scale bar: 500 μm.

(c) A sagittal section of the cerebellum from a 2 month old *beclin 1*$^{flox/flox}$; Pcp2-Cre mouse was stained with anti-Calbindin antibody, showing that almost all Purkinje cells had been lost. Scale bar: 500 μm.

Figure 2-3

a

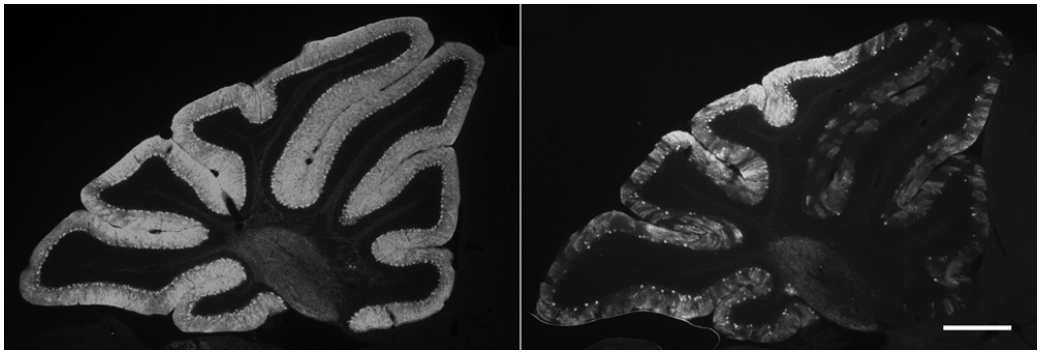

b

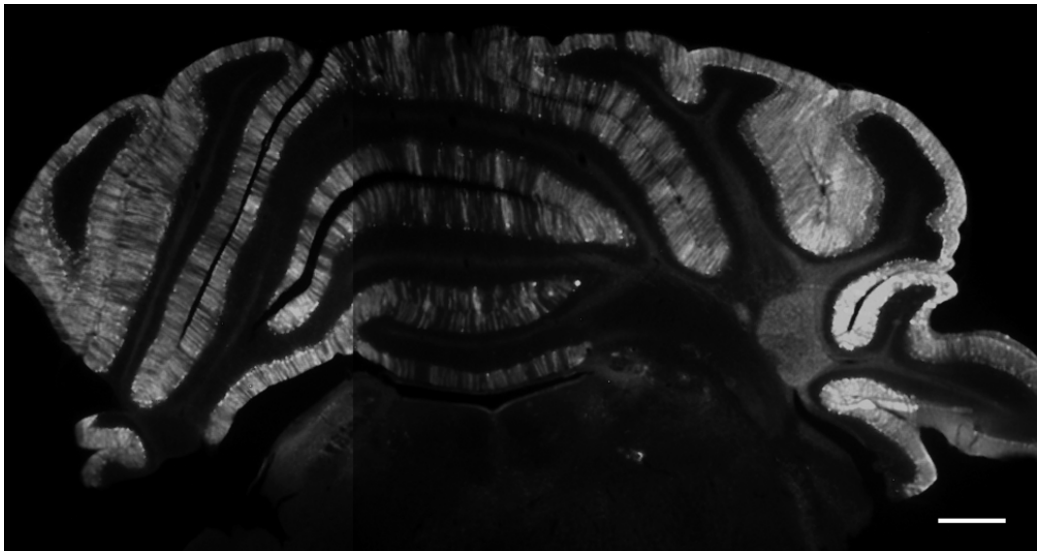

c

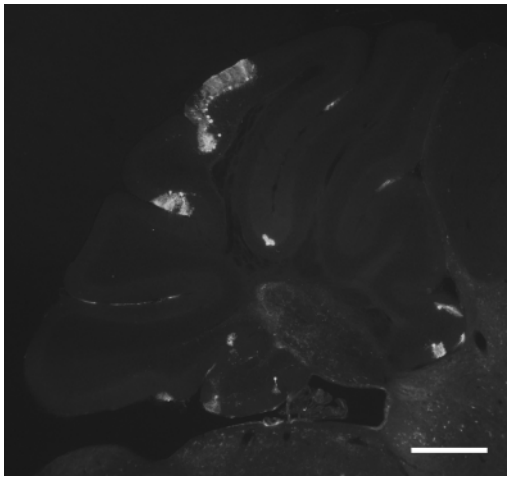

mice were stained with anti-p62/SQSTM1 antibody, no accumulation in the Purkinje cells was observed (data not shown). Meanwhile, anti-activated Caspase3 antibody staining did not detect any activated apoptosis in degenerating *beclin 1*$^{flox/flox}$; Pcp2-Cre Purkinje cells (data not shown).

To search for clues that can lead to possible mechanisms of degeneration of *beclin 1*$^{flox/flox}$; Pcp2-Cre Purkinje cells, electron microscopy (EM) study was performed. To catch the initial stage of the degeneration, a relatively early age (P21) was chosen, and both Purkinje cell bodies and axons in the deep cerebellar nuclei region were examined since neuronal degeneration often starts from the axon region. Semi-thin cerebellar sections (0.5μm) were first cut and stained with Toluidine Blue, and Purkinje cells that showed darker staining than average (and therefore may be the ones undergoing early degeneration) were chosen for further morphological study under EM. In Purkinje cell bodies of *beclin 1*$^{flox/flox}$; Pcp2-Cre mice, numerous electron dense structures were observed, and similar structures were rarely detected in Purkinje cells from control *beclin 1*$^{flox/flox}$ mice. From the localization pattern, the electron dense structures could be divided into two types. One type appeared attached to intracellular membranes although the structures varied in size. Some were about 100nm in diameter, and were attached to Golgi or ER like membranous structures (Fig. 4a&b, bold red arrows); some were smaller in size and were associated with mitochondrial membranes (Fig. 4b&d, red arrowheads); and others were sheet-like structures that extended to longer than 0.5μm and were tightly attached to mitochondrial membranes (Fig. 4a&c, red arrowheads). Interestingly, some of these structures looked like extended tips budding off Golgi or ER membranes that became electron dense (Fig. 4b, thin red arrow). Although most of the structures were

Figure 2-4. Abnormal ultra-structures in degenrating *beclin 1*$^{flox/flox}$; Pcp2-Cre Purkinje cell bodies

P21 *beclin 1*$^{flox/flox}$; Pcp2-Cre Purkinje cell bodies were examined with electron microscopy, and numerous electron dense structures were observed. Some were small in size and were associated with either Golgi-like structures (a & b, bold red arrows), mitochondria (b, red arrowhead) or nuclear envelop (d, green arrowhead); some were in elongated shape and were attached to mitochondria (a & c, red arrowhead); and some looked like condensed tips of Golgi-like membranous structures (b, thin red arrows). In addition to membrane associated small structures, organelle-resembling large structures were also observed (b, c & d, green arrows). Meanwhile, late stage degenerating Purkinje cells showing apoptotic features were also observed (e).

Figure 2-4

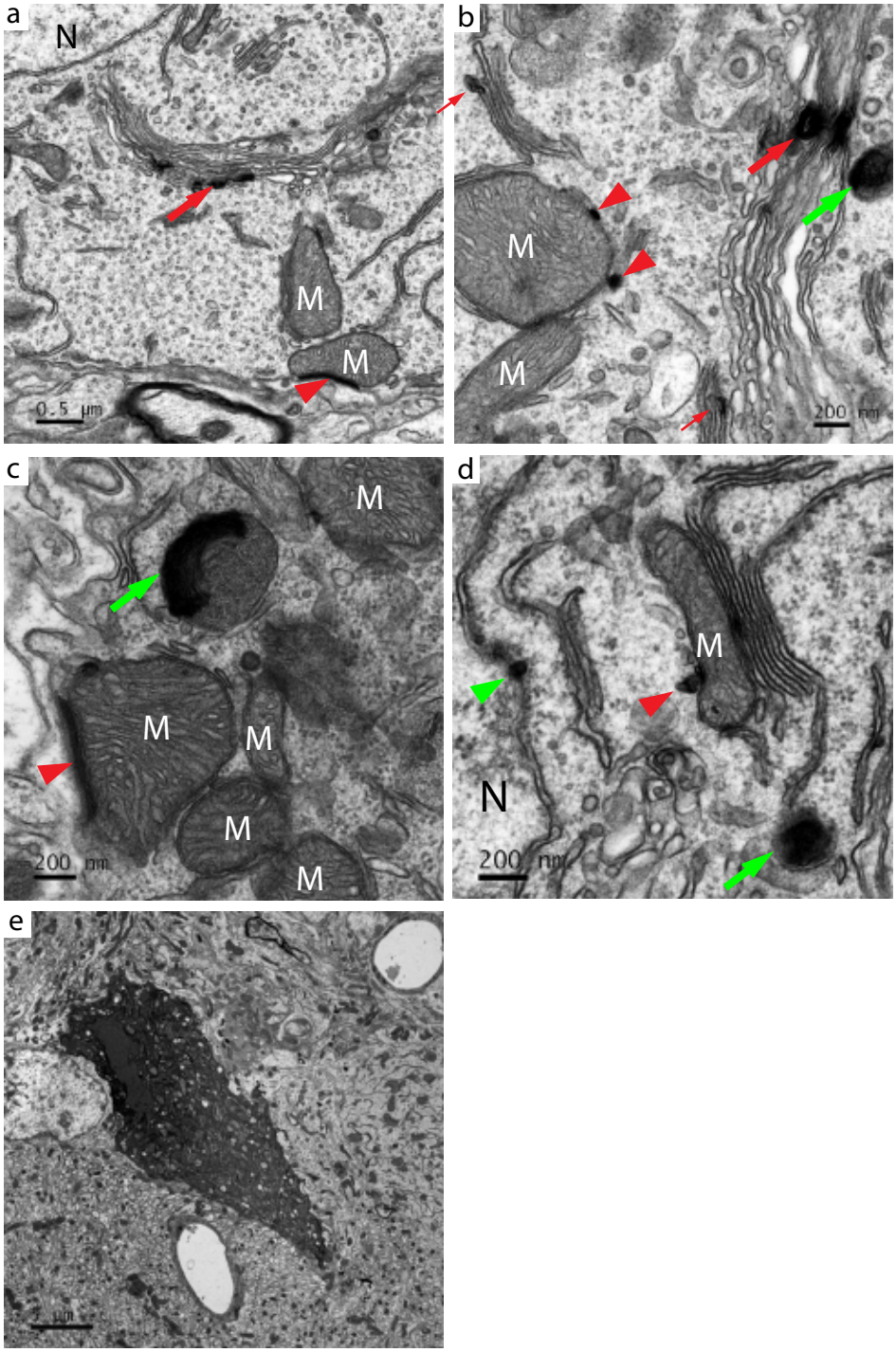

associated with cytosolic membranes, there were also cases when some structures were associated with the nuclear envelop (Fig. 4d, green arrowhead). In addition to these membrane associated structures, there was another type of electron dense structures that were much bigger in size (200nm~ in diameter) and not obviously associated with membranes (Fig. 4b&d, green arrows). Unlike the first type, which appeared to be from condensation of membranes, the second type of structures appeared more likely to be accumulation of electron dense materials in intracellular organelles. In some cases, organelles containing partially electron dense materials were observed, possibly representing an earlier stage in formation of such structures (Fig. 4c, green arrow).

Meanwhile, Purkinje cells at late stages of degeneration were occasionally observed under EM (Fig. 4e). The condensed cell body and nuclear resembled features of apoptotic cell death, although staining the cerebellum sections with activated Caspase 3 antibody did not yield any positive signal (data not shown).

Abnormal structures were also observed in Purkinje cell axons in the deep cerebellar nuclei region of the cerebellum. Purkinje cells send axons to form synapses on deep cerebellar nuclei, and in many case axons can be the first area where degeneration is observed. When deep cerebellar nuclei region of *beclin 1*$^{flox/flox}$; Pcp2-Cre mice was examined under EM, membranous structures were observed in myelinated axons and similar structures were not detected in control mice (Fig. 5a, arrowheads). Under higher magnification, these structures sometimes appeared to be repeatedly folded long membranes that took either regular shape (Fig. 5b) or irregular shape (Fig. 5c), and sometimes appeared as coated vesicles near Golgi like membranes and they resembled

Figure 2-5. Abnormal ultra-structures in degenerating *beclin 1*$^{flox/flox}$; Pcp2-Cre Purkinje cell axons

The deep cerebellar nuclei region of a *beclin 1*$^{flox/flox}$; Pcp2-Cre mouse was examined with electron microscopy. Abnormal membranous structures were observed in myelinated or unmyelinated axons (a, red arrowheads). The structures were regular or irregular in shape and seemed connected to the mitochondria outer membranes (b & c, red arrows). In some cases coated vesicles that resembled clathrin coated vesicles were also observed (d).

Figure 2-5

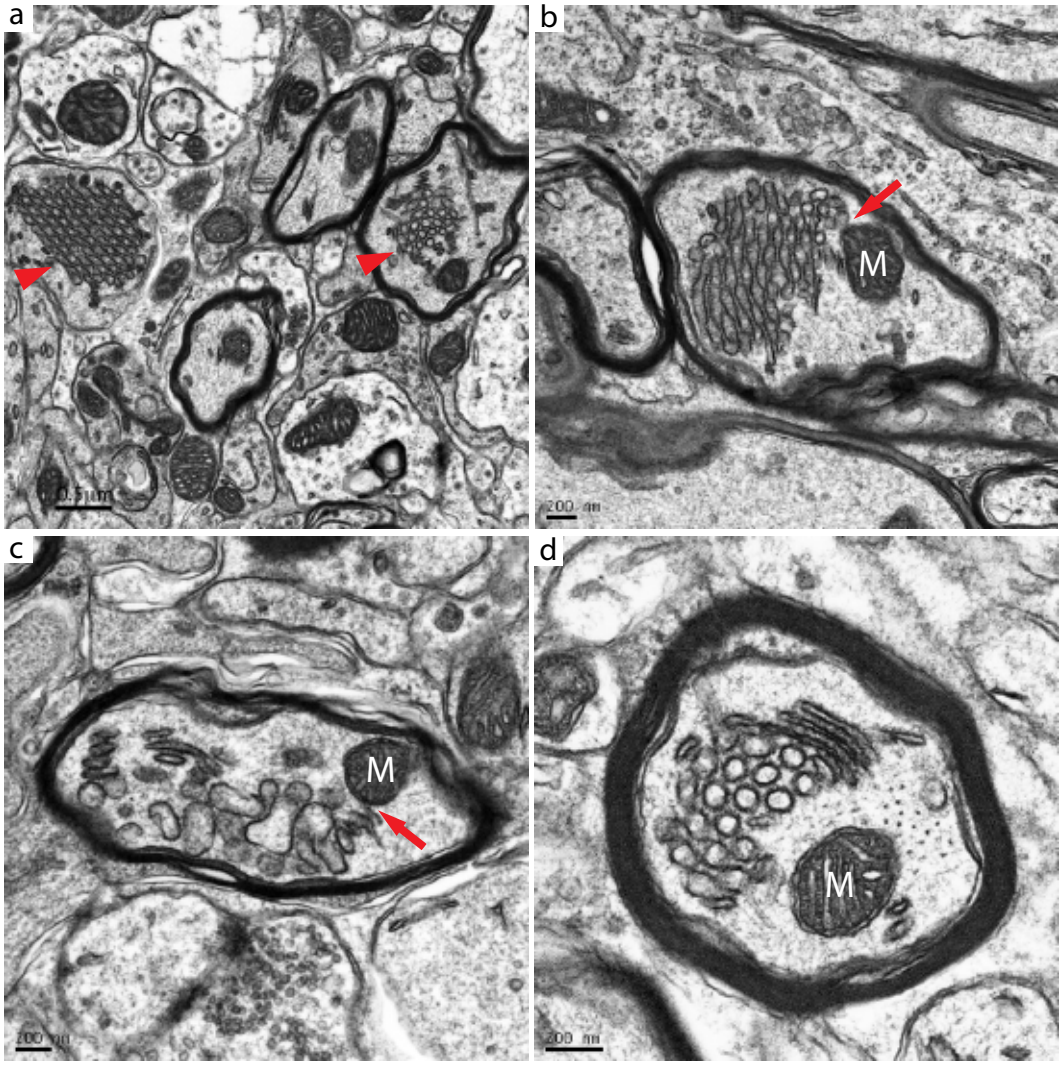

clathrin coated vesicles (Fig. 5d). In most cases, such structures were adjacent to the mitochondria that are often observed in normal myelinated axons, and interestingly sometimes the structures seemed to be connected to the outer membranes of the mitochondria (Fig. 5b&c, arrows).

3.2.4 Deletion of Beclin 1 induces localization change of PtdIns(3)P in Purkinje cells

In C. elegans, deletion of *beclin 1* ortholog *bec-1* caused disappearance of PtdIns(3)P, which is the product of C. elegans class III PI3-kinase LET-512/Vps34, from cytoplasmic membranes and vesicles in larvae (Takacs-Vellai et al., 2005). To test if deletion of *beclin 1* in mice has similar effect, immuno-staining was performed on slices of the cerebellum from P21 mice using anti-PtdIns(3)P antibody. In *beclin 1*$^{flox/flox}$ Purkinje cells, PtdIns(3)P showed punctate localization, while in *beclin 1*$^{flox/flox}$; Pcp2-Cre Purkinje cells its localization became much less confined and was diffuse throughout the whole cytoplasm. Therefore deletion of *beclin 1* changed the localization pattern of PtdIns(3)P from possibly membrane and vesicle bound to largely cytoplasmic.

In summary, deletion of Beclin 1 in Purkinje cells resulted in fast and severe cell degeneration, although the mechanism underlying the degeneration is not clear. Staining with autophagy and apoptosis markers showed that neither of them was activated, therefore the Purkinje cell death may be through alternative pathways, and may be related to altered Vps34/PtdIns3K function.

Figure 2-6. Localization change of PtdIns(3)P in *beclin 1*$^{flox/flox}$; Pcp2-Cre Purkinje cells

(a) Immuno-staining with anti-PtdIns(3)P antibody showed that in *beclin 1*$^{flox/flox}$ Purkinje cells PtdIns(3)P was localized on punctate and vesicular structures that were possibly early endosomes and multivesicular endosomes.

(b) Anti-PtdIns(3)P antibody staining on *beclin 1*$^{flox/flox}$; Pcp2-Cre Purkinje cells showed that the localization of PtdIns(3)P produced was more diffuse and localized throughout the whole cytoplasm.

Figure 2-6

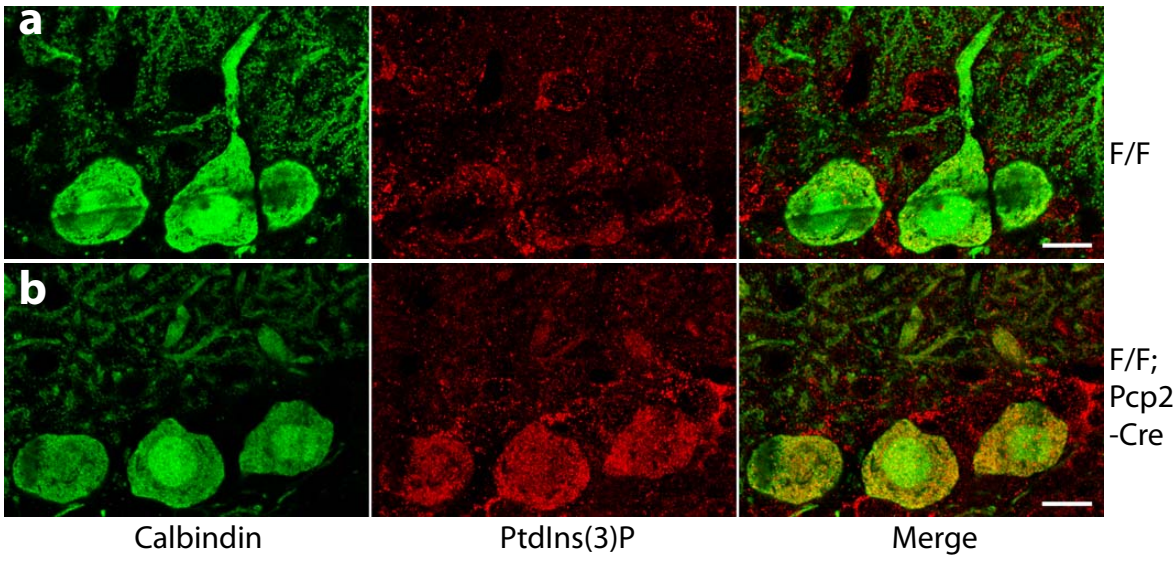

3.3 Characterization of Beclin 1 function in cortical and hippocampal neurons

3.3.1 Beclin 1 expression is reduced in cortical and hippocampal tissues in *beclin 1*$^{flox/flox}$; EMX-Cre mice

Beclin 1$^{flox/flox}$ mice were crossed to transgenic mice that express Cre recombinase under the control of EMX promoter (EMX-Cre) to delete *beclin 1* expression in cortical and hippocampal neurons. The expression of EMX gene and the recombination driven by its promoter both start from early embryonic stage (Guo et al., 2000). Compared to *beclin 1*$^{flox/flox}$ mice, *beclin 1*$^{flox/flox}$; EMX-Cre mice showed reduced body sizes from as early as P15, and this difference persisted along development (Fig. 6a). Compared to *beclin 1*$^{flox/flox}$ mice that rarely showed early death, mortality was observed in *beclin 1*$^{flox/flox}$; EMX-Cre mice from the age of 6 weeks, and almost all mice died by the age of 2 months.

To confirm that Beclin 1 protein level is reduced due to deletion of the gene, the cortex and hippocampus region of the brain was dissected out from a *beclin 1*$^{flox/flox}$; EMX-Cre mouse and a *beclin 1*$^{flox/flox}$ mouse at P25, and lysates were prepared. Western blot with anti-Beclin 1 antibody showed that compared to the level in control mouse, the Beclin 1 protein level in the *beclin 1*$^{flox/flox}$; EMX brain lysate was significantly lower (Fig. 6b).

3.3.2 Accumulation of p62/SQSTM1 protein in *beclin 1*$^{flox/flox}$; EMX-Cre neurons

In cultured NIH/3T3 cells, knockdown of Beclin 1 protein level with RNAi resulted in changes in autophagy level and accumulation of p62/SQSTM1 protein in the cells. In order to study if loss of Beclin 1 induces the same changes in cortical and hippocampal neurons, brain sections were first stained with anti-p62/SQSTM1 antibody.

Figure 2-7. Reduced body size of *beclin 1*$^{flox/flox}$; EMX-Cre mice

(a) *Beclin 1*$^{flox/flox}$; EMX-Cre mice showed reduced body size at P15, and by 1 month, the body size of *beclin 1*$^{flox/flox}$; EMX-Cre is only about half of *beclin 1*$^{flox/flox}$ mice.

(b) Reduced Beclin 1 protein level in *beclin 1*$^{flox/flox}$; EMX-Cre cerebral cortex. Lysates from P25 *beclin 1*$^{flox/flox}$ and *beclin 1*$^{flox/flox}$; EMX-Cre cerebral cortex tissues were used for western blot against anti-Beclin 1 antibody. Beclin 1 protein level was significantly lower in *beclin 1*$^{flox/flox}$; EMX-Cre than in *beclin 1*$^{flox/flox}$ mice.

Figure 2-7

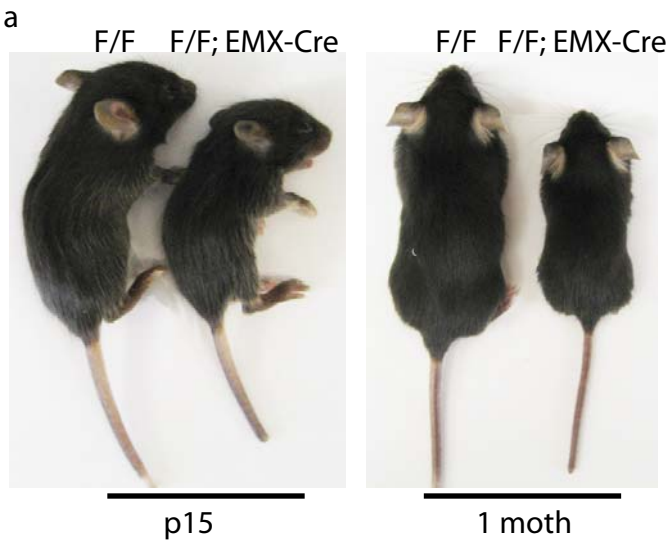
a
F/F
F/F; EMX-Cre
F/F
F/F; EMX-Cre
p15
1 moth

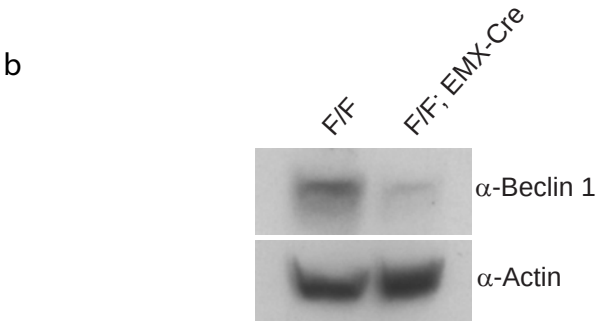
b
F/F
F/F; EMX-Cre
α-Beclin 1
α-Actin

As a result, strong accumulation of p62/SQSTM1 was observed in *beclin 1*$^{flox/flox}$; EMX-Cre hippocampal pyramidal cells in CA1-CA3 area at P12 (Fig. 7a). Such accumulation occurred in the cytosol (Fig. 7b), and was not observed in dendate gyrus neurons or in *beclin 1*$^{flox/flox}$ mice (Fig. 7a and data not shown). This suggested that deletion of Beclin 1 in hippocampal pyramidal cells may have impaired autophagy and caused accumulation of p62/SQSTM1 that failed to be degraded by autophagy. Despite intracellular accumulation of p62/SQSTM1, with anti-NeuN antibody staining, the pyramidal cells in CA1-CA3 areas in *beclin 1*$^{flox/flox}$; EMX-Cre mice showed comparable cell density to *beclin 1*$^{flox/flox}$ mice at P12 (Fig. 7a). However by P15 the cell density in these areas had greatly decreased and p62/SQSTM1 accumulation was still observed in many of the remaining pyramidal cells (Fig. 7c).

Accumulation of p62/SQSTM1 was also observed in cortical neurons of *beclin 1*$^{flox/flox}$; EMX-Cre mice. At P12, only scattered neurons in the pre-frontal area of the cortex showed accumulation (Fig. 8a), and like in hippocampal pyramidal cells, the accumulation was in the cytosol (Fig. 8b). By P15, the p62/SQSTM1 accumulation was observed in a large number of cortical neurons, and interestingly the majority of such neurons were within the top layers in the pre-frontal area (Fig. 8c). Similar pattern was observed in P21 cortex as well (Fig. 8d). However, by the age of one month, p62/SQSTM1 accumulation in the cortex had become less obvious, with only scattered neurons showing accumulation again, and the number of such neurons further decreased by older ages (data not shown)

Figure 2-8. Accumulation of p62/SQSTM1 protein in *beclin 1*$^{flox/flox}$; EMX-Cre hippocampal pyramidal cells

(a) At P12, strong accumulation of p62/SQSTM1 protein was observed in pyramidal cells within CA1 area of the *beclin 1*$^{F/F}$; EMX-Cre hippocampus. Scale bar: 100μm

(b) The p62/SQSTM1 protein was accumulating in the cytosol of the pyramidal cells. Scale bar: 20μm

(c) At P15, strong accumulation of p62/SQSTM1 protein still remains in *beclin 1*$^{flox/flox}$; EMX-Cre hippocampal pyramidal cells. The decreased density of neurons suggested the beginning of cell loss. Scale bar: 100μm

Figure 2-8

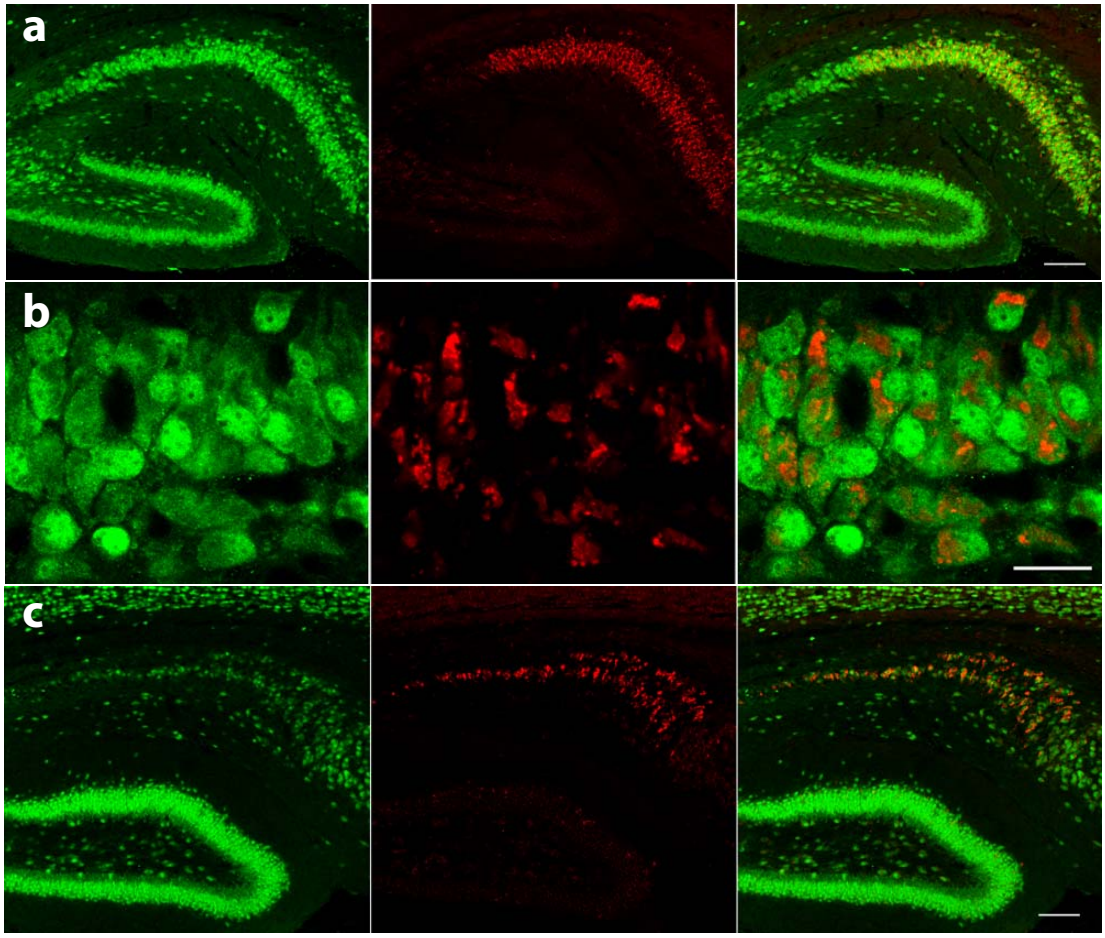

3.3.3 Activation of Caspase3 in *beclin 1*$^{flox/flox}$; EMX-Cre mice

By P15, the density of CA1-CA3 area hippocampal pyramidal cells have decreased significantly in *beclin 1*$^{flox/flox}$; EMX-Cre mice (Fig. 7c). In order to study the possible mechanism underlying the neuronal degeneration, brain sections from *beclin 1*$^{flox/flox}$; EMX mice were stained with antibody against activated Caspase3 to study whether there was activation of apoptotic pathway. At P12 when there was strong accumulation of p62/SQSTM1 in CA1 hippocampal pyramidal cells, no obvious activated Caspase3 signal was observed in that area (data not shown). This is consistent with the observation that the cell density in that area was comparable to control mice at that age. At P15, when the cell density had greatly decreased, strong activated Caspase3 signal was observed in the CA1-CA3 area but not in the dentate gyrus of the hippocampus in *beclin 1*$^{flox/flox}$; EMX-Cre mice, or in control *beclin 1*$^{flox/flox}$ mice (Fig. 9a and data not shown). The activation of Caspase3 reached its peak at P21, as indicated by the massive antibody staining, and gradually decreased after that (Fig. 9b). By the age of 6 weeks, activated Caspase3 signal was still able to be observed in the hippocampus (Fig. 9c).

In contrast to hippocampus where strong activated Caspase3 signal was observed, the signal from the cerebral cortex was much weaker and only very few cells in the cortex showed activation of Caspase3 at P15 (Fig. 10a). By P21, the number of such cells increased and they were mainly distributed in the upper to middle part of layer V of the cortex (Fig. 10b). By the age of 6 weeks, Caspase3activation spread to a wider area within the cortex: signal was also observed in layer II/III in addition to layer V (Fig. 10c). Therefore unlike in the hippocampus of *beclin 1*$^{flox/flox}$; EMX mice where the activation

Figure 2-9. Accumulation of p62/SQSTM1 protein in *beclin 1*$^{flox/flox}$; EMX-Cre cortical neurons

(a) At P12, accumulation of p62/SQSTM1 protein was observed in scattered pyramidal neurons within pre-frontal area of the *beclin 1*$^{flox/flox}$; EMX-Cre cerebral cortex. Scale bar: 100μm

(b) The p62/SQSTM1 protein was accumulating in the cytosol of the pyramidal neurons. Scale bar: 20μm

(c-d) At P15 (c) and P21 (d), strong accumulation of p62/SQSTM1 protein was observed in the top layer (layer II/III) neurons of the *beclin 1*$^{F/F}$; EMX-Cre cerebral cortex. In deeper layers, only limited number of neurons showed p62/SQSTM1 accumulation. Scale bar: 100μm

Figure 2-9

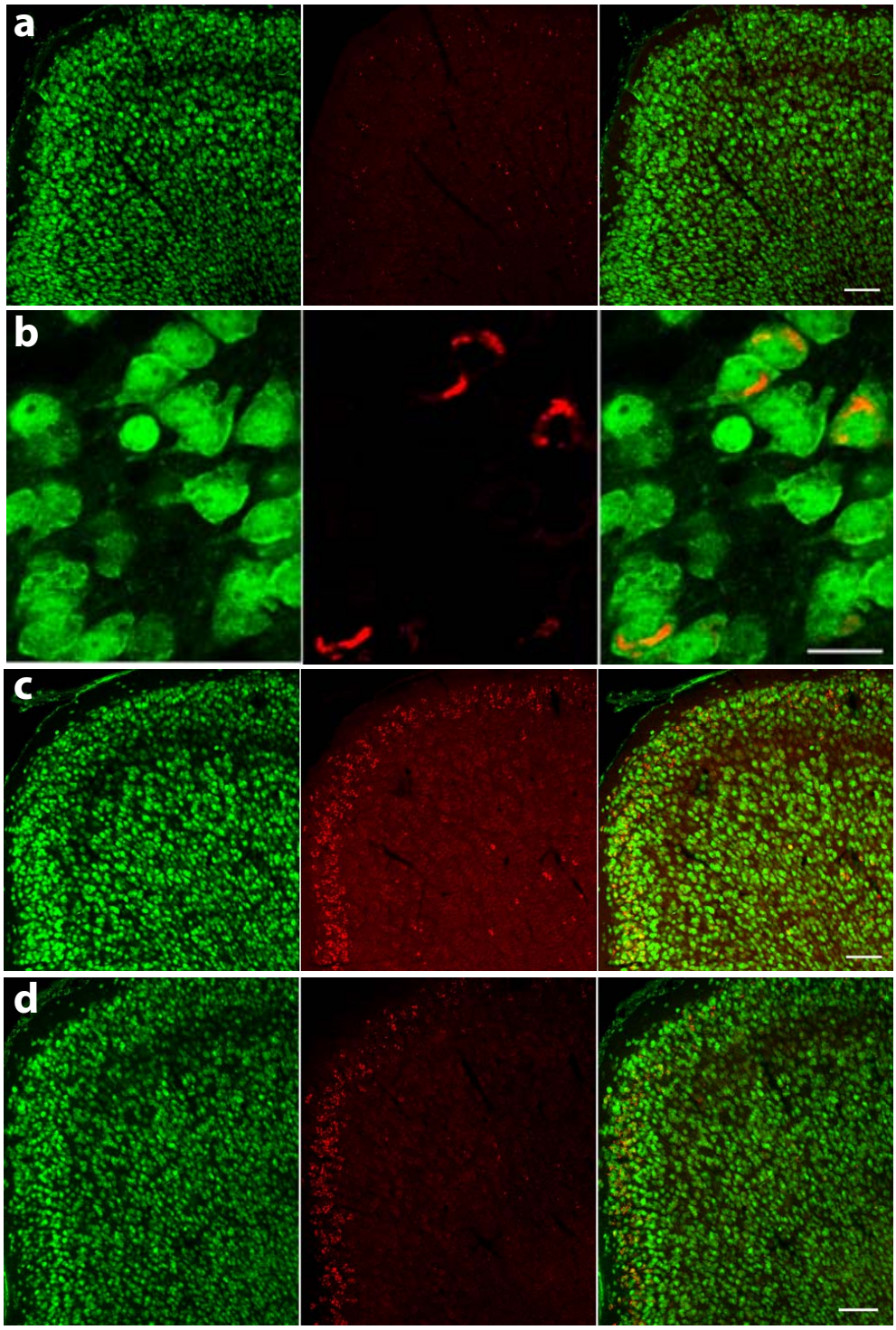

of apoptotic pathway peaked at P21, it gradually increased within the cerebral cortex and showed different layer specificity at different ages.

3.3.4 Aberrant ultra-structures in degenerating *beclin 1*$^{flox/flox}$; EMX-Cre hippocampal pyramidal cells

To further characterize the degeneration of *beclin 1*$^{flox/flox}$; EMX-Cre hippocampal pyramidal cells, electron microscopy was performed. CA1 area in P12 mice was examined because at this age there was severe accumulation of p62/SQSTM1 protein in this area in *beclin 1*$^{flox/flox}$; EMX-Cre cells while the overall cell density was comparable to that in control mice. Therefore degeneration is still at early stage.

As a result, a large number of electron dense structures and aberrant membranous structures were observed in *beclin 1*$^{flox/flox}$; EMX-Cre hippocampal pyramidal cells but not in control cells (Fig. 2-12). Under EM, some pyramidal cells showed severe degeneration and reduced sizes (Fig. 2-12a, arrowheads). In these cells, large electron dense structures were observed and they occupied almost all the remaining cytoplasmic area of the shrinking cells (Fig. 2-12a&b, asterisks). These structures often had concentric membranous structure next to or even connected to them (Fig. 2-12b, arrowheads). In other cells that showed relatively normal sizes, early accumulation of smaller electron dense structures was observed (Fig. 2-12a, area boxed in red and enlarged in Fig. 2-12c). Accumulation possibly started from aberrant less electron dense structures that were widespread in the cytoplasm (Fig. 2-12c&d, asterisk), and they gradually became more electron dense and took up round shape (Fig. 2-12c, arrowheads).

Figure 2-10. Activation of Caspase3 in *beclin 1*$^{flox/flox}$; EMX-Cre hippocampus

(a) At P15, staining with antibody against activated caspase3 showed strong signal in CA1 and CA3 areas of the *beclin 1*$^{flox/flox}$; EMX-Cre hippocampus. Meanwhile, the cell density in these areas was greatly reduced. Scale bar: 100μm

(b) Stronger signal of activated caspase3 was observed at P21 in *beclin 1*$^{flox/flox}$; EMX-Cre hippocampus, and cell density further decreased. Scale bar: 100μm

(c) At the age of 6 weeks, massive activation of caspase3 in *beclin 1*$^{flox/flox}$; EMX-Cre hippocampus was still observed, although the intensity was lower compared to that at P21. Scale bar: 100μm

Figure 2-10

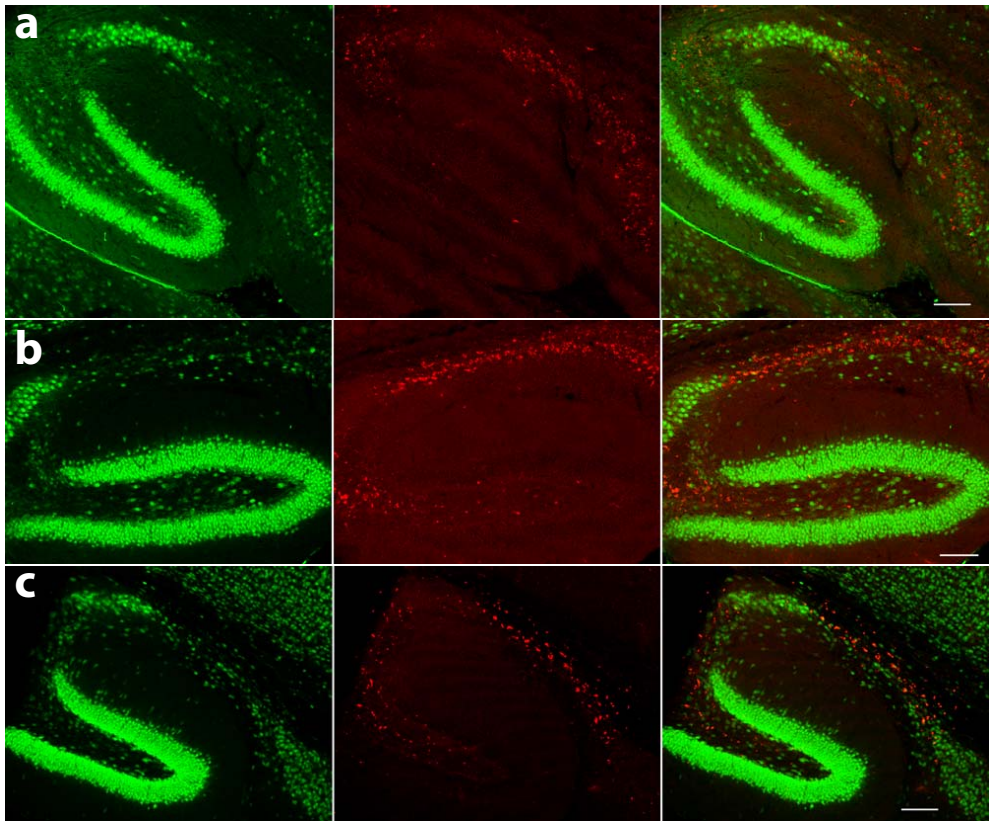

Meanwhile, double membrane vesicles containing electron dense materials were often observed in these cells (Fig. 2-12c, arrows). In some cells, membrane sacs that were possibly in the process of enwrapping electron dense structures (Fig. 2-12d, arrowhead) and newly formed double membrane vesicles (Fig. 2-12d, arrow) were observed. In some other cells, fusion among the small electron dense structures was observed (Fig. 2-12e, arrowheads), and continued fusion of this kind likely accompanied cell degeneration and ultimately generated the large structures observed above (Fig. 2-12a&b, asterisks). Furthermore, these large electron dense structures would fuse with surrounding concentric membranous structures (Fig 2-12f, asterisk).

In summary, deletion of Beclin 1 in cortical and hippocampal pyramidal cells resulted in intracellular accumulation of p62/SQSTM1 protein and activation of Caspase3, suggesting that autophagy in the neurons was disrupted and apoptotic pathway was activated. Furthermore, accumulation p62/SQSTM1 was observed and peaked at earlier ages than activation of Caspase3, suggesting that it preceded and might have been one of the reasons that caused activation of apoptotic pathway. A large number of electron dense structures and abnormal membranous structures were observed in degenerating *beclin* $1^{flox/flox}$; EMX-Cre hippocampal pyramidal cells, suggesting that similar to the degeneration of *beclin* $1^{flox/flox}$; Pcp2-Cre Purkinje cells, the degeneration of pyramidal cells may also be related to disrupted intracellular vesicle formation or trafficking. Interestingly, neither p62/SQSTM1 accumulation nor Caspase3 activation was detected in *beclin* $1^{flox/flox}$; Pcp2-Cre Purkinje cells. Moreover, the electron dense structures observed in Purkinje cells and in pyramidal cells were not identical. This suggests that in response to the same Beclin 1 deletion, cerebellar Purkinje cells and hippocampal

Figure 2-11. Activation of Caspase3 in *beclin 1*$^{flox/flox}$; EMX-Cre cerebral cortex

(a) At P15, only very few cells in the *beclin 1*$^{flox/flox}$; EMX-Cre cerebral cortex showed activated caspase3 signal. Scale bar: 100μm

(b) Stronger signal of activated caspase3 was observed at P21 in *beclin 1*$^{flox/flox}$; EMX-Cre cerebral cortex, and cells that showed activation of caspase3 were mainly distributed in the middle part (layer V) of the cortex, showing layer specificity. Scale bar: 100μm

(c) At the age of 6 weeks, activation of caspase3 was no longer restricted to layer V and more cells in upper layers of the *beclin 1*$^{flox/flox}$; EMX-Cre cerebral cortex was showing activation of caspase3. Scale bar: 100μm

Figure 2-11

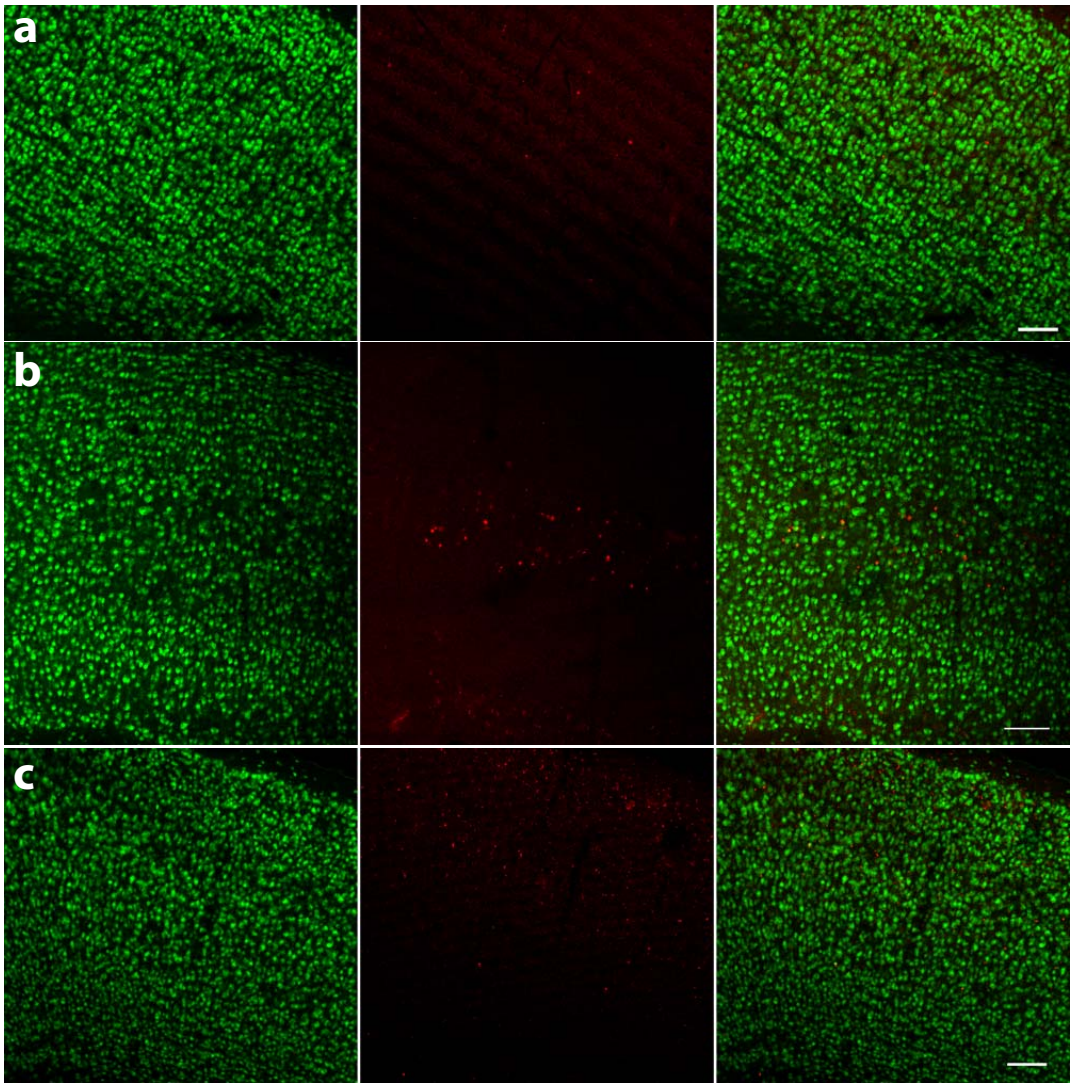

pyramidal cells may activate different pathways and react in different manners, although ultimately they all end up in degeneration.

Figure 2-12. Aberrant ultra-structures in degenerating *beclin 1*$^{flox/flox}$; EMX-Cre hippocampal pyramidal cells

(a) Under electron microscopy, some P12 *beclin 1*$^{flox/flox}$; EMX-Cre hippocampal pyramidal cells showed features of late stage degeneration (arrowheads). Large-sized electron dense structures were observed and occupied almost all the cytoplasmic area of these cells. The area boxed in red is enlarged in (c). Scale bar: 5μm.

(b) Higher magnification image of one degenerating neuron in (a). Concentric membranous structures (arrowheads) were observed next to and connected to the large-sized electron dense structure. Scale bar: 1μm.

(c) Enlarged image of the area boxed in red in (a). A large number of widespread less electron dense structures (asterisk), many round shaped more electron denser structures (arrowheads), and double membrane-enwrapped vesicles (arrows) were observed in the cytoplasm of a neuron that was at a relatively early stage of degeneration. Scale bar: 500nm

(d) Another example of early stage degenerating neurons. An isolation membrane sac was about to enwrap a small electron dense structure (arrowhead). Nearby, there was a newly formed double membrane vesicle containing electron dense materials (arrow). Scale bar: 500nm.

(e) Possible fusion among small electron dense structures to form the large-sized accumulation bodies shown in (a) and (b). Scale bar: 500nm.

(f) A late stage degenerating neuron, in which the multiple-membrane structures (arrowheads) were starting to fuse with the accumulation body (asterisk). Scale bar: 500nm.

Figure 2-12

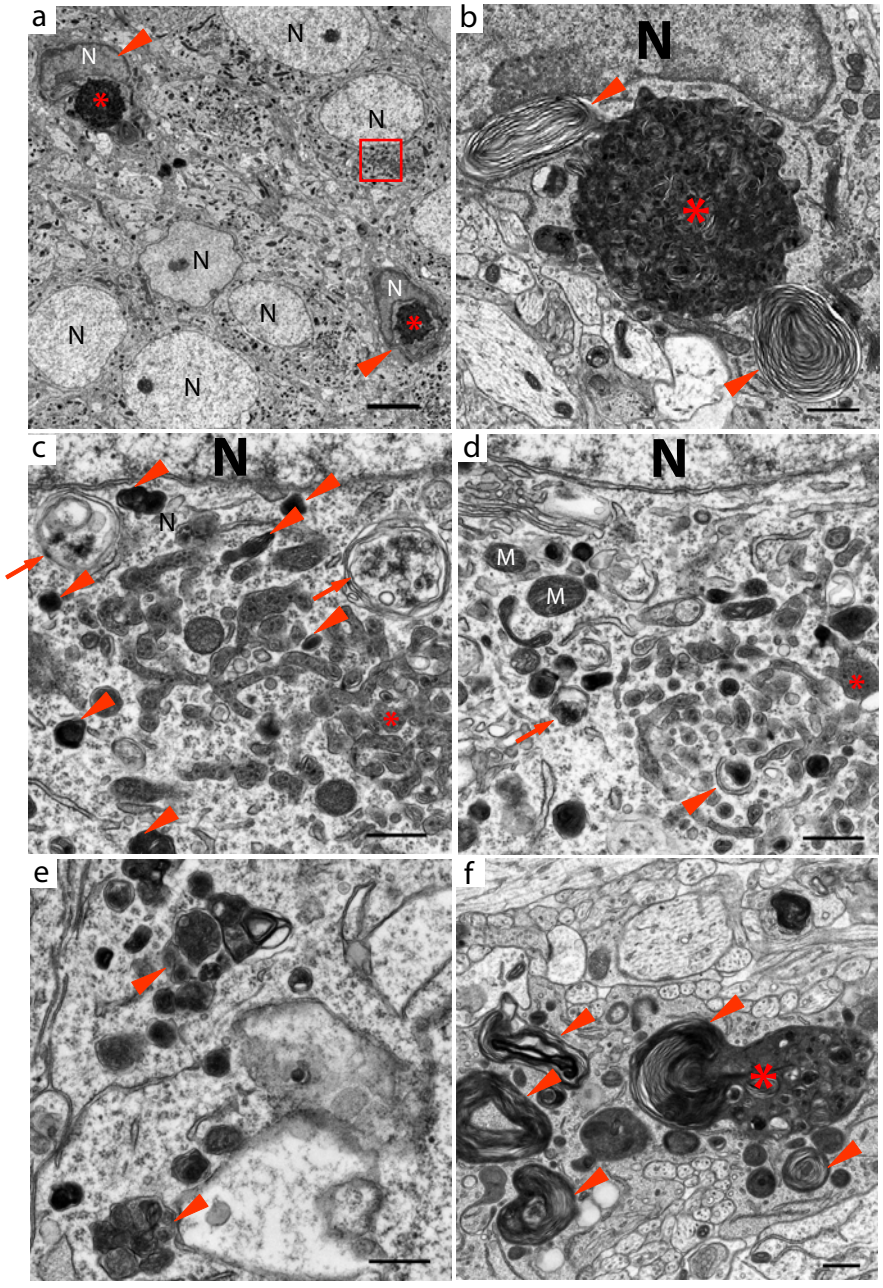

Chapter IV

Discussion

4.1 Identification of Beclin 1 interaction proteins

A rescued mouse was generated and used for identification of Beclin 1 interaction proteins in this study. Under the endogenous promoter and other possible regulatory elements that were contained in the BAC, it could be estimated that expression of *beclin 1-EGFP* followed loyally the expression pattern of the endogenous gene, and this was confirmed with staining tissue sections from Beclin 1-EGFP transgenic mice (Arsov et al., 2008). Homozygous deletion of *beclin* 1 gene expression is embryonic lethal and the embryos die at around embryonic day 7.5 (E7.5). After crossing experiments, mice that have both *beclin 1* alleles deleted but the transgene *beclin 1-EGFP* expressed (*beclin* $1^{-/-}$; *beclin 1-EGFP*, rescued mice) were born normally and the ratio of positive rescued pups to controls followed the Mendel's law. The rescued mice showed no developmental abnormality, and further crossing experiments showed that they were also able to reproduce normally. Therefore it could be concluded that the rescue by Beclin 1-EGFP fusion protein was complete and the fusion protein possesses the physiological functions of the endogenous protein.

In identifying interaction proteins, the rescued mice have several advantages over cultured cell lines, which are often used to over-express tagged proteins with transient or stable transfection. Over-expression of proteins in cultured cells is unphysiological, and often results in production of proteins at levels that are extremely high compared to their endogenous levels *in vivo*. As a result, the proteins produced may simply accumulate in

the cell without functioning properly, or may even start to interact with other proteins non-specifically. Furthermore, a certain protein may have different interaction partners in different tissues, and using a single cell type will not be able to identify all the possible interaction partners. In contrary to cell lines, the rescued mice provided a physiological environment for identification of interaction proteins. The level of fusion protein expression in the Beclin 1-EGFP transgenic mice is comparable to that of the endogenous protein, therefore no excess of fusion protein is created and non-specific binding is unlikely. In addition, since both endogenous *beclin 1* alleles are deleted, there is no competition between endogenous protein and the fusion protein for binding with interaction partners. As a result, all proteins that bind to endogenous Beclin 1 can be expected to bind to Beclin 1-EGFP instead and to be immunoprecipitated. Finally, driven by the endogenous promoter and regulatory elements, the Beclin 1-EGFP fusion protein is expressed ubiquitously in almost all tissue and cell types like endogenous Beclin 1. As a result, it will be possible to use different tissues to study if any identified interaction protein is a general one that most tissues share or is tissue-specific.

Using the rescued mice, at least six interaction proteins were identified from brain, liver and thymus. This suggested that the identified proteins bind to Beclin 1 across different tissue types and therefore are likely to be involved in the general regulation of Beclin 1 function and possibly autophagy as well. Within the six proteins, Vps34/PtdIns3K, Vps15 and UVRAG are already known Beclin 1 interaction proteins. Vps34/PtdIns3K is the major binding partner of Beclin 1, and it was reported that all Beclin 1 protein within the cells is associated with Vps34/PtdIns3K. Meanwhile, Vps15 is the activator essential for Vps34/PtdIns3K function and UVRAG has been shown to

directly bind to Beclin 1. From these three proteins it could be confirmed that the *in vivo* immunoprecipitation from rescued mouse tissues was successful.

Interestingly, the seven bands (six interaction proteins and the Beclin 1-EGFP fusion protein itself) visualized with Coomassie blue staining showed different intensity. Beclin 1-EGFP, Vps34/PtdIns3K, Vps15 and UVRAG showed comparably strong intensity, while the intensity of Rubicon, Atg14L and Nrbf2 was much weaker. *In vivo* immunoprecipitation was repeated and the same pattern was always observed (data not shown). This suggests that the binding affinity among these proteins may be different: Beclin 1 may have stronger or more stable binding with Vps34/PtdIns3K, Vps15 and UVRAG than with Rubicon, Atg14L and Nrbf2. Another possibility is that the different intensity may reflect the stoichiometry of protein complex composition: Beclin 1 may bind to more Vps34/PtdIns3K, Vps15 and UVRAG than to Rubicon, Atg14L and Nrbf2.

Surprisingly, although Beclin 1 was first identified as a Bcl-2 interaction protein, Bcl-2 was not identified from this study. Even western blot with Bcl-2 antibody failed to detect any Bcl-2 in the protein mixture from the *in vivo* immunprecipitation (data not shown). And the recently identified Beclin 1 interaction proteins Bif1 and Ambra1 were not identified either. The tissue lysates used in this study for *in vivo* immunoprecipitation was prepared under mild detergent condition, using Triton X100 at the final concentration of 0.2%. Under this condition, the pellet after centrifugation that was not used still contained a certain amount of Beclin 1 (data not shown). Therefore, it is likely that only some insoluble membrane-bound Beclin 1 is interacting with Bcl-2 and this is consistent with a previous report that unlike the major Beclin 1 interaction protein Vps34/PtdIns3K that is localized predominantly on endosomes and trans Golgi network

(Gillooly et al., 2000), Bcl-2 is localized mainly on the outer mitochondrial and ER membranes (Germain and Shore, 2003; Pattingre et al., 2005). Interestingly it has also been reported that full-length Beclin 1 does not interact with Bcl-2 in the yeast two-hybrid system (Liang et al., 1998) and that the interaction between endogenous Beclin 1 and Bcl-2 was not detected in certain cell lines (Zeng et al., 2006). Therefore this interaction may also be transient or unstable that only occurs under specific conditions and therefore was not detected from *in vivo* immunoprecipitation in this study. The same scenario may also be true for interaction between Beclin 1 and Bif1 or Ambra1. Moreover, although the interaction proteins identified in this study seem to be general ones that are shared by multiple tissues, the possibility can not be ruled out that Beclin 1 may have tissue or cell type specific binding partners. Further thorough study focusing on specific tissues will be able to answer this question.

4.2 Beclin 1 containing protein complexes in mammalian cells

Three novel Beclin 1 interaction proteins Atg14L, Rubicon and Nrbf2 and three already known proteins Vps34/PtdIns3K, Vps15 and UVRAG were identified in this study. It is an interesting question how many protein complexes may exist in mammalian cells. In yeast Atg6p forms two distinctive protein complexes with either Atg14p to regulate autophagy, or with Vps38p to mediated CPY sorting (Kihara et al., 2001b). However forced expression of *beclin 1* in yeast strains that are deficient in *atg6* only restored autophagy but did not rescue the disrupted CPY sorting pathway (Liang 1999). It is not due to the stable protein expressed, and this defect persisted even when Vps38p

was over-expressed (Melendez et al., 2003). Therefore Beclin 1 may be able to functionally interact with Atg14p but not with Vps38p.

It is not clear how many Beclin 1-containing protein complexes exist in mammalian cells and what their composition is. In this study, endogenous immunoprecipitation using Atg14L and Rubicon antibodies initially suggested that they might exist in different protein complexes, since they failed to pull down each other although they both were able to pull down Beclin 1 and Vps34/PtdIns3K. However, gel filtration from both wild type and rescued mouse tissues showed that Beclin 1, Vps34/PtdIns3K, Atg14L and Rubicon all eluted in the same fractions, although Atg14L and Rubicon both eluted in later fractions as well that may represent smaller protein complexes. This strongly suggests that all these proteins can co-exist in one same large protein complex, and this was confirmed from transient transfection and co-immunoprecipitation experiments. Although the gel filtration experiment in this study was not able to show distribution of UVRAG, it should be reasonable to hypothesize that it also exists in this large complex given the fact that UVRAG and Beclin 1 bind directly to each other (Liang et al., 2006), and this hypothesis is supported by co-immunoprecipitation as well. In addition to this large complex, it is possible that there are multiple smaller Beclin 1-related protein complexes in mammalian cells. Some complexes may contain only Atg14L while others may contain only Rubicon, which is consistent with the results from endogenous immunoprecipitation using Atg14L and Rubicon antibodies. These smaller complexes may be derived from the initial large complex, and may be the ones that actually mediate Beclin 1's function.

4.3 Beclin 1-Atg14L interaction

The protein Atg14L identified in this study showed moderate homology to yeast protein Atg14p, and the homology was shared mainly in the coiled-coil domain region that was shown to be essential for interaction between Beclin 1 and Atg14L. Like yeast Atg14p, Atg14L showed strong binding affinity to Beclin 1. Upon co-transfection Atg14L and Beclin 1 both changed intracellular localization pattern dramatically and became co-localized with each other completely. In yeast, Atg6p and Atg14p are both peripherally associated with membrane fractions, and pretreatment of cell extract with detergent did not disrupt the interaction between Atg6p and Atg14p, indicating that they are binding directly (Kametaka et al., 1998). Whether Beclin 1 and Atg14L bind to each other directly in mammalian cells was not characterized in this study and future binding assay using recombinant proteins will provide an answer to this question. In yeast, Atg6p is important for the stabilization of Atg14p, because Atg14p was barely detectable in Atg6 mutant cells (Kihara et al., 2001b). Similarly, in mammalian cells Beclin 1 is essential for stabilization of Atg14L too, since transfection of Beclin 1 siRNA resulted in significant decrease of Atg14L protein level. And in consistence with this, when Atg14L-EGFP alone was transfected into cells, only dim fluorescence was observed, indicating the lack of abundance of the protein in the cells. However when Beclin 1 was co-transfected, the fluorescent signal of Atg14L-EGFP became much stronger, possibly because more protein was stabilized through forming complexes with over-expressed Beclin 1.

Atg14L also share some functional similarity with yeast Atg14p. Atg14L positively regulates both Vps34/PtdIns3K kinase activity and autophagy levels in the

cells, and co-transfection of Beclin 1 and Atg14L induced electron dense structures that were not observed in cells transfected with either Beclin 1 or Atg14L alone. Such structures were clearly not aggresomes that arose from over-production of proteins since they were surrounded by double membranes. Autophagy proteins that participate in autophagosome formation such as Atg5, Atg12 and LC3 were found co-localized on these structures, suggesting that these structures were possibly pre-autophagosomal structures (PAS) that Atg6p and Atg14p in yeast are localized on. Therefore it is likely that Beclin 1 and Atg14L function together to promote the initial steps of autophagosome formation. In consistence with this, co-transfection of Beclin 1 and Atg14L induced membrane rearrangement in the cells and increased number of autophagosomes were observed in the transfected cells.

It is likely that Atg14L may promote autophagy levels by positively regulating Vps34/PtdIns3K kinase activity, and Beclin 1 is essential for this since only with co-transfection of Beclin 1 did Atg14L increase the kinase activity of Vps34/PtdIns3K. Beclin 1 increased the binding between Atg14L and Vps34/PtdIns3K, and meanwhile, with the presence of Atg14L, Vps34/PtdIns3K was able to pull down more Beclin 1. Therefore Beclin 1 and Atg14L enable each other to form a more stable complex with Vps34/PtdIn3K and this complex that contains these three proteins and possibly Vps15 may be one of the smaller functioning complexes, which promotes induction of autophagy and autophagosome biogenesis.

However to determine whether *Atg14L* is truly the ortholog of yeast *Atg14*, a complement experiment showing that forced expression of *Atg14L* in *Atg14* null yeast cells can restore the autophagy level will be necessary. And if that is the case, then the

yeast Atg6p-Atg14p-Vps34p-Vps15p sub-complex is also well conserved from yeast to mammalian cells like other autophagy proteins.

Treatment of *Bax/Bak*$^{-/-}$ cells with Beclin 1 siRNA also reduced Atg5-Atg12 protein levels (Shimizu et al., 2004), indicating that like Atg14L, protein stabilization of Atg5-Atg12 may also be dependent on Beclin 1. Therefore combining the data from this study, it can be concluded that Beclin 1 is genuinely a key protein in autophagy induction.

4.4 The functions of Rubicon

Atg6p forms a second protein complex in yeast with Vps38p, and whether Rubicon might be its mammalian ortholog was studied. However no homology was observed between Rubicon and Vps38p and there is very little functional similarity between Rubicon and Vps38p. Previous studies (Kihara et al., 2001b) show that Vps38p mediates interaction between Atg6p and Vps34p, since the interaction is disrupted in *Vps38* mutant cells. However, Rubicon is showing a rather inhibitory effect on interaction between Beclin 1 and Vps34/PtdIns3K. Vps38p level is not detectable in *Atg6* mutant cells, indicating that Atg6p is essential for Vps38p stabilization. When Beclin 1 protein level was knocked down with RNAi in NIH/3T3 cells, Rubicon protein level showed little change compared to control conditions. Moreover, deletion of *Vps38* in yeast significantly reduced the PtdIns 3-kinase activity, indicating the positive regulatory function of Vps38p. On the contrary, Rubicon negatively regulates the kinase activity of Vps34/PtdIns3K. Therefore *Rubicon* is clearly not the mammalian ortholog of *Vps38* and if a mammalian ortholog does exist it still remains to be identified.

In contrast to Atg14L, Rubicon negatively regulates autophagy, and it may also be through its negative regulation on Vps34/PtdIns3K kinase activity. Interestingly unlike in the case of positive regulation by Atg14L, this negative regulation is inhibited by Beclin 1, since it diminished in the presence of over-expressed Beclin 1. Meanwhile, over-expression of Rubicon decreased the amount of Vps34/PtdIns3K that Beclin 1 was able to bind, although Beclin 1 did not interfere with the binding between Rubicon and Vps34/PtdIns3K. Therefore Rubicon and Beclin 1 may be inhibitory on each other's binding to Vps34/PtdIns3K, or may be competing to bind to it in an exclusive manner. And the inhibition of Rubicon's negative regulation on autophagy by Beclin 1 may be part of the functions of Beclin 1 in promoting autophagy induction. Interestingly, in cells transiently transfected with Rubicon-EGFP, starvation induced significant increase of binding between Rubicon-EGFP and Beclin 1. This increase of binding may be important for starvation induced autophagy activation because it inhibits the negative regulation by Rubicon on Vps34/PtdIns3K and therefore results in a positive regulation.

Over-expression of Rubicon resulted in massive abnormal vesicle structures that were labeled positive for late endosome/early lysosome marker LAMP1 and multi-vesicular body marker LBPA, suggesting that Rubicon is likely to be involved in endocytic pathway in addition to its function in autophagy regulation. To test whether endocytosis is affected by over-expression or protein knock-down of Rubicon, horse radish peroxidase (HRP) intake and epidermal growth factor (EGF) induced receptor (EGFR) internalization was examined in cells transfected with either Rubicon-EGFP or Rubicon siRNA. In both cases, no significant difference was observed between Rubicon transfected cells and control cells. Therefore the internalization step of endocytosis

appears not significantly affected by Rubicon, and this is consistent with the observation that only a small number of Rubicon induced structures were positive for early endosome marker EEA1. Rubicon blocks autophagosome maturation, and the reason can be either that the fusion step of autophagosomes with lysosomes is inhibited, or that lysosomes themselves fail to develop normally. Therefore, the involvement of Rubicon in endocytic pathway may also be at a relatively late stage, such as maturation of endosomes and their fusion with lysosomes.

The functions of Rubicon in endocytic pathway may also be closely related to Vps34/PtdIns3K. Although the C-terminal cysteine-rich domain of Rubicon is not identical to the FYVE domain and does not bind directly to PtdIns(3)P, the product of Vps34/PtdIns3K, nevertheless they showed extensive co-localization. It is likely that Vps34/PtdIns3K binds to Rubicon and is localized on the Rubicon-associated structures, and therefore its product is enriched where Rubicon is localized. However co-transfection experiments showed that Beclin 1 is not co-localized on the Rubicon-associated structures. A previous report showed that knocking down Beclin 1 protein level in cells did not affect the endocytic pathway (Zeng et al., 2006). Moreover, in mammalian cells, quantitative analyses with a cross-linker showed that although all Beclin 1 is associated with Vps34/PtdIns3K complex, ~50% of Vps34/PtdIns3K is free of Beclin 1. And partial overlap between Vps34/PtdIns3K and late endosome/mutli-vesicular body (MVB) marker LBPA is observed (Kihara et al., 2001a). Therefore a small Rubicon functioning complex that contains Vps34/PtdIns3K but not Beclin 1 may exist on the Rubicon-associated structures.

Both immunoprecipitation from wild type cells using anti-Rubicon antibody and immunoprecipitation from Rubicon-EGFP stable cells using GFP antibody showed that UVRAG binds to Rubicon but not to Atg14L. This suggested that UVRAG may be in the smaller functioning complex with Rubicon although anti-UVRAG antibody failed to detect clear signal from fractions collected from gel filtration. Interestingly, UVRAG has been shown to be closely related to autophagosome maturation and endocytic trafficking as well (Liang et al., 2008) However in that study, both endogenous and epitope-tagged UVRAG consistently showed colocalization with early endosomal marker EEA1 but not with late endosomal markers. Moreover, UVRAG was shown to facilitate autophagosome maturation and fusion of endosomes with lysosomes through its interaction with class C Vps complex, and Beclin 1 was not necessary for that function. Therefore Rubicon and UVRAG seem to function at similar steps of the same pathways, but in directly opposite directions. However this does not argue against the possibility that Rubicon and UVRAG may co-exist in the small functioning complex: their opposite functions may be important for keeping autophagy and endocytosis levels well balanced and under control in the cells.

From the data of this study, a model can be proposed. There is a large Beclin 1 protein complex that contains at least most of the Beclin 1 interaction proteins identified in this study: Vps34/PtdIns3K, Vps15, UVRAG, Atg14L and Rubicon. Within this large complex, Beclin 1, Vps34/PtdIns3K, Vps15 and UVRAG may be the core component given their similar stoechiometry as identified from the *in vivo* immunoprecipitation. Although Atg14L was detected at a much lower intensity, from its high binding affinity with Beclin 1, it is possible that Atg14L is also one of the core components. Multiple smaller protein complexes can be generated from this initial large complex and may be

the ones that actually function in various cellular pathways. One such complex contains Beclin 1, Vps34/PtdIns3K and Atg14L, and it functions at the initial step of autophagy and promotes antuphagosome biogenesis. Another complex contains Vps34/PtdIns3K and Rubicon, and may contain UVRAG as well but not Beclin 1. Its function is in inhibiting endocytic pathway and autophagosome maturation (Fig. 1-19). Through interaction with either Atg14L or Rubicon, Beclin 1 may be playing a critical role in regulating the balance of autophagy and thereby in maintaining the homeostasis of the cells.

4.5 Function of Beclin 1 in autophagy and development

Specific deletion of *beclin 1* in several populations of neurons caused degeneration, and different cell types showed different phenotypes. In cortical and hippocampal pyramidal cells, deletion of *beclin 1* induced intracellular accumulation of p62/SQSTM1, indicating that autophagy in these neurons was disrupted. Activation of apoptotic pathway and massive cell death were also observed. Interestingly, p62/SQSTM1 accumulation preceded the activation of apoptotic pathway and cell death by a few days, suggesting that the failure to degrade intracellular proteins might have been one of the reasons that induced apoptosis activation. It is also consistent with previous reports that deletion of *Atg5* or *Atg7* in the central nervous system induced inhibition of basal level of autophagy and caused accumulation of ubiquitinated proteins and activation of apoptosis (Hara et al., 2006; Komatsu et al., 2006).

Electron microscopy studies revealed accumulation of electron dense structures in *beclin* $1^{-/-}$; EMX-Cre hippocampal pyramidal cells. The accumulation likely starts from

protein aggregates that fail to be degraded by autophagy, and gradually include aberrant membrane structures that are generated possibly also due to disruption of autophagy. The degeneration of the cells proceeds as the accumulation bodies grow, and at the late stages of degeneration, the accumulation bodies will likely occupy almost all the cytoplasmic area. Interestingly, a large number of double membrane vesicles that resembled autophagosomes were observed in *beclin 1*$^{-/-}$; EMX-Cre hippocampal pyramidal cells, suggesting that the deletion of beclin 1 may not inhibit autophagosome formation but rather may block the clearance of autophagosomes. And this is consistent with the observation that knocking down Beclin 1 protein level in NIH/3T3 cells increased LC3II form level. Furthermore, it is also consistent with the functional interaction between Beclin 1 and its newly identified interaction protein Rubicon. Since Rubicon blocks autophagosome maturation and this activity may be inhibited by Beclin 1, deletion of *beclin 1* may result in an increase in blocking of autophagosome maturation. Although studies have shown that Beclin 1 is essential for autophagy, its exact function is still unclear. Therefore further *in vivo* characterization of autophagy pathway in *beclin 1*$^{-/-}$; EMX-Cre hippocampal pyramidal cells will provide important information.

In contrast to cortical and hippocampal pyramidal cells, when *beclin 1* was deleted in Purkinje cells, despite severe degeneration and massive cell loss, no obvious p62/SQSTM1 accumulation and activation of apoptosis was observed. Instead Purkinje cells at early stage of degeneration showed many electron dense structures that from their morphology seemed closely related to the intracellular membranes. Since Beclin 1 is part of the Vps34/PtdIns3K complex and the complex has important functions in membrane trafficking in the cells, it can be speculated that the phenotype induced by deletion of

beclin 1 may be related to Vps34/PtdIns3K function. In yeast, Atg6p is not essential for activation of Vps34p, since *Atg6* mutant cells showed only a slight decrease in PtdIns 3-kinase activity (~80% of wild type cells) (Kihara et al., 2001b). Similarly siRNA mediated knockdown of Beclin 1 in NIH/3T3 cells did not significantly affect the Vps34/PtdIns3K kinase activity in the cells (data not shown). Therefore, it is likely that Beclin 1 does not catalytically regulate Vps34/PtdIns3K activity but rather mediates its intracellular localization, possibly by selectively forming different small functioning protein complexes. Therefore deletion of *beclin 1* in Purkinje cells may have induced aberrant localization of Vps34/PtdIns3K. Since Vps34/PtdIns3K has important function in membrane trafficking and lysosomal enzyme sorting, its mislocalization can result in defect in membrane genesis and lysosome development in the cells. Immuno-staining with anti-PtdIns(3)P antibody showed that deletion of *beclin 1* induced changes in localization of PtdIns(3)P, the product of Vps34/PtdIns(3)K, in Purkinje cells. Future electron microscopy experiments using PtdIns(3)P probes such as tagged 2xFYVE domains will be performed to confirm the specific localization of PtdIns(3)P in both control and *beclin* $1^{-/-}$; Pcp-2 Cre Purkinje cells. Meanwhile, immuno-staining studies using lysosomal markers will be performed to examine whether there is abnormality in lysosome development and maturation in *beclin* $1^{-/-}$; Pcp-2 Cre Purkinje cells.

Comparing the phenotypes of *beclin 1* neuronal knockout mice and *Atg5*/*Atg7* neuronal knockout mice, some big differences can be immediately noticed. *Atg7*$^{flox/flox}$; nextin-Cre mice can live as long as 28 weeks (Komatsu et al., 2004), while almost all *beclin 1*$^{flox/flox}$; EMX-Cre mice, though with much more limited cell populations affected, die by 8 weeks. *Atg7*$^{flox/flox}$; Pcp2-Cre mice don't show severe Purkinje cell death until

P56 while in *beclin 1*$^{flox/flox}$; Pcp2-Cre mice Purkinje cell degeneration starts from as early as P21 and by the age of one month almost half of the Purkinje cells are dead (Komatsu et al., 2007a). Similar difference exists between beclin $1^{-/-}$ and $Atg5^{-/-}$/$Atg7^{-/-}$ mice. Both $Atg5^{-/-}$ and $Atg7^{-/-}$ mice survive to be born while beclin $1^{-/-}$ die at early developmental stage at E7.5 (Yue et al., 2003; Kuma et al., 2004; Komatsu et al., 2005). Therefore it is suggested that Beclin 1 has other critical function than just regulating autophagy and therefore is more important for development than other autophagy proteins. The results from this study suggest that Beclin 1 may also regulate membrane trafficking and lysosome development in the cells, possibly through interaction with Vps34/PtdIns(3)K. Future study focusing on this direction will likely provide useful information to help better understand the functions of Beclin 1.

Methods and materials

Reagents and antibodies

Dynabeads M-270 epoxy, NuPAGE Bis-Tris gels, Western blot transfer buffer, MES SDS running buffer, antioxidant, Lipofectamine 2000 and Lipofectamine RNAi MAX kits were purchased from Invitrogen (Carlsbad, CA). Modified Trypsin, EDTA-free protease inhibitor cocktail tablets, and FuGene 6 transfection reagent were purchased from Roche Diagnostics (Indianapolis, IN). Immobilon-P PVDF membrane was purchased from Millipore (Billerica, MA). GelCode Blue Stain Reagent, Trifluoroacetic acid, Tris(2-carboxyethyl)-phosphine hydrochloride, and the Micro BCA Protein Assay Reagent Kit were purchased from Pierce (Rockford, IL). Gel filtration calibrant mixtures were purchased from BioRad (Hercules, CA). Phosphatidylinositol was purchased from Avanti Polar Lipids (Alabaster, AL). Radio-active ^{32}P-ATP was purchased from PerkinElmer (Waltham, MA). G418, anti-myc affinity gel beads, 3,3'-Diaminobenzidine (DAB) and urea tablets were purchased from Sigma (St Louis, MO). Beclin 1 siRNA was purchanse from Dharmacon (Lafayette, CO); Atg14L siRNA was purchased from Invitrogen (Carlsbad, CA); and Rubicon and control siRNA were purchased from Ambion (Austin, TX). Coated silica gel was purchased from EMD (Gibbstown, NJ). Fluorescence mounting medium was purchased from Abcam (Cambridge, MA). Vectastain Elite ABC kit was purchased from Vector Laboratories (Burlingame, CA).

Commercial antibodies used in this study include rabbit polyclonal LC3 antibody (1:1000, MBL, Woburn, MA), rabbit polyclonal antibody raised against the C-terminal of UVRAG (1:500, Abgent, San Diego, CA), rabbit polyclonal Beclin 1 antibody (1:600; Santa Cruz Biotechnology, Santa Cruz, CA), guinea pig polyclonal p62/SQSTM1

antibody (1:1000, American Research Products, Inc., Belmont, MA), mouse monoclonal Lamp 1 antibody (1:10, Developmental Studies Hybridoma Bank at the University of Iowa, Iowa City, IA), mouse monoclonal LBPA antibody (1:200, Echelon Biosciences Inc. Salt Lake City, UT), rabbit polyclonal Vps34antibody (1:250, Zymed Laboratories, San Francisco, CA), mouse monoclonal syntaxin 6 antibody (1:600, BD Tranduction Laboratories, , San Jose, CA), mouse monoclonal EEA1 antibody (1:600, BD Tranduction Laboratories, San Jose, CA), mouse monoclonal protein disulphide isomerase (PDI) antibody (1:100, Abcam, Cambridge, MA), mouse monoclonal c-myc antibody (1:1000; Santa Cruz Biotechnology, Inc., Santa Cruz, CA; Zymed Laboratories, San Francisco, CA), mouse monoclonal M2 FLAG and β-actin antibodies (Sigma, St. Louis, MO), anti-rabbit Alexa Fluo 555 and Alexa 488 (1:1000, Invitrogen, Carlsbad, CA), Rhodomine red conjugated secondary antibody (Jackson ImmunoResearch, West Grove, PA), anti-mouse and anti-rabbit Cy5 (1:500, Zymed Laboratories, San Francisco, CA), rabbit IgG (1:6000; Amersham, Pittsburgh, PA), mouse IgG (1:10000; Pierce, Rockford, IL).

Rabbit polyclonal GFP antibody was raised against GST-tagged GFP and affinity purified in house as described previously (Cristea et al., 2005). Rabbit polyclonal Atg14L and Rubicon antibodies were generated as described below. Full length cDNA of Atg14L was cloned into NdeI and BamHI sites of bacterial expression vector pET-28a(+) (Novagen, USA). Partial cDNA of Rubicon that corresponds to amino acids 220-941 was cloned into NheI and BamHI sites of pET-28a(+) vector. Recombinant 6× His-tagged Atg14L and Rubicon proteins were expressed in BL21-Codon-Plus (DE3)-RIL competent cells and purified with Ni-NTA agarose beads (Qiagen, USA). A total of 500

μg of purified recombinant protein was used for injections to produce polyclonal antibodies in rabbits (Cocalico Biologicals, Inc. Reamstown, PA). Sera were either purified with protein-G column (GE Healthcare, Piscataway, NJ) (Rubicon) or further affinity purified with recombinant protein (Atg14L).

Generation and genotyping of the *Beclin1-EGFP* BAC transgenic mice

Beclin1-EGFP mice were generated using BAC mouse transgenic techniques (Gong et al., 2002). In brief, a 455-base pair homology region immediately upstream of stop codon of *Becn1* gene ("A box") was PCR amplified and inserted between AscI and SmaI sites of pLD53.SCA-E-B, and another 507-base pair homology region immediately downstream of stop codon was PCR amplified and inserted between PacI and StuI sites of the vector ("B box") (Gong et al., 2002). Through homologous recombination, DNA sequence encoding EGFP protein followed by a stop codon was inserted into the BAC clone RP24-392C4 which contains all regulatory elements of *Beclin 1* gene to replace the original stop codon of *Beclin 1*. The modified BAC clone was purified using CsCl gradient ultra-centrifugation, and used for pronuclear injection in FVB/NJ mice. All mice were backcrossed to C57BL/6J background for more than 10 generations before analysis.

Genotype of mice from pronuclear injection was determined with either southern blot or PCR reaction. For southern blot, a 0.5 inch piece of mouse tail was clipped from the tail end and incubated in lysis buffer (27% sucrose, 1× SSC, 1 mM EDTA, 1% SDS, 200 μg/ml proteinase K) at 55°C overnight. After extractions with phenol:chloroform (1:1) and with chloroform, DNA was precipitated with ethanol and dissolved in TE buffer. Genomic DNA was digested with XhoI and XbaI, and was analyzed with southern blot

using “A box” as the hybridization probe. For PCR reaction, the EGFP forward and reverse primer pairs are:

Forward: CCTACGGCGTGCAGTGCTTCAGC

Reverse: CGGCGAGCTGCACGCTGCCGTCCTC

Generation of rescued mice

Beclin 1-EGFP/+ transgenic mice were genetically crossed with *beclin 1* $^{+/-}$ mice to generate rescued mice, in which both endogenous *beclin 1* alleles are deleted and only *beclin 1*-EGFP transgene is expressed. First, *beclin 1*-EGFP mice were crossed with *beclin 1* $^{+/-}$ mice to obtain *beclin 1* $^{+/-}$; *beclin 1*-EGFP mice. Then mice of this genotype were further crossed with *beclin 1* $^{+/-}$ mice to obtain *beclin 1* $^{-/-}$; *beclin 1*-EGFP mice. Tails were clipped from mice and protein was extracted in protein lysis buffer (20mM HEPES, pH7.4/ 1mM MgCl2/0.25mM mM CaCl2/ 0.2% Triton X-100/150mM NaCl/ protease inhibitor and PMSF-pepstatin/DNaseI), after which western blot with anti-Beclin 1 antibody was performed to confirm the deletion of endogenous Beclin1 protein. Multiple litters were produced and the numbers of mice of each genotype were counted to examine whether the Mendel’s law was followed.

Affinity purification and mass spectrometric analysis

Affinity purification of Beclin 1 interacting proteins and mass spectrometric identification of these proteins were carried out as described (Wang et al., 2006), with slight modification. In brief, tissue extracts were obtained from both *Becn1*$^{+/-}$ and *Becn1*$^{-/-}$; *Becn1-EGFP* mice (4 months of age) by homogenizing 2 brains or 1 liver with a

motor-driven homogenizer (speed 2.5, 12 strokes) in 4 ml buffer containing 0.32 M sucrose, 1 mM $NaHCO_3$, 20 mM HEPEs/pH 7.4, 1 mM $MgCl_2$, 0.25 mM $CaCl_2$, PIC, 200 μg/mL PMSF, pepstatin 4 μg/mL and DNase I. The tissue extracts were centrifuge at 1,400 g for 10 min and the pellets were homogenized again in 4 ml buffer for 8 strokes and centrifuged again. Supernatants from the two homogenization steps were pooled, centrifuged at 750 g for 10 min. Aliquots of the resulting supernatants were used for gel filtration experiments. The remaining supernatants were diluted with equal volumes of 2× pull-out buffer and then 2 volumes of 1× pull-out buffer containing 20 mM HEPEs/pH 7.4, 1 mM $MgCl_2$, PIC, 100 μg/mL PMSF, 2 μg/mL pepstatin, 0.2% triton X-100 and 150 mM NaCl. Each sample was incubated with 5 mg M-270 Epoxy Dyanbeads, which were pre-coated with affinity purified polyclonal anti-GFP antibody, for 1.5 hours at 4°C. Dynabeads were washed 5 times with 1× pull-out buffer and then incubated with 250 μl elution buffer containing 0.5 mM EDTA and 0.5 M $NH_3 \cdot H_2O$ for 20 min at room temperature. The eluents were collected, frozen in liquid nitrogen and dried in a Speedvac. The purified complexes were resolved on SDS-PAGE and stained with colloidal Coomassie. The entire gel lane of the *Becn1*$^{-/-}$; *Becn1-EGFP*/+ sample was sliced into ~30 2-mm wide pieces. Each gel piece was reduced, alkylated with iodoacetamide, and subject to in-gel digestion with trypsin. The resulting tryptic peptides were analyzed by MS and MS/MS, using either in-house-constructed MALDI-QqTOF and MALDI-ion trap (LCQ DECA XP; Thermo Electron Corporation) mass spectrometers or ESI-LTQ mass spectrometer (Thermo Electron Corporation). Accurate masses of the tryptic peptides and the masses of their product ions were used to identify proteins in each gel piece, using the computer search engines ProFound

(http://prowl.rockefeller.edu/prowl-cgi/profound.exe), Xproteo (http://www.xproteo.com) and GPM (http://prowl.rockefeller.edu/tandem/thegpm_tandem.html) to search the most up-to-date NCBI non-redundant mouse protein database.

Plasmid constructs and stable cell lines

Total RNA was extracted from postnatal day 12 mouse whole brain using RNeasy mini kit (Qiagen, USA). Full length cDNA was synthesized with Omniscript RT kit (Qiagen, USA) and used as templates for PCR amplifications with KOD HiFi DNA polymerase (Novagen, USA). *Beclin1* was cloned into EcoRI and BamHI sites of pEGFP-N3 and pAs-Red vectors (Clonetech, USA). *Atg14L* was cloned into EcoRI and BamHI sites of pEGFP-N3, pAsRed and pCMV-FLAG (Sigma, St Louis, MO) vectors. *Rubicon* was cloned into HindIII and BamHI sites of pEGFP-N3, pAs-Red and pCMV-FLAG2 vectors. *UVRAG* was cloned into XhoI and BamHI sites of pEGFP-N3 vector. Single or combinations of *Beclin1* domains were cloned into EcoRI and BamHI sites of pCMV-FLAG2 vector. Truncated *Atg14L* mutants were cloned into EcoRI and BamHI sites of pEGFP-N3 vector. Truncated *Rubicon* mutants were cloned into KpnI and BamHI sites of pEGFP-N3 vector. EGFP-Atg12 and EGFP-Atg5 constructs were generously provided by Dr. X. Jiang. Myc-hVps34-hVps15-V5-His/pVITRO2 plasmid was described previously (Yan et al., 2008).

Cell cultures and transfections

Human embryonic kidney (HEK) 293 and 293T, Hela and NIH/3T3 cells were maintained in standard medium, i.e., Dulbecco's modified Eagle's medium (DMEM)

supplemented with 10% fetal bovine serum (FBS) and 1% penicillin-streptomycin (Invitrogen, Carlsbad, CA). MLE12 cells were generously provided by Dr. C Münz and maintained in DMEM/F12 medium (ATCC, Manassas, VA) supplemented with 0.005 mg/ml insulin, 0.01 mg/ml transferrin, 30 nM sodium selenite, 10 nM hydrocortisone, 10 nM beta-estradiol, 10 mM HEPEs, 2 mM L-glutamine, 2% FBS and 1% penicillin-streptomycin. Transient DNA transfection was performed with standard calcium phosphate precipitation procedure, FuGene 6 or Lipofectamine 2000 kit, following the protocols provided by the manufacturers (Invitrogen, Carlsbad, CA). siRNA transfection of NIH/3T3 cells and GFP-LC3 MLE12 stable cells was performed with Lipofectamine RNAi MAX kit following the reverse transfection protocol provided by the manufacturer. The sequences of siRNAs are:

Beclin 1: CAGUUUGGCACAAUCAAUA

Atg14L: UUUGCGUUCAGUUUCCUCACUGCGC

Rubicon: GCCUUCAGUCUAUGCCACA

Generation of stable cell lines

HEK293 cells were transfected with pEGFP-N3 vector, Beclin 1-EGFP, Atg14L-EGFP or Rubicon-EGFP, and were selected with 800 μg/ml G418 for one week. Single colonies with EGFP expression were picked and culture was continued in medium supplemented with 200μg/ml G418. Correct expression of EGFP-fusion protein was confirmed with western blot using anti-GFP antibody, after which cells were maintained in culture medium supplemented with 200μg/ml G418.

***In vitro* protein immunoprecipitation (IP)**

DNA plasmids were transfected into HEK293T cells for IP. For Co-IP experiments, two or three plasmids were transfected simultaneously in equal amount. Cells were lysed in IP lysis buffer (20mM HEPES, pH7.4/ 1mM MgCl2/0.25mM mM CaCl2/ 0.2% Triton X-100/150mM NaCl/ protease inhibitor and PMSF-pepstatin/DNaseI). For IP with anti-GFP, anti-Atg14L or anti-Rubicon antibody, Dynabeads M-270 E-proxy (Invitrogen, Carlsbad, CA) were conjugated with each antibody, and incubated with cell lysate at 4°C for 2 hours. After the beads were washed in IP lysis buffer for 5 times, proteins were eluted by incubating beads in elution buffer (0.5mM EDTA, pH8/0.5N $NH_3 \cdot H_2O$) at room temperature for 20 minutes and dried with vacuum speed centrifuge. For FLAG-tagged protein IP, Anti-FLAG M2 affinity resin (Sigma, St Louis, MO) was used and the manufacture's protocol was followed.

Vps34kinase assay

Vps34kinase assay was performed as described (Miled et al., 2007). Myc-hVps34-hVps15-V5-His/pVITRO2 plasmid was transfected into HEK293T cells in combination with other FLAG-tagged or EGFP-tagged plasmids. Cells were lysed in 1% Nonidet P-40 lysis buffer (20 mM Tris/pH 7.5, supplemented with 137 mM NaCl, 1 mM $MgC1_2$, 1 mM $CaC1_2$, 100 mM NaF, 10 mM sodium pyrophosphate, 100 μM Na_3VO_4, 10% glycerol, and 0.35 mg/ml phenylmethylsulfonyl fluoride/protease and phosphatase inhibitors). Immunoprecipitation was performed with anti-myc affinity gel beads (Sigma, St Louis, MO), following manufacture's protocol. Beads were washed in lysis buffer three times, followed by three washes in washing buffer (100 mM Tris-HCl/pH7.4 and

500 mM LiCl) and two washes in reaction buffer (10 mM Tri-HCl/pH7.4, 100 mM NaCl and 1 mM EDTA). Beads were re-suspended in 60 μl of reaction buffer, followed by addition of 10 μ1 of 100 mM $MnCl_2$ and 10 μl of sonicated phosphatidylinositol (2 μg/μl). The reaction was started by the addition of 10 μl of 440 μM ATP containing 10 μCi of γ-^{32}P-ATP, and beads were incubated for 10 min at room temperature. Reaction was terminated by adding 20 μl 8 M HCl, and organic phase was extracted with 160 μl chloroform:methanol (1:1). Extracted phospholipids products were resolved by thin layer chromatography (TLC) using a coated silica gel and a solvent composed of chloroform:methanol:H_2O:ammonium hydroxide (v/v/v/v, 9:7:1.7:0.3), followed by visualization with Typhoon 9400 Variable Imager (GE Healthcare Biosciences, Piscataway, NJ).

Immuno-staining

Cultured cells were fixed in fresh 4% paraformaldihyde in 1x PBS, and permeablized in PBS with either 0.05%-0.1% Triton X-100 or 0.01% saponin for 10-30 min at room temperature. After blocking in PBS containing 10% goat serum for 30 min-1 h at room temperature, cells were incubated in primary antibodies overnight at 4°C. After three washes in PBS, cells were incubated with fluorescent secondary antibodies for one hour at room temperature, followed by four washes in PBS. Cells were mounted with fluorescence mounting medium and examined under Zeiss (Göttingen, Germany) upright and invert confocal microscopes.

Brain sections were permeabilized in blocking buffer (10% goat serum and 0.1% Triton X-100 in PBS), and were incubated in primary antibodies diluted in blocking

buffer overnight at 4°C. Sections were then washed in PBS and incubated in Alexa Fluor conjugated secondary antibodies (Invitrogen) in PBS for 1 hour at room temperature. After washes in PBS, sections were mounted and examined in the same way as above. For HRP staining with paraffin sections, antigen retrieval was first performed and sections were incubated in 0.5% H_2O_2 for 15 minutes at room temperature to block the endogenous peroxidase activity. After permeabilization in the same blocking buffer as above, sections were incubated in primary antibodies diluted in blocking buffer overnight at 4°C. Vectastain Elite ABC Kit (Vector Laboratories) was used for secondary antibody reaction and signal detection following the manufacturer's protocol.

Electron microscopy

For morphology EM, transfected HEK293T cells were fixed in 2.5% glutaraldehyde (2.5GA) in 0.1M cacodylate buffer, pH 7.4. Animals were perfusion fixed with 2% paraformaldehyde and 2% glutaraldehyde in 0.1M PB (pH7.4), and 200μm sections were cut with vibrotme. After sample processing and embedding, 0.5 mm thin sections were cut and stained with 1% Toluidine Blue, and areas for further examination were selected under light microscope. Samples were then processed by routine transmission electron microscopy procedure and embedded in Epon (Yue et al., 2002).

For immuno-EM, transfected HEK293T cells were fixed in fresh PLP fixative (4% paraformaldehyde, 0.01M periodate, 0.075M lysine, and 0.075M phosphate buffer/pH7.4) supplemented with 0.05% glutaraldehyde for one hour. After three washes in PBS, cells were permeabilized with 0.01% saponin in PBS supplemented with 0.1% BSA for 15 minutes at room temperature, and were incubated with primary antibody

(anti-GFP) diluted in the same buffer overnight at 4°C. Vectastain Elite ABC kit was used for secondary antibody reaction, and cells were fixed again in 1.5% glutaraldehyde in 0.1 M cacodylate buffer supplemented with 5% sucrose. After three washes with 50 mM Tris/pH 7.4 supplemented with 7.5% sucrose, DAB reaction was performed with the same kit. The reaction was stopped with 50 mM Tris/pH 7.4 supplemented with 7.5% sucrose, and cells were processed for silver enhancement as described (Teclemariam-Mesbah et al., 1997).

Sample blocks were cut with a diamond knife on a Leica UltracutE and ultra-thin (~70 nm) sections were collected on uncoated 200-mesh grids and stained with Uranium and Lead. Grids were viewed with a TecnaiSpiritBT Transmissiiom Electron Microscope (FEI) at 80 KV and pictures were taken with Gatan 895 ULTRASCAN Digital Camera. Image levels were processed in Adobe Photoshop (Adobe Systems, San Jose, CA) to enhance contrast.

Gel Filtration

Liver and brain extracts from both *beclin 1* $^{+/-}$ and *beclin 1* $^{-/-}$; *beclin 1*-GFP/+ mice at 4 month of age were prepared as described above. Cell extracts were prepared as previously described (Wang et al., 2006). Tissue and cell extracts were diluted with equal volumes of 2× pull-out buffer (see above) and incubated for 15 min at 4°C. The samples were then subject to ultracentrifugation at 100,000 g and the resulting supernatants were used for gel filtration experiments. Superdex 200 HR10/30 column (Pharmacia) was equilibrated with 2 bed volumes of filtered running buffer containing 20 mM HEPEs/pH 7.4, 1 mM $MgCl_2$, 500 μg/mL PMSF, 1 μg/mL pepstatin and 150 mM

NaCl. The column was calibrated using Biorad gel filtration calibrant mixture, which are composed of thyroglobulin (670 kDa), γ-globulin (158 kDa), ovalbumin (44 kDa), myoglobin (17 kDa) and vitamin B_{12} (1,350 Da). A spike of these calibrants (10 μl) was also added to each sample (240 μl) as internal calibrants. Both calibrants and samples were run at a flow rate of 0.2 ml/min. For each run, 2 bed volumes of buffer were used to elute the sample and a total of 80 fractions were collected 25-29 min after starting the runs and at a rate of 1 fraction/min. Two bed volumes of buffer were used to wash the column at the same flow rate in between two runs.

Long-lived protein degradation assay

Long-lived protein degradation was accessed as described (Gronostajski and Pardee, 1984). In brief, NIH/3T3 cells were transfected with either control or Atg14L siRNA and plated in 12-well plates. After 48 h, standard medium was changed to leucine-free medium supplemented with 1 μCi/ml ^{3}H-L-leucine. After being pulse-labeled for 24 h, cells were washed 3 times and further cultured in standard medium supplemented with excess unlabeled leucine (5 mM) for 16 h to chase out short-lived proteins. Cells were then washed 3 times and further cultured for 4 h in standard medium, Earle's Balanced Salt Solution (EBSS), or EBSS supplemented with 10 mM 3-MA, all containing 5 mM unlabeled leucine. Both media and cell lysate were subject to trichloroacetic acid (TCA) precipitation. Long-lived protein degradation was calculated as the ratio of TCA-soluble medium radioactivity to TCA-precipitated cell lysate radioactivity.

Construction of *beclin 1* targeting vector

Two shuttle vectors were used to generate the final vector for BAC modification. S351 contains the diphtheria toxin A-fragment gene (DT-A) for negative selection at gene targeting against random integration, and S385 contains the two loxP sites and the pGKneo cassette flanked by two FRT sites. An DNA fragment about 1000 base pair (bp) in size (box A1), starting from around 1060 bp upstream of start codon of beclin 1 gene to around 60 bp upstream of start codon, was PCR amplified using BAC DNA as template and inserted into AscI and EcoRV sites of S351. A DNA fragment about 500 bp (box A2) immediately downstream of box A1 (and containing the second exon of *beclin 1* gene) was PCR amplified and inserted into EcoRV and KpnI sites of S385. A third DNA fragment about 2000 bp (box B) immediately downstream of box A2 was subcloned into FseI and SmaI sites of S351 and was later used as short arm for homologous recombination in gene targeting. Another DNA fragment about 2000 bp (box C) downstream of box B was subcloned into XbaI site of S351, and was used for homologous recombination in the process of BAC modification. Finally all the elements in S385 were linearized with NotI and PmeI digestion and ligated into NotI and SwaI sites of S351, generating the complete shuttle vector for BAC modification. Through modification, the loxP-A2-FRT-pGKneo-FRT-loxP fragment was replaced into the BAC clone. After linearization with PI-SceI digestion, the BAC clone was used as the targeting vector for gene targeting.

Gene targeting and blastocyst injection

Linearized targeting vector was electroporated into embryonic stem (ES) cells derived from C57BL/6J-*Tyr*$^{c\text{-}2J}$/J mice, and selection was performed with G418 treatment. 50 surviving clones were picked and genomic DNA was extracted, followed by digestion with BamHI. Southern blot was performed using a 500 bp DNA fragment downstream of box B (short arm of the targeting vector) as the probe. Clones that gave a 5700 bp band were picked as possible positive clones, while negative clones gave a 4000 bp band. Genomic DNA from selected positive clones was purified and digested with SwaI and BglII, and southern blot was performed with the same probe as above. Clones that gave a band of 5500 bp were confirmed to be true positive clones from correct homologous recombination, and were used for blastocyst injection. For southern blot, genomic DNA was digested with restriction enzymes and separated on agarose gels, followed by transfer to nylon membrane (NP0HYB0010, GE). Probe synthesis and hybridization was performed using Prime-It II random primer labeling kit (Stratagene), following the manufacturer's manual.

Mouse genotyping

Chimera mice from blastocyst injection were crossed to wild type C57BL/6J mice, and pups with white coat color were tail clipped for genotyping. Genomic DNA was extracted as described above and was used for southern blot. For genotyping analyses starting from F2 generation, the following primers were used.

Forward: 5'-CCACCACCAAGGCAGCGGGTAG-3'

Reverse: 5'-TCACTGATGGCTCTAACCTCAACTCGTC-3'

Generation of conditional knockout mice

Positive mice were first crossed to transgenic mice that express FLP recombinase under the control of a broad promoter ROSA26 to remove the PGK-neo cassette flanked by two FRT sites from the genome, and the deletion was confirmed with southern blot. For genotyping FLP mice, the following primers were used

Forward: 5'-CTAATGTTGTGGGAAATTGGAGC-3'

Reverse: 5'-CTCGAGGATAACTTGTTTATTGC-3'

Beclin 1$^{flox/+}$ mice were crossed to each other to generate *beclin 1*$^{flox/flox}$ mice. Meanwhile they were crossed with either Pcp2-Cre or EMX-Cre mice to generate *beclin 1*$^{flox/+}$; Cre/+ mice. Finally *beclin 1*$^{flox/flox}$ mice were crossed with *beclin 1*$^{flox/+}$; Cre/+ mice to generate *beclin 1*$^{flox/flox}$; Cre/+ mice, in which *beclin 1* expression is specifically deleted in either cerebellar Purkinje cells (Pcp2-Cre) or cortical and hippocampal pyramidal cells (EMX-Cre). For genotyping Cre mice, the following primers were used.

Forward: 5'-CCGGTGAACGTGCAAAACAGGCTCTA-3'

Reverse: 3'-CTTCCAGGGCGCGAGTTGATAGC-3'

Preparation of brain slices

Mice at different ages were put into anesthesia with intraperitoneal Nembutal injection at dose of 0.01ml/g body weight. Perfusion was performed with 4% paraformaldehyde in 0.1M phosphate buffer (pH7.4), and dissected brains were post fixed in the same fixative at 4°C for overnight. For floating sections, brains were embedded into 5% low melting agarose gel and 40μm sections were cut with vibrotome (Vibrotome). For cryosections, brains were subjected to cryo-protection in 30% sucrose

at 4°C for overnight, and then were embedded into Neg-50 compound (Richard-Allan Scientific). 20μm sections were cut with cryostat (Leica). For paraffin sections, brains were dehydrated in series of ethanol (70%, 80%, 90%, and 100%) for 30 minutes x 2, followed by incubation in Xylene for 3 days, and were embedded into wax. 10 μm sections were cut with a microtome (Leica).

References

Aita VM, Liang XH, Murty VV, Pincus DL, Yu W, Cayanis E, Kalachikov S, Gilliam TC, Levine B (1999) Cloning and genomic organization of beclin 1, a candidate tumor suppressor gene on chromosome 17q21. Genomics 59:59-65.

Arsov I, Li X, Matthews G, Coradin J, Hartmann B, Simon AK, Sealfon SC, Yue Z (2008) BAC-mediated transgenic expression of fluorescent autophagic protein Beclin 1 reveals a role for Beclin 1 in lymphocyte development. Cell Death Differ 15:1385-1395.

Boya P, Gonzalez-Polo R-A, Casares N, Perfettini J-L, Dessen P, Larochette N, Metivier D, Meley D, Souquere S, Yoshimori T, Pierron G, Codogno P, Kroemer G (2005) Inhibition of Macroautophagy Triggers Apoptosis. Mol Cell Biol 25:1025-1040.

Cristea IM, Williams R, Chait BT, Rout MP (2005) Fluorescent proteins as proteomic probes. Mol Cell Proteomics 4:1933-1941.

Diskin T, Tal-Or P, Erlich S, Mizrachy L, Alexandrovich A, Shohami E, Pinkas-Kramarski R (2005) Closed head injury induces upregulation of Beclin 1 at the cortical site of injury. J Neurotrauma 22:750-762.

Ellson CD, Andrews S, Stephens LR, Hawkins PT (2002) The PX domain: a new phosphoinositide-binding module. J Cell Sci 115:1099-1105.

Fiering S, Kim CG, Epner EM, Groudine M (1993) An "in-out" strategy using gene targeting and FLP recombinase for the functional dissection of complex DNA regulatory elements: analysis of the beta-globin locus control region. Proc Natl Acad Sci U S A 90:8469-8473.

Fimia GM, Stoykova A, Romagnoli A, Giunta L, Di Bartolomeo S, Nardacci R, Corazzari M, Fuoco C, Ucar A, Schwartz P, Gruss P, Piacentini M, Chowdhury K, Cecconi F (2007) Ambra1 regulates autophagy and development of the nervous system. Nature 447:1121-1125.

Furuya N, Yu J, Byfield M, Pattingre S, Levine B (2005) The evolutionarily conserved domain of Beclin 1 is required for Vps34 binding, autophagy and tumor suppressor function. Autophagy 1:46-52.

Germain M, Shore GC (2003) Cellular distribution of Bcl-2 family proteins. Sci STKE 2003:pe10.

Gillooly DJ, Morrow IC, Lindsay M, Gould R, Bryant NJ, Gaullier JM, Parton RG, Stenmark H (2000) Localization of phosphatidylinositol 3-phosphate in yeast and mammalian cells. Embo J 19:4577-4588.

Gong S, Yang XW, Li C, Heintz N (2002) Highly efficient modification of bacterial artificial chromosomes (BACs) using novel shuttle vectors containing the R6Kgamma origin of replication. Genome Res 12:1992-1998.

Gonzalez-Polo RA, Boya P, Pauleau AL, Jalil A, Larochette N, Souquere S, Eskelinen EL, Pierron G, Saftig P, Kroemer G (2005) The apoptosis/autophagy paradox: autophagic vacuolization before apoptotic death. J Cell Sci 118:3091-3102.

Gronostajski RM, Pardee AB (1984) Protein degradation in 3T3 cells and tumorigenic transformed 3T3 cells. J Cell Physiol 119:127-132.

Guo H, Hong S, Jin XL, Chen RS, Avasthi PP, Tu YT, Ivanco TL, Li Y (2000) Specificity and efficiency of Cre-mediated recombination in Emx1-Cre knock-in mice. Biochem Biophys Res Commun 273:661-665.

Hara T, Nakamura K, Matsui M, Yamamoto A, Nakahara Y, Suzuki-Migishima R, Yokoyama M, Mishima K, Saito I, Okano H, Mizushima N (2006) Suppression of basal autophagy in neural cells causes neurodegenerative disease in mice. Nature 441:885.

Horazdovsky BF, DeWald DB, Emr SD (1995) Protein transport to the yeast vacuole. Curr Opin Cell Biol 7:544-551.

Ichimura Y, Kirisako T, Takao T, Satomi Y, Shimonishi Y, Ishihara N, Mizushima N, Tanida I, Kominami E, Ohsumi M, Noda T, Ohsumi Y (2000) A ubiquitin-like system mediates protein lipidation. Nature 408, (2000): 488 - 492.

Kabeya Y, Mizushima N, Ueno T, Yamamoto A, Kirisako T, Noda T, Kominami E, Ohsumi Y, Yoshimori T (2000) LC3, a mammalian homologue of yeast Apg8p, is localized in autophagosome membranes after processing. EMBO J 19:5720-5728.

Kametaka S, Okano T, Ohsumi M, Ohsumi Y (1998) Apg14p and Apg6/Vps30p Form a Protein Complex Essential for Autophagy in the Yeast, Saccharomyces cerevisiae. J Biol Chem 273:22284-22291.

Kanai F, Liu H, Field SJ, Akbary H, Matsuo T, Brown GE, Cantley LC, Yaffe MB (2001) The PX domains of p47phox and p40phox bind to lipid products of PI(3)K. Nat Cell Biol 3:675.

Kihara A, Kabeya Y, Ohsumi Y, Yoshimori T (2001a) Beclin-phosphatidylinositol 3-kinase complex functions at the trans-Golgi network. EMBO Rep 2:330-335.

Kihara A, Noda T, Ishihara N, Ohsumi Y (2001b) Two distinct Vps34 phosphatidylinositol 3-kinase complexes function in autophagy and carboxypeptidase Y sorting in Saccharomyces cerevisiae. J Cell Biol 152:519-530.

Klionsky DJ, Emr SD (2000) Autophagy as a Regulated Pathway of Cellular Degradation. Science 290:1717-1721.

Klionsky DJ, Cregg JM, Dunn WA, Emr SD, Sakai Y, Sandoval IV, Sibirny A, Subramani S, Thumm M, Veenhuis M, Ohsumi Y (2003) A Unified Nomenclature for Yeast Autophagy-Related Genes. Developmental Cell 5:539.

Komatsu M, Wang QJ, Holstein GR, Friedrich VL, Jr., Iwata J-i, Kominami E, Chait BT, Tanaka K, Yue Z (2007a) Essential role for autophagy protein Atg7 in the maintenance of axonal homeostasis and the prevention of axonal degeneration. Proceedings of the National Academy of Sciences 104:14489-14494.

Komatsu M, Waguri S, Chiba T, Murata S, Iwata J-i, Tanida I, Ueno T, Koike M, Uchiyama Y, Kominami E, Tanaka K (2006) Loss of autophagy in the central nervous system causes neurodegeneration in mice. Nature 441:880.

Komatsu M, Waguri S, Ueno T, Iwata J, Murata S, Tanida I, Ezaki J, Mizushima N, Ohsumi Y, Uchiyama Y, Kominami E, Tanaka K, Chiba T (2005) Impairment of starvation-induced and constitutive autophagy in Atg7-deficient mice. J Cell Biol 169:425-434.

Komatsu M, Waguri S, Koike M, Sou YS, Ueno T, Hara T, Mizushima N, Iwata J, Ezaki J, Murata S, Hamazaki J, Nishito Y, Iemura S, Natsume T, Yanagawa T, Uwayama J, Warabi E, Yoshida H, Ishii T, Kobayashi A, Yamamoto M, Yue Z, Uchiyama Y, Kominami E, Tanaka K (2007b) Homeostatic levels of p62 control cytoplasmic inclusion body formation in autophagy-deficient mice. Cell 131:1149-1163.

Kuma A, Mizushima N, Ishihara N, Ohsumi Y (2002) Formation of the ~350-kDa Apg12-Apg5{middle dot}Apg16 Multimeric Complex, Mediated by Apg16 Oligomerization, Is Essential for Autophagy in Yeast. J Biol Chem 277:18619-18625.

Kuma A, Hatano M, Matsui M, Yamamoto A, Nakaya H, Yoshimori T, Ohsumi Y, Tokuhisa T, Mizushima N (2004) The role of autophagy during the early neonatal starvation period. Nature 432:1032-1036.

Larsen KE, Sulzer D (2002) Autophagy in neurons: a review. Histol Histopathol 17:897-908.

Levine B, Klionsky DJ (2004) Development by Self-Digestion: Molecular Mechanisms and Biological Functions of Autophagy. Developmental Cell 6:463.

Levine B, Kroemer G (2008) Autophagy in the Pathogenesis of Disease. Cell 132:27.

Liang C, Feng P, Ku B, Dotan I, Canaani D, Oh BH, Jung JU (2006) Autophagic and tumour suppressor activity of a novel Beclin1-binding protein UVRAG. Nat Cell Biol 8:688-699.

Liang C, Lee JS, Inn KS, Gack MU, Li Q, Roberts EA, Vergne I, Deretic V, Feng P, Akazawa C, Jung JU (2008) Beclin1-binding UVRAG targets the class C Vps complex to coordinate autophagosome maturation and endocytic trafficking. Nat Cell Biol 10:776-787.

Liang XH, Jackson S, Seaman M, Brown K, Kempkes B, Hibshoosh H, Levine B (1999) Induction of autophagy and inhibition of tumorigenesis by beclin 1. Nature 402:672.

Liang XH, Kleeman LK, Jiang HH, Gordon G, Goldman JE, Berry G, Herman B, Levine B (1998) Protection against fatal Sindbis virus encephalitis by beclin, a novel Bcl-2-Interacting protein. J Virol 72:8586-8596.

Lindmo K, Stenmark H (2006) Regulation of membrane traffic by phosphoinositide 3-kinases. J Cell Sci 119:605-614.

Lum JJ, Bauer DE, Kong M, Harris MH, Li C, Lindsten T, Thompson CB (2005) Growth factor regulation of autophagy and cell survival in the absence of apoptosis. Cell 120:237-248.

Maiuri MC, Le Toumelin G, Criollo A, Rain JC, Gautier F, Juin P, Tasdemir E, Pierron G, Troulinaki K, Tavernarakis N, Hickman JA, Geneste O, Kroemer G (2007) Functional and physical interaction between Bcl-X(L) and a BH3-like domain in Beclin-1. Embo J 26:2527-2539.

Massey AC, Zhang C, Cuervo AM (2006) Chaperone-mediated autophagy in aging and disease. Curr Top Dev Biol 73:205-235.

Melendez A, Talloczy Z, Seaman M, Eskelinen EL, Hall DH, Levine B (2003) Autophagy genes are essential for dauer development and life-span extension in C. elegans. Science 301:1387-1391.

Miled N, Yan Y, Hon W-C, Perisic O, Zvelebil M, Inbar Y, Schneidman-Duhovny D, Wolfson HJ, Backer JM, Williams RL (2007) Mechanism of two classes of cancer mutations in the phosphoinositide 3-kinase catalytic subunit. Science 317:239-242.

Mizushima N, Noda T, Ohsumi Y (1999) Apg16p is required for the function of the Apg12p-Apg5p conjugate in the yeast autophagy pathway. EMBO J 18:3888-3896.

Mizushima N, Sugita H, Yoshimori T, Ohsumi Y (1998a) A New Protein Conjugation System in Human. THE COUNTERPART OF THE YEAST Apg12p

CONJUGATION SYSTEM ESSENTIAL FOR AUTOPHAGY. J Biol Chem 273:33889-33892.

Mizushima N, Yamamoto A, Matsui M, Yoshimori T, Ohsumi Y (2004) In Vivo Analysis of Autophagy in Response to Nutrient Starvation Using Transgenic Mice Expressing a Fluorescent Autophagosome Marker. Mol Biol Cell 15:1101-1111.

Mizushima N, Noda T, Yoshimori T, Tanaka Y, Ishii T, George MD, J. KD, Mariko O, Yoshinori O (1998b) A protein conjugation system essential for autophagy. Nature 395:395-398.

Mizushima N, Yamamoto A, Hatano M, Kobayashi Y, Kabeya Y, Suzuki K, Tokuhisa T, Ohsumi Y, Yoshimori T (2001) Dissection of Autophagosome Formation using Apg5-deficient Mouse Embryonic Stem Cells. J Cell Biol 152:657-668.

Nagy A (2000) Cre recombinase: the universal reagent for genome tailoring. Genesis 26:99-109.

Nemoto T, Tanida I, Tanida-Miyake E, Minematsu-Ikeguchi N, Yokota M, Ohsumi M, Ueno T, Kominami E (2003) The mouse APG10 homologue, an E2-like enzyme for Apg12p conjugation, facilitates MAP-LC3 modification. Journal of Biological Chemistry 278:39517-39526.

Nordquist DT, Kozak CA, Orr HT (1988) cDNA cloning and characterization of three genes uniquely expressed in cerebellum by Purkinje neurons. J Neurosci 8:4780-4789.

Oberdick J, Smeyne RJ, Mann JR, Zackson S, Morgan JI (1990) A promoter that drives transgene expression in cerebellar Purkinje and retinal bipolar neurons. Science 248:223-226.

Oberstein A, Jeffrey PD, Shi Y (2007) Crystal structure of the Bcl-XL-Beclin 1 peptide complex: Beclin 1 is a novel BH3-only protein. J Biol Chem 282:13123-13132.

Ogura K, Wicky C, Magnenat L, Tobler H, Mori I, Muller F, Ohshima Y (1994) Caenorhabditis elegans unc-51 gene required for axonal elongation encodes a novel serine/threonine kinase. Genes Dev 8:2389-2400.

Pacheco CD, Kunkel R, Lieberman AP (2007) Autophagy in Niemann-Pick C disease is dependent upon Beclin-1 and responsive to lipid trafficking defects. Hum Mol Genet 16:1495-1503.

Pankiv S, Clausen TH, Lamark T, Brech A, Bruun J-A, Outzen H, Overvatn A, Bjorkoy G, Johansen T (2007) p62/SQSTM1 binds directly to Atg8/LC3 to facilitatedegradation of ubiquitinated protein aggregates by autophagy. J Biol Chem 282:24131-24145.

Pattingre S, Tassa A, Qu X, Garuti R, Liang XH, Mizushima N, Packer M, Schneider MD, Levine B (2005) Bcl-2 Antiapoptotic Proteins Inhibit Beclin 1-Dependent Autophagy. Cell 122:927.

Petiot A, Ogier-Denis E, Blommaart EF, Meijer AJ, Codogno P (2000) Distinct classes of phosphatidylinositol 3'-kinases are involved in signaling pathways that control macroautophagy in HT-29 cells. J Biol Chem 275:992-998.

Pickford F, Masliah E, Britschgi M, Lucin K, Narasimhan R, Jaeger PA, Small S, Spencer B, Rockenstein E, Levine B, Wyss-Coray T (2008) The autophagy-related protein beclin 1 shows reduced expression in early Alzheimer disease and regulates amyloid beta accumulation in mice. J Clin Invest 118:2190-2199.

Pyo JO, Jang MH, Kwon YK, Lee HJ, Jun JI, Woo HN, Cho DH, Choi B, Lee H, Kim JH, Mizushima N, Oshumi Y, Jung YK (2005) Essential roles of Atg5 and FADD in autophagic cell death: dissection of autophagic cell death into vacuole formation and cell death. J Biol Chem 280:20722-20729.

Qu X, Yu J, Bhagat G, Furuya N, Hibshoosh H, Troxel A, Rosen J, Eskelinen E-L, Mizushima N, Ohsumi Y, Cattoretti G, Levine B (2003) Promotion of tumorigenesis by heterozygous disruption of the beclin 1 autophagy gene. J Clin Invest 112:1809-1820.

Rubinsztein DC, Gestwicki JE, Murphy LO, Klionsky DJ (2007) Potential therapeutic applications of autophagy. Nat Rev Drug Discov 6:304-312.

Rusten TE, Lindmo K, Juhasz G, Sass M, Seglen PO, Brech A, Stenmark H (2004) Programmed autophagy in the Drosophila fat body is induced by ecdysone through regulation of the PI3K pathway. Dev Cell 7:179-192.

Saeki K, Yuo A, Okuma E, Yazaki Y, Susin SA, Kroemer G, Takaku F (2000) Bcl-2 down-regulation causes autophagy in a caspase-independent manner in human leukemic HL60 cells. Cell Death Differ 7:1263-1269.

Schu PV, Takegawa K, Fry MJ, Stack JH, Waterfield MD, Emr SD (1993) Phosphatidylinositol 3-kinase encoded by yeast VPS34 gene essential for protein sorting. Science 260:88-91.

Scott RC, Schuldiner O, Neufeld TP (2004) Role and regulation of starvation-induced autophagy in the Drosophila fat body. Dev Cell 7:167-178.

Shibata M, Lu T, Furuya T, Degterev A, Mizushima N, Yoshimori T, MacDonald M, Yankner B, Yuan J (2006) Regulation of intracellular accumulation of mutant Huntingtin by Beclin 1. J Biol Chem 281:14474-14485.

Shimizu S, Kanaseki T, Mizushima N, Mizuta T, Arakawa-Kobayashi S, Thompson CB, Tsujimoto Y (2004) Role of Bcl-2 family proteins in a non-apoptotic programmed cell death dependent on autophagy genes. Nat Cell Biol 6:1221-1228.

Simonsen A, Wurmser AE, Emr SD, Stenmark H (2001) The role of phosphoinositides in membrane transport. Current Opinion in Cell Biology 13:485.

Stack JH, Herman PK, Schu PV, Emr SD (1993) A membrane-associated complex containing the Vps15 protein kinase and the Vps34 PI 3-kinase is essential for protein sorting to the yeast lysosome-like vacuole. Embo J 12:2195-2204.

Stack JH, DeWald DB, Takegawa K, Emr SD (1995) Vesicle-mediated protein transport: regulatory interactions between the Vps15 protein kinase and the Vps34 PtdIns 3-kinase essential for protein sorting to the vacuole in yeast. J Cell Biol 129:321-334.

Stenmark H, Aasland R, Driscoll PC (2002) The phosphatidylinositol 3-phosphate-binding FYVE finger. FEBS Letters 513:77.

Suzuki K, Kirisako T, Kamada Y, Mizushima N, Noda T, Ohsumi Y (2001) The pre-autophagosomal structure organized by concerted functions of APG genes is essential for autophagosome formation. EMBO J 20:5971-5981.

Takacs-Vellai K, Vellai T, Puoti A, Passannante M, Wicky C, Streit A, Kovacs AL, Muller F (2005) Inactivation of the autophagy gene bec-1 triggers apoptotic cell death in C. elegans. Curr Biol 15:1513-1517.

Takahashi Y, Coppola D, Matsushita N, Cualing HD, Sun M, Sato Y, Liang C, Jung JU, Cheng JQ, Mul JJ, Pledger WJ, Wang HG (2007) Bif-1 interacts with Beclin 1 through UVRAG and regulates autophagy and tumorigenesis. Nat Cell Biol 9:1142-1151.

Tanida I, Mizushima N, Kiyooka M, Ohsumi M, Ueno T, Ohsumi Y, Kominami E (1999) Apg7p/Cvt2p: A Novel Protein-activating Enzyme Essential for Autophagy. Mol Biol Cell 10:1367-1379.

Teclemariam-Mesbah R, Wortel J, Romijn HJ, Buijs RM (1997) A simple silver-gold intensification procedure for double DAB labeling studies in electron microscopy. J Histochem Cytochem 45:619-622.

Thumm M, Kadowaki T (2001) The loss of Drosophila APG4/AUT2 function modifies the phenotypes of cut and Notch signaling pathway mutants. Mol Genet Genomics 266:657-663.

Tsukada M, Ohsumi Y (1993) Isolation and characterization of autophagy-defective mutants of Saccharomyces cerevisiae. FEBS Lett 333:169-174.

Uttenweiler A, Mayer A (2008) Microautophagy in the yeast Saccharomyces cerevisiae. Methods Mol Biol 445:245-259.

Wang J, Lian H, Zhao Y, Kauss MA, Spindel S (2008) Vitamin D3 induces autophagy of human myeloid leukemia cells. J Biol Chem 283:25596-25605.

Wang QJ, Ding Y, Kohtz DS, Mizushima N, Cristea IM, Rout MP, Chait BT, Zhong Y, Heintz N, Yue Z (2006) Induction of autophagy in axonal dystrophy and degeneration. J Neurosci 26:8057-8068.

Williams A, Jahreiss L, Sarkar S, Saiki S, Menzies FM, Ravikumar B, Rubinsztein DC (2006) Aggregate-prone proteins are cleared from the cytosol by autophagy: therapeutic implications. Curr Top Dev Biol 76:89-101.

Yan Y, Flinn RJ, Wu H, Schnur RS, Backer JM (2008) hVps15 but not calcium/calmodulin is required for the activity and regulation of hVps34 in mammalian cells. Biochem J.

Yu L, Alva A, Su H, Dutt P, Freundt E, Welsh S, Baehrecke EH, Lenardo MJ (2004) Regulation of an ATG7-beclin 1 program of autophagic cell death by caspase-8. Science 304:1500-1502.

Yue Z, Jin S, Yang C, Levine AJ, Heintz N (2003) Beclin 1, an autophagy gene essential for early embryonic development, is a haploinsufficient tumor suppressor. Proceedings of the National Academy of Sciences of the United States of America 100:15077-15082.

Yue Z, Horton A, Bravin M, DeJager PL, Selimi F, Heintz N (2002) A novel protein complex linking the delta 2 glutamate receptor and autophagy: implications for neurodegeneration in lurcher mice. Neuron 35:921-933.

Zeng X, Overmeyer JH, Maltese WA (2006) Functional specificity of the mammalian Beclin-Vps34 PI 3-kinase complex in macroautophagy versus endocytosis and lysosomal enzyme trafficking. J Cell Sci 119:259-270.

Zuo J, De Jager PL, Takahashi KA, Jiang W, Linden DJ, Heintz N (1997) Neurodegeneration in Lurcher mice caused by mutation in delta2 glutamate receptor gene. Nature 388:769-773.